PHYSICO-CHEMICAL STUDY OF COPPER-CARBON SYSTEM FOR PREPARATION OF GRAPHITE DISPERSED COPPER ALLOY COMPOSITE

（黒鉛分散銅基複合材料の開発に関する基礎研究）

July, 2017

Doctor of Engineering

Abdul Muizz Bin Mohd Noor

Toyohashi University of Technology

別紙４（課程博士）

Date of Submission:

平成 29 年 8 月 29 日

Department. of Mechanical Engineering	Student ID Number 学籍番号	D149105
Applicant's name 氏名	ABDUL MUIZZ BIN MOHD NOOR	

Supervisors 指導教員	SEIJI YOKOYAMA 横山誠二 MASANOBU IZAKI 伊崎昌伸 MASAHIRO FUKUMOTO 福本昌宏

Abstract

論文内容の要旨 (博士)

Title of Thesis 博士学位論文名	PHYSICO-CHEMICAL STUDY OF COPPER-CARBON SYSTEM FOR PREPARATION OF GRAPHITE DISPERSED COPPER ALLOY COMPOSITE (黒鉛分散銅基複合材料の開発に関する基礎研究)

(Approx. 800 words)

Graphite-dispersed copper composites is known to have good thermal and electrical conductivities, self-lubrication and low thermal expansion coefficient. These characteristic of it are derived from both characteristic of copper and graphite. Therefore, this composite is expected to be used for a sliding contact which an electric current flows in and friction acts on.

First, a Cu-Ni alloy in which the nickel was included up to approximately 5 mass% was melted in a graphite crucible with a high frequency induction furnace to prepare the Cu-Ni-C_{sat} (saturated carbon) alloy. Solubility of carbon into Cu-Ni alloy increased with the nickel content and with the melting temperature. The particles precipitated from the melt were graphite. The relation between the activity coefficient of carbon for Cu-Ni-C_{sat} and the temperature could be expressed by numerical formulas. This work proposed that the interaction parameter, ω_C^{Ni}, for Cu-Ni-C_{sat} was -17.1. Vickers hardness of Cu-Ni-C_{sat} system increased with C content. The Cu-Ni-C_{sat} alloy prepared in this study was hardened by precipitation hardening of the graphite particles and solution hardening of Ni.

Second, solubility of nitrogen gas into pure copper at temperature range of 1993 K to 2443 K was studied with using a levitation melting apparatus. The solubility of nitrogen which was equilibrated with nitrogen gas with a pressure of 101.3 kPa increased with the temperature of molten copper. However, the solubility was approximately 1.5 massppm even at 2443 K. The solubility obeyed the Sieverts' law. The relation between the change of Gibbs energy for this reaction, $\Delta_r G^0 = 61573 + 48.75T$ and thermodynamic temperature of the molten copper, T [K], was expressed as : $\ln[\text{mass\%N}] = -\frac{7406}{T} - 5.863$

Third, it was attempted that graphite dispersed copper composite was prepared only on the surface of a copper plate using a spot welding machine which could heat a material beyond 2073 K for short time. Experiments were carried out with changing the compressive load, the repetition number of the compression and the electrical

current in order to study their effects on carbon content and Vickers hardness of the composite. Generally, the carbon content of the composite prepared without an electrical current flow was smaller than that prepared with an electrical current flow. The former composite was prepared with that relatively small angular graphite particles were pushed into the copper plate. In the case of flowing electrical current, graphite particles was heated, and partially or wholly dissolved into molten copper. Therefore, this composite was prepared with undissolved graphite and precipitated graphite from the copper melt. The Vickers hardness of the copper matrix in the composite prepared without an electrical current flow was larger than that prepared with an electrical current flow, because the electrical heating annealed the composite. The relation between the Vickers hardness of the copper matrix in the composite and the volume fraction of graphite were expressed by the rule of mixtures.

Fourth, laser irradiation was used to prepare the graphite dispersed copper composite on a copper plate. The carbon dioxide laser was irradiated on the copper plate on which the graphite particles were plunged by rolling. Most plunged particles except the small angular graphite particles which were stuck in the copper plate were eliminated, when the rolled plate was dipped in the ultrasonic bath. When the laser was irradiated to the rolled plate, the number of graphite particles in the laser spot decreased with the laser irradiation time, because the particles was eliminated by the laser trapping. However, the fixing of the particles resulted from improvement of the wettability between the graphite particle and the molten copper. When the copper around the graphite particles further melted, the particles on the plate disappeared by the laser trapping. The number of the graphite particles on the outside of the laser spot increased with time. The laser trapping hardly acted on the graphite particles at this place. The copper at the outside of the laser spot were heated by the conduction from the laser spot, and melted. The particles were fixed by the wetting. The Vickers hardness decreased with an increase with the laser irradiation time due to annealing by the laser heat. The Vickers hardness at the outside of the laser spot was higher than that at the center of the laser spot.

Finally, it was tried to prepare the bulk of the graphite dispersed copper composite. The influence of the temperature, the way of addition of the graphite particles and the alloying elements (nickel, iron) were studied. The graphite particles were formed by the precipitation from the melt. When the temperature was above approximately 2073 K, copper could wet to the graphite, and this enhanced the dissolution of graphite into the molten copper. Therefore, the composite prepared at 2073 K included more graphite particles than that at 1673 K. In addition, the composite prepared by the addition of graphite particles on the melt hold at 2073 K contained more graphite than the composite prepared by the addition of them before heating. This resulted from the quantity of scattering graphite under heating and the wettability. The graphite particles in the composite contained nickel larger than that in pure copper because the solubility of carbon in copper-nickel system was larger than that in copper. The graphite particles in the composite contained iron were smaller than that in pure copper, and mainly existed in iron rich phase. The Vickers hardness of the composite after annealing was smaller than that before annealing because of the relaxation of solid-solution strengthening of carbon. The hardness of the graphite dispersed copper alloy was largest due to the solid-solution hardening of the alloying elements.

CONTENTS

CHAPTER 1

INTRODUCTION

1.1 Background

History of electric vehicle can be traced back in the 1800s when the first vehicle powered by battery was invented [1]. In 1890, first successful electric vehicle with a top speed of 14 miles per hour debuted and sparked interest in electric vehicles. In 1899, the first automobile powered by electricity exceeded 60 miles per hour [2]. Electric motor vehicles competed against steam and petrol engine vehicles from 1890s to 1900s [3]. By 1900 in the United State of America, the number of the electric vehicles was third highest among cars [4]. However, electric vehicles industries were in adversity when Henry Ford mass-produced Model T which was powered by internal-combustion engine and widely affordable to consumer [5]. After that, internal-combustion vehicles continued to grow it sell among consumer [6]. Continuing improvement in the internal combustion engine technology, reducing manufacturing cost and abundant amount of petrol had hampered the demand for electric vehicles until the late of 1990s [7]. From late 1990s to the recent, electric motor vehicles have regained its popularity among consumer due to improvement of the driving capability and economical. Now, electric vehicle is on a par with a petrol vehicle [8].

Vehicles account for approximately 20% of total primary energy consumption, where 95% of the usage derived from oil-based fuel [9,10]. In the past several years, high petrol consumption, worsening of environment pollution and increase of industrial waste have prompted researchers and car manufactures to produce more environmental friendly

devices and machines with low maintenance cost [11-13]. For example, in recent years an increase of public demand for nature friendly car such as electric motor vehicle causes rapid development in automotive engineering [14, 15]. Since modern electric cars have first introduced in 1997 to consumers, more than 11 million of them have been sold worldwide until April 2016 [16, 17]. Until now, the selling of eco-friendly vehicles have been increased and been popular among road user. Japan is top in sale with 5 million, followed by the United State of America (4 million), European (1.5 million) and rest of the world (0.5 million) [16]. Toyota Motor Company which has manufactured electric motor cars (hybrid car), until April 2016 leads the electric motor car industries with 9 million cars worldwide [17]. In future, more environment-friendly machine will be produced, not only limited to vehicles.

Electric motor vehicles usually use DC motors because of their lightweight, compact and efficiency [18, 19]. For example, large type of a DC motor is used in train [20]. However, the brushes used in a DC motor need to be replaced periodically due to wear [21]. As shown in Fig. 1.1, the brushes are used as a contact material with the commutator. When electric current passes through the coiled conducting cable in a magnetic field, the coil will produce a magnetic force. Torque from this force will rotate the coil the axes of with the motor [22]. Inside this motor, there are two parts which rotate and non-rotate. The rotating part is the commutator, while the non-rotating is the brushes [22]. As the DC motor has been used for a period of time, the brushes are eroded, and need to be replaced. This is due to the friction occurred between brushes and the commutator [23]. Beside copper brushes, carbon brushes are used in DC motor. However electric current flow in carbon brushes leads themselves to high temperature, which copper presented in commutators can be oxidized [24]. Another type of DC motor is a

brushless DC motor which requires permanent magnet. The demerit of this type of motor is that permanent magnet is necessary to this motor. The permanent magnet which is inferior to an electro-magnet is generated by the rotor rotation [25]. Beside that, in the case of high rotation, temperature of the rotor of the motor in which permanent magnet is becomes high. The increase in eddy current loss at the permanent magnet will reduce the efficiency [26, 27].

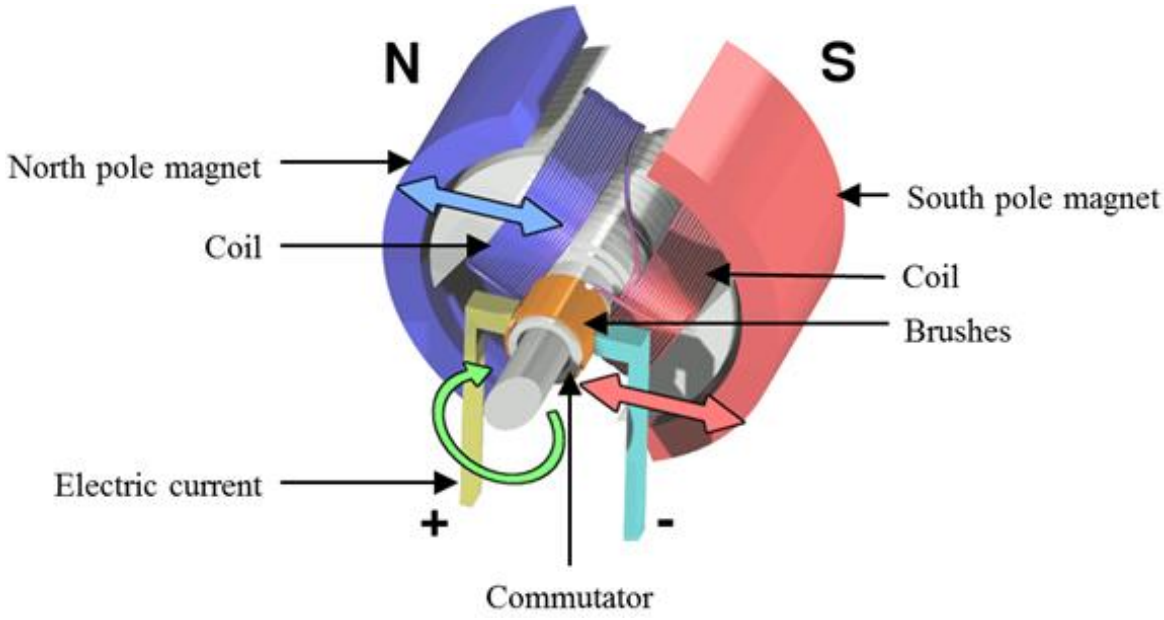

Fig. 1.1 Schematic of DC motor.

Both copper and graphite brushes have advantage and disadvantages. Copper brushes have better electrical conductivity than graphite brushes, but carbon brushes have a self-lubricating property [28-30]. These materials are not only used as brushes but also other sliding contact component such as pantograph [31].

If a material with advantages originated from both copper and graphite are

developed, the material should have good electrical and thermal conductivities, a high wear resistance and low thermal expansion. In this thesis, graphite dispersed copper composite which has characteristics as, above described, is introduced to be an alternative material for a component which is made of copper or graphite.

1.2 Fundamentals of copper

1.2.1 Brief history

Copper metal has been widely used in various applications and purposes. Copper is one of the earliest metals used by human because it can be discovered as a relatively pure metal naturally [32]. It was the first source of metal, and was used in 8000s BC. It was smelted in 5000s BC, casted to form something in 4000s BC, and alloyed to create bronze in 3500s BC [33]. Pure copper is usually too soft for most uses. About 3500 years ago, human learned for the first time that copper could be strengthened by mixing with other metals [34]. Today, copper has been mainly used as a conducting cable. It has also been used in heat exchanger because of its good thermal conductivity. In addition, it and its alloy are also used in some musical instruments, screws and other hardware that must resist corrosion [35].

1.2.2 Physical properties

Copper, silver and gold are in group 11 of the periodic table, and they have certain properties in common. They are characterized by high ductility, high electrical and thermal conductivity. Copper can be easily joined and hardened. It is non-magnetic, catalytic, and recyclable [36-40]. Copper metal appearance can be described as reddish color. Table 1.1 and Table 1.2 show mechanical and thermal properties of copper [41-43].

Table 1.1 Mechanical properties of copper.

Mechanical Property	Annealed (soft) copper	Cold-worked (hard) copper
Elastic modulus	100-120 GPa	120-130 GPa
Shearing modulus	40-45 GPa	45-50 GPa
Poisson's ratio	0.35	-
Tensile strength	200-250 MPa	300-360 MPa
Yield strength	40-120 MPa	250-320 MPa
Elongation	30-40 %	3-5 %
Vickers hardness	40-50 HV	800-1100 MPa
Brinell hardness	45-55 HB	90-120 HB
Scratch hardness	3	-

Table 1.2 Thermal properties of copper

Thermal property	Value
Melting point	1356 K
Boiling point	2868 K
Heat of fusion	13.1 kJ / mol
Heat of vaporization	300 kJ / mol
Vapor pressure at 2089 K	1 kPa
Specific heat capacity at 298 K	8.527 J / (K·mol)
Average specific heat capacity 298 K to 2750 K	18.7687 J / (K·mol)
Coefficient of linear thermal expansion	19.8 K^{-1}
Thermal conductivity at 293 K	394 W / (m·K)

1.2.3 Physical chemistry of copper

Like many other metal, copper is oxidized whenever it is exposed to air at high temperature. [44]. In the air, the copper reacts with oxygen, carbon dioxide, moisture and so on. It forms verdigris that are layered on the copper surface [45, 46]. This verdigris is not like the rust that forms on iron or other metals, but actually covers the copper surface as a passive state. Therefore, it protects the copper beneath it [47]. In the periodic table, copper is placed in period 4 and group 11. It behaves as a typical transition metal. It forms a wide variety of compounds with oxidation states of +I to +II. Its compounds are colored, and tends to form complex ions in aqueous solution. The crystal structure of copper is a face-centered cubic (FCC) structure, and inter-atomic distance is 0.255 nm [48].

1.3 Fundamentals of graphite

1.3.1 Brief history

Enormous deposits of natural graphite was discovered on the approach to Grey Knotts from the hamlet of Seathwaite in Borrowdale parish, Cumbria, England before 1565. It was then used by locals to mark sheep [49, 50]. In the reign of Queen Elizabeth I, Borrowdale graphite was used as a refractory material to line molds for cannonballs. Because of its military importance, it was strictly controlled by the Crown [51]. Graphite got it’s named by Abraham Gottlob Werner which mean “writing stone”. Until then, graphite had been known as a black lead or a plumbago [52-54].

1.3.2 Physical properties

Graphite is a naturally-occurring form of crystalline allotrope of carbon and

blackish in color [55, 56]. It is a native element mineral which is found in metamorphic and igneous rocks [57]. Graphite is extremely soft, fragile, cleft with very small force, and has a very low specific gravity [56-59]. It has an extremely heat resisting property and is nearly inert to almost any other materials [60]. These extreme properties give a wide range of uses in metallurgy and manufacturing [61]. Graphite can be found in organic-rich shale's and coal beds. In these cases, the graphite itself probably resulted from metamorphosis of dead plant and animal matter. Graphite is also found in veins sometimes basalt, and meteorites [62]. Table 1.3 shows the mechanical and thermal properties of graphite [63-65].

Table 1.3 Mechanical and thermal properties of graphite.

Property	Value
Bulk Density	1.3 - 1.95 g / cm^3
Porosity	0.7 – 53%
Modulus Elasticity	8 – 15 GPa
Compressive Strength	20 – 200 MPa
Flexural Strength	6.9 – 100 MPa
Coefficient of Thermal Expansion	1.2 – 8.2 ˚C
Thermal Conductivity	25 – 470 W / (m.K)
Specific Heat Capacity at 298 K	8.527 J / (K·mol)
Electrical Resistivity	1375.0×10^{-6} (Ω.cm)

1.3.3 Physical chemistry of graphite

Graphite is a mineral composed exclusively of the elemental carbons, C. It has the

same chemical composition as diamond, but the crystalline structures of graphite and diamond are entirely different [66]. This causes almost opposite characteristics in their physical properties. Diamond is transparent and known to be one of the hardest materials [67]. Diamond is widely used as abrasive and cutting medium in industries [68]. In contrast, graphite is soft and easily broken [56]. However graphite resists to heat and thermal shock [60]. Graphite also is used a as a solid lubricant and writing medium [69].

Graphite consists of layers in which six carbon atoms closely bond together hexagonally. The distance between the layers is 0.335mm, and is relatively large. In comparison with diamond, the density of graphite is small, and it is more stable than diamond thermodynamically [66]. Fig. 1.2 shows atomic structure of graphite and diamond. In graphite, the bond within one layer are strong, but the bonds between the layers are weak than that in one layer. The autonomic coordination at the first and third layers of graphite crystal are the same. Similarly, the coordination at the second and fourth layer are the same. As mentioned earlier, because the distance between the layers is relatively large, the interlayer forces are small. Therefore, the layers can be easily sheared. This explains the lubricity of graphite [66].

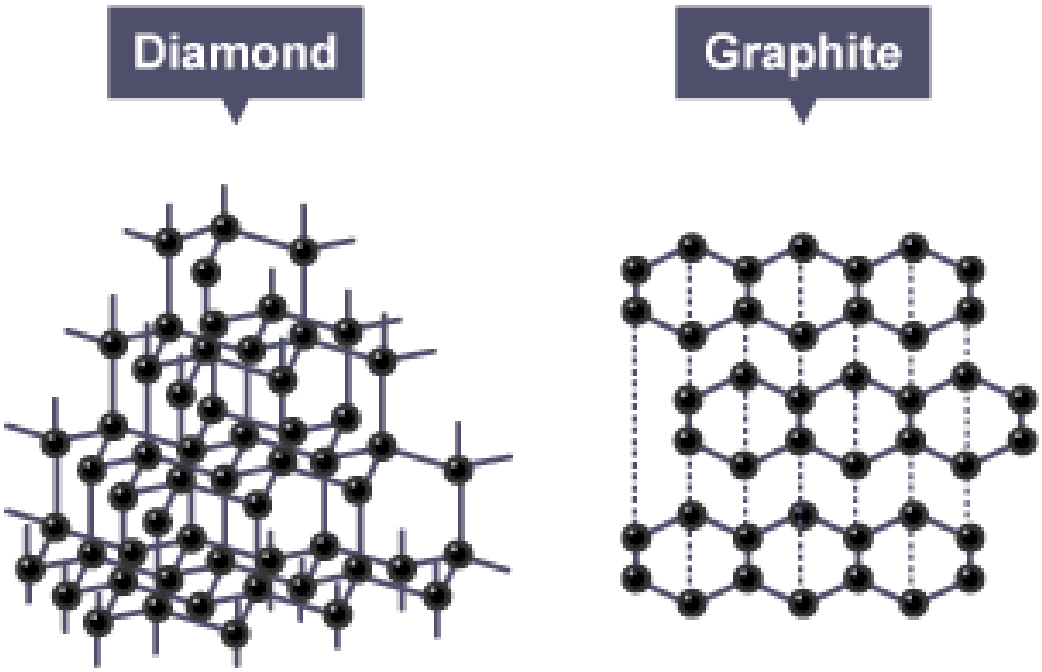

Fig. 1.2 Atomic structures of diamond and graphite

1.4. Copper-graphite composite

1.4.1 Characteristic of graphite dispersed copper composite

Characteristic of graphite dispersed copper composite derived are from both characteristic of copper and graphite. Copper is known to have good electrical and thermal conductivities and thermal expansion. On the other hand, graphite has a high wear resistance or self-lubrication and low thermal expansion. As a result, graphite-dispersed copper composites is known to have good thermal and electrical conductivities, self-lubrication and low thermal expansion coefficient. Therefore, this composite is expected to be used for a sliding contact which an electric current flows in and friction acts on.

1.4.2 Phase diagram for C-Cu system

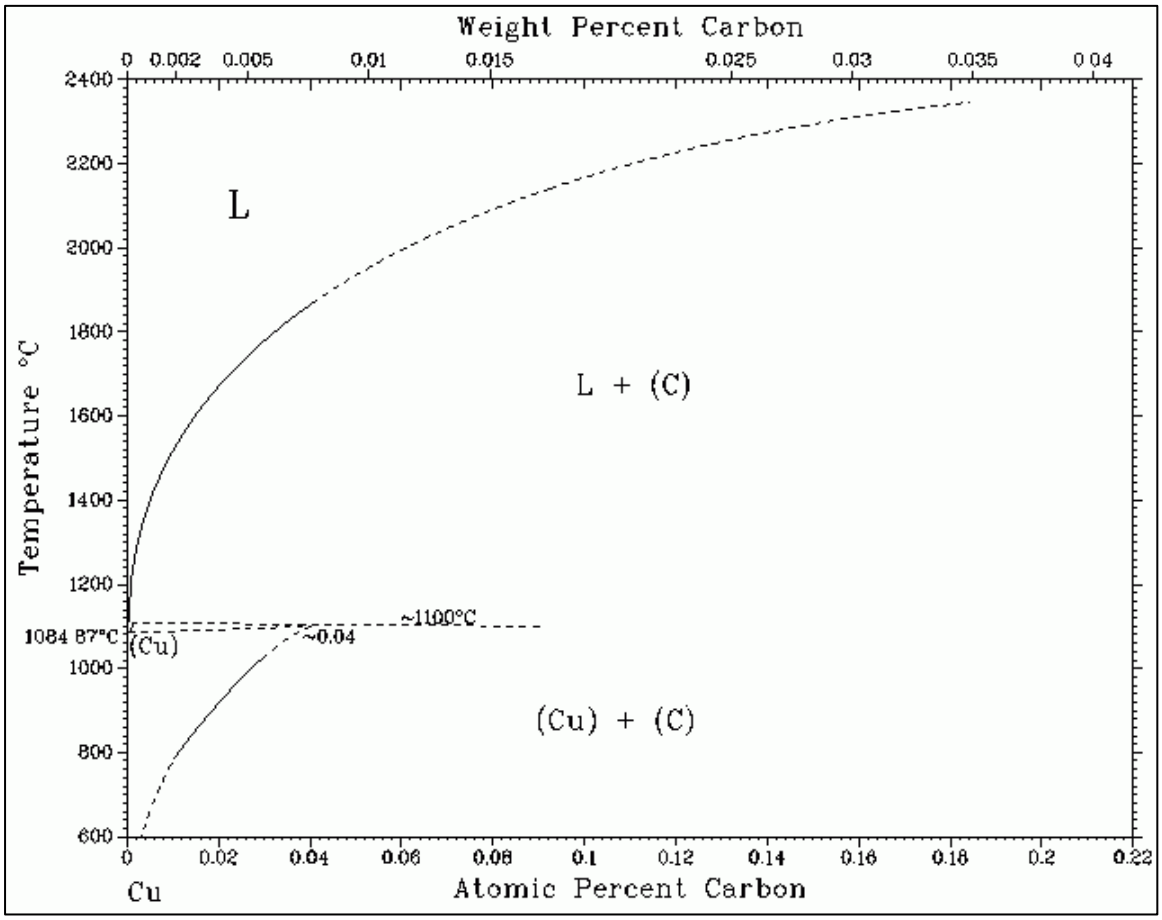

Fig. 1.3 Binary phase diagram of C-Cu [72]

The solubility of carbon in molten copper has been investigated. M. B. Bever et al. found that the solubility of carbon in molten copper were only 0.0001 mass% of carbon at 1100 ˚C (1373 K), 0.00015 mass% at 1200 ˚C (1473 K), 0.0005 mass% at 1500 ˚C (1773 K) and 0.003 mass% at 1700 ˚C (1973 K) [70]. Fischer and Schumid experimentally measured solubility of carbon with about 0.0005 mass% at 1200 ˚C (1473 K) [71]. Fig. 1.3 shows the phase diagram of C-Cu system [72]. This phase diagram was determined from the works [70-75]. It can be seen that carbon content increases with temperature.

According to the phase diagram, no carbide phase has been reported [72].

The solubilities of carbon into liquid copper measured by different researchers accords well each others. In contrast to the solubility of carbon in liquid copper, the solubilities of carbon in solid copper measured by Mc. Lellan [73] and G. Mathieu et al. [74] are different. In Mc. Lellan's work, solubility of carbon was measured from the temperature of 1058 K to 1314 K by carbon potential control technique. Foils of copper were equilibrated with graphite in presence of a small amount of air. The carbon was introduced into copper foil through gas mixture of CO and CO_2. The carbon content was analyzed with the conventional combustion method. The solubility was 250 atomic ppm at 1273 K which was near melting point, and was two orders of magnitude higher than solubility of carbon in molten copper. It was speculated later that this high solubility value was caused by the adsorption of carbon, CO and CO_2, or trapped carbon at intergranular [76]. As a result, this data were regarded as tentative. It was reported that the solubility at 1173 K was smaller than 0.5 at. ppm using a radiochemical technique [77]. In that work, the copper was aquilibrated by holding the copper speciments at 1173 K for 20 days in presence of a millicurie of ethylene or glucose. This data were not incorporated in the newest assesment of the Cu-C equilibrium phase diagram [72].

In recent work by Yokoyama et al. [78], the solubility of carbon in pure molten copper was measured up to 2273 K. It was found that the saturated carbon content could tremendously increase beyond 2073 K. In Yokoyama et al.'s work, the solubility of carbon in copper at 2273 K was 0.0297 mass%, which was analyzed with the combustion method. The solubility by them was also shown in Fig. 1.4 [72]. Until now, there is no other work which investigated carbon content in molten copper at the temperature higher than their work.

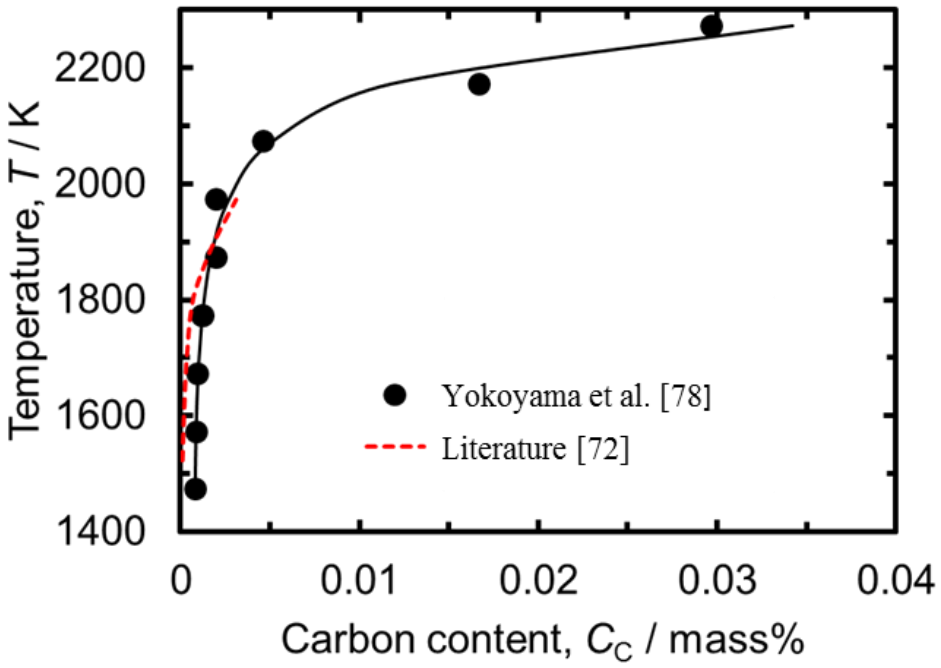

Fig. 1.4 Solubility of carbon in pure molten copper by Yokoyama et al. [78]

1.4.3 Preparation method for graphite dispersed copper composite

Various methods have been developed by researchers in order to prepare copper-graphite composite. The works concerning the preparation of Copper-Graphite are summarized as follows:

1) Addition of alloying element

P. B. Anderson and M. B. Bever studied the carbon solubility in copper-manganese and copper-nickel alloys [79]. However, they limited to the temperature of the molten copper alloy up to 1748 K. By adding 1 mass% or 9 mass% of nickel in copper, the solubility of carbon in molten copper alloy were 0.002 mass% and 0.053 mass %. However, their work concerned the solubility, not the preparation of graphite dispersed copper composite. Although saturated carbon content increased with nickel content in

copper-nickel alloy, the electric resistivity of copper alloy decreased [80]. As other works, adding chromium [81, 82] and titanium [83] in the composite to improve the wettability of molten copper alloy to the graphite. It was the largest problem in the preparation of copper-graphite composite that molten copper could not wet to graphite. According to Abel et al. [83], wettability of graphite with copper-chromium or copper-titanium was dependent on chromium or titanium concentration respectively. They concluded that chromium or titanium was in a thin layer as carbides between copper and graphite phases.

2) Other material processing methods

There are other methods without using high temperature. Powder metallurgy is one of the methods for preparing graphite dispersed copper composite. Powder metallurgy requires special equipment and is relatively expensive. In addition, composite prepared with this method tends to be porous [84].

Another method was the MG, (mechanical grinding). The advantages of this method is that it can produce various non-equilibrium phases such as highly supersaturated solid solution, nano-quasicrystalline, amorphous phases and so on [85-89]. A copper-graphite composite powder were prepared using this method [90]. A metastable solid solution Cu(C) can be obtained by high energy ball milling at room temperature.

In other work using MG in which high energy mechanical milling, MG was used to downsize the Cu-10 at% C to 30 nm [91]. The Vickers hardness of the composite was 2000 MPa. The grain boundary strengthening was the major strengthening mechanism for this composite [91]. However, sintering is necessary for preparation of the bulk composite, because the MG method only produces particles.

Brazing method has also been used to improve the wettability of copper to graphite

[92]. This method is equal to the surface modification. In this method, copper of which surface was modified by the other substances and graphite were melted at around 1200 K. Element such chromium, phosphorous and nickel were used as modifier to wet copper with graphite. This modifying additive acts as bridge at the interface between copper and graphite.

K. Rajkumar et al. [93] had prepared the graphite dispersed copper composite using microwave.

1.5 Objectives of this work

The graphite dispersed copper composite has promising features such as high wear resistance and good electrical and thermal conductivities which are useful for sliding contact like a brush of DC motor. There are two problems for preparation of this composite. Firstly, the solubility of carbon in copper is very low. If the solubility of carbon in molten copper can be enlarged, graphite particles will be able to be precipitated from the copper melt in which much carbon dissolved. This method for preparation of graphite dispersed copper composite is alike with the method for preparation of cast iron. Secondly, the molten copper cannot wet to graphite. As described earlier, Yokoyama et al. [78] revealed the following two things: First is that the solubility of carbon in liquid copper steeply increased with the temperature beyond approximately 2073 K. Second is that the wetting of molten copper to graphite improves beyond this temperature.

Main objective of this study was to prepare the graphite dispersed copper composite. Therefore, it was studied in this study to influence of alloying element on the solubility of carbon in molten copper so as to enlarge the solubility. In addition, it was intended to prepare the composite with high temperature processes more than 2073 K

where the wettability was improved. The mechanisms of formations of graphite and so on were discussed physico-chemically. The Vickers hardness of the composite was discussed from the view point of material engineering.

Graphite dispersed copper alloy composite demand carbon content from approximately 20 mass% to 85 mass%. In this study it was tried to prepare the graphite dispersed copper composite whose carbon content was in this range.

The increase in the solubility brings about the improvement of the wettability. So in this study, the concentrate objectives are listed as follows:

1) Influence of nickel content in molten copper-nickel alloy on the solubility of carbon in this liquid alloy. Effects of the dissolved carbon, precipitated graphite and nickel content in the solidified alloy on Vickers hardness were studied.

2) It was found that solubility of carbon steeply increased when the temperature exceed approximately 2100 K. As a fundamental study, the solubility of nitrogen gas into liquid copper was measured at temperature range of 1993 K to 2443 K to prepare nitride dispersed copper composite.

3) The copper-graphite composite was tried to be prepared only on the copper surface with using a spot welding machine.

4) Preparation of the copper-graphite composite only on the copper surface using a carbon dioxide laser process was attempted.

5) It was tried to prepare the bulk of the graphite-dispersed copper composite with conventional melting process with high temperature.

In order to achieve this target, some guiding questions are posed as follows:

Q1- How much is the carbon saturated content for copper-nickel alloy at temperature

2073 K and above?

Q2-What is the equation to express solubility of carbon as a function of thermodynamic temperature?

Q3-Is graphite equilibrated with Cu-Ni alloy? How are the relation among activity coefficient of carbon, temperature and molar fraction of nickel expressed?

Q4-What are the morphologies of the precipitated inside the composite?

Q5-How large does carbon content affect the hardness of the copper-graphite composite?

Q6-Can the nitride dispersed copper alloy be prepared with the high temperature process?

Q7- What is the equation to express solubility of nitrogen gas as a function of thermodynamic temperature?

Q8-Is the dissolution of nitrogen in copper expressed by with Sievert's law?

Q9-Spot welding provides locally high temperature for very short time. Can it be used to prepare this composite?

Q10-How do the compression force and the electrical current influence the preparation of the composite?

Q11-How does temperature influence the composite formation?

Q12-What is hardening mechanism of spot welding process?

Q13-Carbon dioxide laser provides locally high temperature. Can it be used to prepare this composite?

Q14-How does the graphite particles behave during laser irradiation?

Q15-how do the laser heating and trapping influence the preparation of the composite?

Q16-How do the graphite particles behave in molten copper in a magnesia crucible?

Thus all the guiding questions will be discussed and answered in each chapter of this

thesis.

1.6 Outline of this study

The overall outline of this thesis is summerized in Table 1.4. This thesis is consisted of 7 chapters.

Table 1.4 Overview of thesis outline

Chapter	Topic
1	Introduction
2	Influence of nickel content on solubility of carbon into molten copper-nickel alloy and Vickers hardness
3	Solubility of nitrogen into molten copper at temperature range of 1993 K to 2443 K
4	Preparation of graphite dispersed copper composite with spot welding
5	Preparation of graphite dispersed copper composite on surface of copper plate with carbon dioxide laser
6	Preparation of graphite dispersed copper composite with addition of graphite into molten copper
7	Summary

In **Chapter 1**, the following is described: the background of the research, the potential of graphite dispersed copper composite, physical and chemical properties of copper and graphite, previous work related with preparation of this composite, idea of proposing a new method to prepare this composite and finally the objective of this study.

In **Chapter 2,** the influence of nickel content and temperature on the carbon

solubility was discussed. These influences were analyzed thermodynamically. Graphite particles that were precipitated under cooling were observed using SEM and laser microscope. Mechanical property, which was the Vickers hardness of the Cu-Ni-C_{sat} composite, was mainly discussed from the influence of carbon and nickel contents on the Vickers hardness.

In **Chapter 3**, the solubility of nitrogen into molten copper was described. As shown in previous chapter, higher temperature could increase saturated carbon content in molten copper. Then, there was a possibility that nitrogen gas dissolves in molten copper at a higher temperature. The solubility of nitrogen obeyed with the Sievert's law. Relation between Gibbs energy and thermodynamic temperature was discussed in this chapter.

In **Chapter 4,** the preparation of graphite dispersed copper composite using a spot welding machine was described. Spot welding machine was used because it could raise the temperature high for a short time. A SEM and an EDX were used to observe microstructure of the sample surface and cross-section of it. Vickers hardness was also measured at the surface and the cross-section of the sample. Influences of the compression forces and electric current were discussed..

In **Chapter 5**, the preparation of graphite dispersed using a carbon dioxide laser was described. As similar to the spot welding in previous chapter, the laser could produce high temperature for an instant time. A SEM observation and an EDX analysis were done to study microstructures and compositions of the sample surface and cross-section. Vickers hardness was also measured at the surface and the cross-section of the sample.

In **Chapter 6**, the preparation of graphite dispersed copper composite with addition of graphite particles into molten copper was described. This work was almost as similar to the work in chapter 2, but, instead a graphite crucible, the copper with graphite powder

had been melted in a magnesia crucible. Much smaller graphite powder and mechanically ground copper with the graphite powder were also used for the preparation of the composite. The cross-section of the solidified copper was observed to clear how graphite particles participated inside copper. The Vickers hardness of the composite was also measured.

Finally, in **Chapter 7**, main results and discussion that were obtained from Chapter 2 to Chapter 6 were summarized in this chapter.

1.7 Flow of this study

Solubility of carbon in molten copper steeply increased with an increased in the temperature when the temperature of the copper melt exceeded around 2073 K. In addition, liquid copper could wet to the graphite above this temperature. the main objective of this work is to prepare the graphite dispersed copper composite with using these knowledge. The flow of this study is described as follows:

Chapter 2: Because the solubility of carbon in liquid copper was small, quantity of precipitated graphite was small. Then, in this chapter, it was tried that addition of nickel increased the carbon solubility.

Chapter 3: the solubility of carbon increased by the addition of nickel. However, the solubility did not become so large. Then, the solubility of nitrogen into liquid copper was studied in order to prepare a nitride dispersed copper composite instead a graphite dispersed copper composite.

As a result, the solubility of nitrogen in liquid copper was small. It seemed to be difficult that graphite or nitride dispersed copper composite to be prepared with the precipitation from the carbon or nitrogen saturated copper. Then, it was attempted to

prepare the graphite dispersed copper composite with using the phenomena that the wetting of molten copper to graphite improved beyond 2100 K.

Chapter 4: it was tried that the graphite dispersed copper composite was prepared only on the copper plate with a spot welder which could heat a substances to a higher temperature for a short time.

Chapter 5: It was tried that the graphite dispersed copper composite was prepared only on the copper plate with a carbon dioxide laser which could heat a material to a higher temperature for a short time like a spot welder.

Chapter 6: It was tried to prepare bulk of the graphite dispersed copper composite. Copper, graphite particles and alloying elements (nickel, iron) were melted in a magnesia crucible. Influence of temperature, was of the addition of graphite and alloying elements on the formation of the composite were studied in this chapter.

REFERENCES

[1] M. Guarnieri: “Looking back to electric cars”, Third HISTELCON, (2012) pp. 1-6

[2] E. Gregersen: “The complete history of wheeled transportation: From cars and trucks to buses and bikes”, Britannica Educational Publishing, (2011) pp. 31

[3] David A. Kirsch: “Part two - Histories, the electric vehicle and the burden of history”, Rutgers University Press United State of America, (2000) pp. 29-189

[4] Joseph W. Weiss: “Business ethics: a stakeholder and issues management approach with cases”, Cengage Learning Inc., Ohio, US (2009) pp. 204

[5] J. Merrill, R. Sharp and S. Usborne, Model T Ford: “The car that changed our world”, Independent online, 3rd March (2008)

[6] F. Clymer: “Treasury of early American automobiles 1877–1925”, Bonanza Books, New York, (1950) pp. 178

[7] Francis C. Moon: “Chapter 3 Social networks of the internal combustion engine and automobile”, History of Mechanism and Machine Science, Social Networks in the History of Innovation and Invention, Springer, vol. 22 (2014) pp. 65-84

[8] Matt Lake: “How it works; A Tale of 2 Engines: How Hybrid Cars Tame Emissions”, The New York Times, 8th Nov. (2001)

[9] Exxon Mobil: “The outlook for energy: a view to 2040”, ExxonMobil (2014)

[10] B. Metz, O.R. Davidson, P.R. Bosch, R. Dave, L.A. Meyer (Eds.): “Climate change 2007: mitigation. Contribution of working group III to the fourth assessment report of the intergovernmental panel on climate change”, Cambridge University Press, Cambridge, UK and New York, USA (2007)

[11] M. H. M. Ashnani, T. Miremadi., A. Johari, A. Danekar: “Environmental impact of alternative fuels and vehicle technologies: A life cycle assessment perspective”, Procedia

Environmental Sciences, vol. 30 (2015) pp. 205-210

[12] B.L. Salvi, K.A. Subramanian: “Sustainable development of road transportation sector using hydrogen energy system”, Renew. Sustain. Energy Rev., 51 (2015), pp. 1132–1155

[13] L. Lei, S. Wang, Y. Lin, W. Liu, T. Chi; “A covering model application on Chinese industrial hazardous waste management based on integer program method”, Ecol. Indic., vol. 51 (2015), pp. 237–243

[14] L. Situ: “Electric vehicle development: the past, present and future”, PESA, (2009), pp. 1–3

[15] H. Yua, A. L. Stuarta: “Impacts of compact growth and electric vehicles on future air quality and urban exposures may be mixed”, Sci. Total Environ., vol. 576, (2017) pp. 148–158

[16] J. Cobb: “American buy their four-millionth hybrid car”, HybridCar.com, 6th June (2016)

[17] Toyota: “Worldwide sales of Toyota hybrid surpass 9 million units”, Press release, Toyota City Japan, 20th May (2016)

[18] R. Hodkinson and J. Fenton: “Lightweight electric/hybrid vehicle design”, A volume in Automotive Engineering Series, (2000) pp. 3–28

[19] K. Hameyer, R. J. M. Belmans: “Permanent magnet excited brushed DC motors”, IEEE T. Ind. Electron., vol. 43 (1996) pp. 247–255

[20] S. Liu, Y. Tian, W.J.T. (Bill) Daniel, P. A. Meehan: “Modelling of track wear damage due to changes in friction conditions: A comparison between AC and DC electric drive locomotives”, Wear, vol. 366-367 (2016) pp. 338–345

[21] R.J. Hamilton: “DC motor brush life”, IEEE T. Ind. Appl., vol. 36 (2000) pp.

1682-1687

[22] Y. Zhou: “DC motors, speed controls, servo systems: An engineering handbook”, Electro-craft Corporation USA, Pergamon Press Ltd., (1977)

[23] Z. L. Hu, Z. H. Chen, J. T. Xia: “Study on surface film in the wear of electrographite brushes against copper commutators for variable current and humidity”, Wear, vol. 264 (2008) pp. 11–17.

[24] D.W. McKee, R.H. Savage, G. Gunnoe: “Chemical factors in carbon brush wear”, Wear, 22 (1972), pp. 193–214

[25] A. Alla, M. Hinze, O. Lass, S. Ulbrich: “Model order reduction approaches for the optimal design of permanent magnets in electro-magnetic machines”, IFAC Papersonline, vol. 48 (2015) pp. 242-247

[26] Kea-Ho Leea, Hyun-Rok Chab, Young-Bae Kim: “Development of an interior permanent magnet motor through rotor cooling for electric vehicles”, Appl. Therm. Eng., vol. 95 (2016) pp. 348–356

[27] C. Ruschettia, C. Verucchib, G. Bossioa, C. De Angeloa, G. García: “Rotor demagnetization effects on permanent magnet synchronous machines”, Energ. Convers. Manage., vol. 74 (2013) pp. 1–8

[28] P. Jenei, J. Gubicza, E. Y. Yoon, H. S. Kim, J. L. Lábár: “High temperature thermal stability of pure copper and copper–carbon nanotube composites consolidated by high pressure torsion”, Compos. Part A Appl. Sci. Manuf., vol. 51 (2013) pp. 71–79

[29] Y. Feng, S. L. Burkett: “Modeling a copper/carbon nanotube composite for applications in electronic packaging”, Comput. Mater. Sci., vol. 97 (2015) pp. 1–5

[30] K.T. Kim, S.I. Cha, S.H. Hong, S.H. Hong: “Microstructures and tensile behavior of carbon nanotube reinforced Cu matrix nanocomposites”, Mater. Sci. Eng. A, vol. 430

(2006), pp. 27–33

[31] T. Ding, G. X. Chen, Y. M. Li, Q. D. He, W. J. Xuan: “Friction and wear behavior of pantograph strips sliding against copper contact wire with electric”, AASRI Procedia, vol. 2, (2012) pp. 288-292

[32] S. K. Lothrop: “Cocle: an archeological study of central Panama: Memoirs of the Peabody museum of archeology and ethnology”, Harvard University, Cambridge, (1937)

[33] C. McHenry: “The New Encyclopedia Britannica 3 (15 Edition)”, Chicago: Encyclopedia Britannica Inc., (1992) pp. 612

[34] I. McNeil: “Encyclopaedia of the History of Technology”, Taylor & Francis London, (2002) pp. 48–66

[35] B. Carter: “Boom, bust, boom: a story about copper, the metal that runs the world”, Schaffner Press, Inc. (2014)

[36] W. K. Kuhn, R. A. Campbell, D. W. Goodman: “Structural, chemical and electronic properties of copper/tantalum (110)”, J. Phys. Chem., vol. 97 (1993) pp. 446–453

[37] David R. Lide: CRC Handbook of Chemistry and Physics, 88th Edition, Taylor & Francis (2007) 4-61

[38] S. Chandra, A. Kumar: “Recyclable copper nanoparticles: Efficient catalyst for selective cyclization of Schiff bases”, J. Saudi Chem. Soc., vol. 20 (2016) pp. 367–372

[39] W. F. Steiner: “A method for producing non-magnetic castings of copper, brass, and aluminum”, J. Geophys. Res., vol. (43) (1) (1938) pp. 47-48

[40] K. V. Raman, J. S. Moodera: “Materials chemistry: A magnetic facelift for non-magnetic metals”, Nature, vol. 524 (2015) pp. 42–43

[41] David R. Lide, CRC Handbook of Chemistry and Physics, 88th Edition, Taylor & Francis (2007) 4-61

[42] J. R. Davis: “Copper and copper alloys”, ASM Specialty Handbook, ASM International, (2001) pp. 446-452

[43] H. Wayne Richardson: “Handbook of Copper Compounds and Applications”, Marcel Dekker Inc., New York, (1997) pp. 13-30

[44] Jian Li and J. W. Mayer: “Oxidation and protection in copper and copper alloy thin films”, J. Appl. Phys., vol. 70 (1991) pp. 2820

[45] R.P.B. Hernández, Z. Pászti, H.G. de Melo, I.V. Aoki: “Corrosion behaviour of copper under chloride-containing thin electrolyte layer”, Corros. Sci., vol. 52 (2010), pp. 826–837

[46] K. P. Fitz Gerald, J. Nairn, G. Skennerton, A. Atrens: “Atmospheric corrosion of copper and the colour, structure and composition of natural patinas on copper”, Corros. Sci., vol. 48 (9) (2006) pp. 2480-2509

[47] T. E. Graedel, K. Nassau, J.P. Franey: “Copper patinas formed in the atmosphere-I. Introduction”, Corrosion Science, vol. 27 (1987) pp. 639-649

[48] R. E. Smallman, R. J. Bishop: “Modern physical metallurgy and materials engineering”, Sixth Edition, Butterworth Heinemann, Oxford, (1999) pp. 20

[49] M. Norgate, J. Norgate: “Old Cumbria Gazetteer, black lead mine”, Seathwaite Geography Department, Portsmouth University, (2008)

[50] A. Wainwright: “A Pictorial Guide to the Lakeland Fells, Western Fells London”, Frances Lincoln, (2005)

[51] The Bavarian State Library: “The Statutes at Large: From the ... Year of the Reign of ... to the ... Year of the Reign of ..”, (1764) pp. 415

[52] J. W. Evans: “V.— the Meanings and Synonyms of Plumbago”, Transactions of the Philological Society, 26 (1908) pp. 133

[53] J. F. W. Widenmann: “Handbuch des oryktognostischen Theils der Mineralogie: Mit einer Farbentabelle und einer Kupfertafel”, Crusius, (1794) pp. 653

[54] C. W. K. Scheele: “1779). Versuche mit Wasserbley;Molybdaena”, Svenska vetensk. Academ. Handlingar. vol. 40 (1779) pp. 238

[55] International Committee for Characterization and Terminology of Carbon: “Carbon”, vol. 28 (1990) pp. 445-449

[56] Hugh O. Pierson: “Handbook of Carbon, Graphite, Diamonds and Fullerenes”, Noyes Publications, Park Ridge, New Jersey, U.S.A., (1993) pp. 43

[57] J. C. Bokros: “Chemistry and Physics of Carbon”, Marcel Dekker Inc., New York vol. 5 (1969)

[58] P. Mukhopadhyay, R. K. Gupta: “Graphite, graphene, and their polymer nanocomposites”, CRC Press, U.S.A., (2013) pp. 56

[59] X. C. Tong: “Advanced Materials and Design for Electromagnetic Interference Shielding”, CRC Press, U.S.A., (2009) pp. 154

[60] J. R. Davis: “ASM Specialty Handbook: Tool Materials”, ASM Int. (1995) pp. 265

[61] AZO Materials: “Graphite (C) - Classifications, Properties and Applications of Graphite”, http://www.azom.com/article.aspx?ArticleID=1630 Sept. 10 (2002)

[62] Earth Science Museum, University of Waterloo: “Graphite”, https://uwaterloo.ca/earth-sciences-museum/resources/detailed-rocks-and-minerals-articles/graphite available online March (2009)

[63] David R. Lide, CRC Handbook of Chemistry and Physics, 88th Edition, Taylor & Francis (2007) 4-56

[64] J. W. Anthony, R. A. Bideaux, K. W. Bladh, M. C. Nichols: “Graphite”, Handbook of Mineralogy, Mineralogical Society of America, Chantilly, VA, US (1990)

[65] T.D. Burchell: “2.10 – Graphite: Properties and Characteristics”, Comprehensive Nuclear Materials, vol. 2 (2012) pp. 285-305

[66] R. E. Smallman, R. J. Bishop: “Modern physical metallurgy and materials Engineering”, Sixth Edition, Butterworth Heinemann, Oxford, (1999) pp. 21

[67] M. A. Prelas, G. Popovici, L. K. Bigelow: “Handbook of Industrial Diamonds and Diamond Films”, CRC Press, U.S.A., (1997) pp. 78

[68] J. Konstanty: “Powder metallurgy diamond tools”, Elsevier Ltd., U. K., (2005) pp. 21-38

[69] R. H. Savage: “Graphite lubrication”, J. Appl. Phys., vol. 19 (1948) pp. 1

[70] M. B. Bever, C. F. Floe: “The solubility of carbon in molten copper”, Trans. AIME, vol. 166 (1946) pp. 128

[71] J. Fisher and W. Schidt: *Z. Erbergbau Metalluettenw*., vol. 9 (1956) pp. 284

[72] P.R. Subramaniam, D.E. Laughlin: “Phase diagrams of binary copper alloys. Monograph series on alloy phase diagrams”, Material Park, OH: ASM International ,vol. 10 (1994) pp. 109

[73] O. Ruff, B. Bergdahl: “Arbeiten im gebiet hoher temperaturen. XII. Die messung von dampfspannungen bei sehr hohen temperaturen nebst einigen beobachtungen über die löslichkeit von kohlenstoff in metallen”, Z. Anorg. Allg. Chem., vol. 106 (1919) pp.76-94

[74] M.C. Snead, J.L. Maynard, R.C. Brasted: “Comprehensive Inorganic Chemistry, Copper, Silver, and Gold”, van Nostrand, Princeton, vol. 2 (1954) pp. 110-111

[75] R.B. McLellan: “The solubility of carbon in solid gold, copper, and silver”, Scr. Metall., vol. 3 (1969) pp. 389-391

[76] L. L. Oden, N. A. Gokcen: “Cu-C and Al-Cu-C phase diagrams and thermodynamic

properties of c in the alloys from 1550 °C to 2300 °C", Metall. Trans. B, vol. 23 (4) (1992) pp .453–458

[77] G. Mathieu, S. Guiot, J. Cabane: "Solubilite du carbone dans l'argent, le cuivre et l'or", Scripta Metall., vol. 7 (1973) pp. 421

[78] S. Yokoyama, Y. Takashima, M. Nor, Y. Murata, H. Kanematsu, J. Sasano, M. Izaki: "Solubility of carbon and Vickers hardness of copper saturated with carbon", AMPT, Sept. (2012) pp. 1-8

[79] P. B. Anderson, M. B. Bever: "Solubility of carbon in molten copper-manganese and copper-nickel alloys", Metals Tech., vol. 14 (1947) pp. 2151

[80] G. Iannone, D. Zola, A. Angrisani Armenio, M. Polichetti, and C. Attanasio: "Electrical resistivity and magnetic behavior of PdNi and CuNi thin films", Phys. Rev. B, vol. 75 (2007) 064409.

[81] S. M. Devincent, G. M. Michal: "Reaction Layer Formation at the Alloy Interface," Contractor, vol. 24 (1992) pp. 53–60

[82] L. Yang, P. Shen, Q. Lin, F. Qiu, and Q. Jiang: "Effect of Cr on the wetting in Cu/graphite system," Appl. Surf. Sci., vol. 257 (14) (2011) pp. 6276–6281

[83] P. B. Abel, A. L. Korenyi-Both, F. S. Honecy, S. V. Pepper: "Study of copper on graphite with titanium or chromium bond layer", J. Mater. Res., vol. 9 (3) (1994) pp. 617–624

[84] W. D. W. Ángel, L. T. Jurado, J. F. C. Alcalá, E. C. Martínez, Víctor F. V. Cedeño: "Effect of copper on the mechanical properties of alloys formed by powder metallurgy", Materials & Design, vol. 58 (2014) pp. 12–18

[85] S. Saji, T. Kadokura, H. Anada, K. Notoya, N. Takano: "Solid Solubility of Carbon in Copper During Mechanical Alloying", Mater. Trans. JIM, vol. 39 (7) (1998) pp.

778-781

[86] S. Abe, S. Saji, S. Hori: “Mechanical alloying of Al-20 mass%Ti mixed powders”, Japan Inst. Metals, vol. 54 (1990) pp. 895-902

[87] K. Uenishi, K. Kobayashi, S. Nasu, H. Hatano, K Ishihara, P. Shingu: “Mechanical alloying in the Fe-Cu system”, Z. Metallk., vol. 83 (1992) pp. 132

[88] S. Saji, H. Araki, K. Hashimoto, E. Murata: “Amorphization of Al-12at.%Ti-X (X=Cr,Fe,Ni,Cu) mixed powders by mechanical alloying”, Mater. Trans. JIM, vol. 37 (1996) pp. 1061-1066

[89] U. Mizutani, T. Takeuchi, T. Fukunaga: “Formation of quasicrystals and approximant crystals by mechanical alloying in Mg-Al-Zn alloy system”, Trans. JIM, vol. 34 (1993) pp. 102-108

[90] J. Wang: “Research on Preparation of Copper-Graphite Composite Powder by Mechanical Alloying”, Composite Powder vol. vol. 34 (4) (2016) pp. 291-294

[91] W. Zhang, DS. Zhou, D. Zhang, X. Li: “Microstructural evolution of Cu-10at%C nanocomposite powder during high energy mechanical milling”, Mat. Res., vol. 18 (2015) pp. 152-157

[92] J. Zhang, T. Wang, C. Liu, Y. He: “Effect of brazing temperature on microstructure and mechanical properties of graphite/copper joints”, Mater. Sci. Eng., vol. 594 (2014) pp. 26-31

[93] K. Rajkumar, S. Aravindan: “Microwave sintering of copper–graphite composites”, J. Mater. Process. Tech., vol. 209 (2009) pp. 5601-5605

CHAPTER 2

INFLUENCE OF NICKEL CONTENT ON SOLUBILITY OF CARBON INTO MOLTEN COPPER-NICKEL ALLOY AND VICKERS HARDNESS

2.1 Introduction

Graphite-dispersed copper composites have been known to have good thermal and electrical conductivities, self-lubrication and low thermal expansion coefficient [1, 2]. The former two properties and the latter two properties are mainly originated from copper and graphite respectively. Therefore, this composite is expected to be used for a sliding contact which an electric current flows in and friction acts on. One of the applications of this material is a brush for a direct current (DC) motor and a generator [3, 4]. The brushes determine the lifetime of a DC motor and a generator. Because the brush is worn by the friction, the brush should be replaced as needed.

The most important thing for the preparation of this composite is that copper can not wet graphite. Therefore, a surface modification of graphite and/or alloying a copper with the element such as Ti and Cr are needed so as to improve the wetting [5-7]. Generally, a liquid metal can wet a solid which forms endogenously. If graphite is precipitated from a molten copper as graphite from cast iron, this problem of the wetting between copper and graphite will be able to be solved. The phase diagram shows that the solubility of carbon in liquid copper at the temperature below approximately 2000 K is less than or equal to approximately 50 mass ppm [8]. Then, in the previous work [9], copper in a graphite crucible was heated up to approximately 2300 K so as to study the

solubility of graphite into molten copper at a higher temperature. The saturated content of carbon in molten copper steeply increased when the temperature exceeded approximately 2100 K. The solubility of carbon in molten copper at 2273 K was approximately 300 mass ppm. In addition, spheres and flakes of graphite were precipitated at the final solidification place of a molten copper saturated with carbon. However, the saturated carbon content was too small that the quantity of precipitated graphite was small. Then, in this work, it was attempted to increase the solubility of carbon by addition of alloying element in copper. Because the carbon can dissolve in a nickel, it is anticipated that the solubility of carbon in Cu-Ni alloy increases with an increase in the nickel content in the alloy. J. R. Anderson and M. B. Bever investigated the solubility of carbon in copper-nickel alloy at the temperature of 1748 K [10]. Until now, there is no research on carbon solubility in molten copper-nickel alloy above 1748 K. In addition, whereas Ni_3C has been known as carbide of nickel, it can be estimated from Gibbs energy that the Ni_3C does not form in the Cu-Ni-C_{sat} alloy [11]. A nickel is chosen as an alloying element from these two reasons. Then, as a series of fundamental study of preparation of graphite dispersed copper composite, influence of nickel content in molten Cu-Ni alloy on the solubility of carbon was investigated. In addition, the Vickers hardness of the solidified alloy was measured to clear the effects of the dissolved carbon, precipitated graphite and nickel content on the hardness.

2.2 Experimental

2.2.1 Preparation of Cu-Ni alloy

1) Metals used

Commercially available pure copper (the purity: 99.9 mass%) and nickel (99.9

mass%) were used for preparation of Cu-Ni alloy. The copper and the nickel were cut from these bulks and were arranged so that total weight of them was approximately 300g. The mixing weight of copper and nickel was shown in Table 2.1. The materials were cleaned in an ultrasonic-bath which ethanol was in for 15 minutes to eliminate from house dust, grease and so on.

Table 2.1 Mixing quantity of Cu and Ni, anticipated content of Ni and actual content of Ni.

Symbol of alloy	Copper, W_{Cu} / g	Nickel, W_{Ni} / g	Anticipated nickel content, C_{Ni} / mass %	Measured content of Ni, C_{Ni} / mass %
CuNi 1 wt%	304	3.328	1.08	1.35
CuNi 3 wt%	283	9.709	2.99	3.13
CuNi 5 wt%	287	15.03	4.98	5.02

2) Apparatus

The apparatus to prepare copper-nickel alloy was shown in Fig. 2.1 The maximum reaching temperature was approximately 2200 K. It could be controlled manually within ±10 K by adjusting the voltage. The inner diameter and length of the quartz furnace tube were 100 mm and 505 mm respectively.

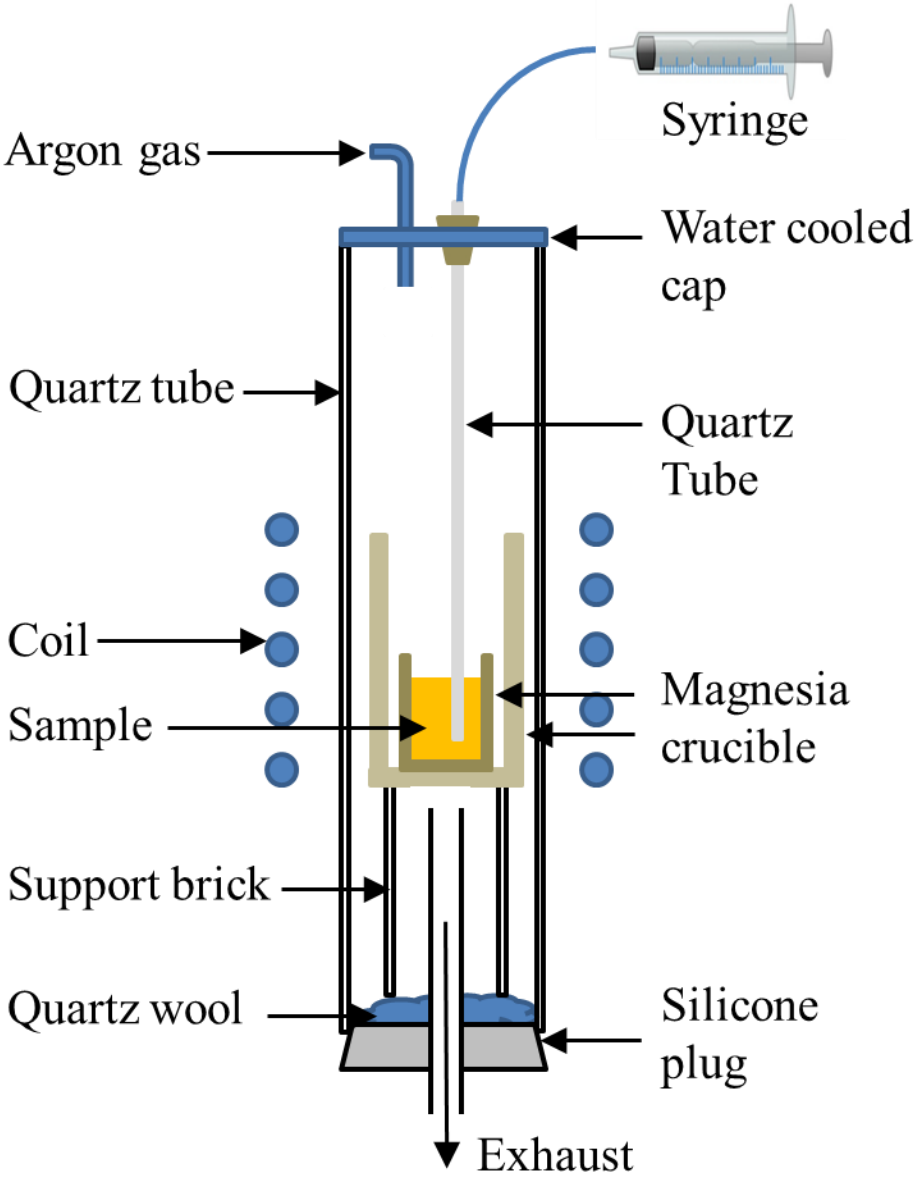

Fig. 2.1 Apparatus to prepare copper-nickel alloy.

3) Melting

The mixture of copper and nickel was placed inside a magnesia crucible, and were melted under argon gas flow with a high frequency induction furnace (EG53S Fuji Electric). An argon with a purity of 99.999 mol% was introduced in the furnace with the flow rate of 0.4 L/min (NTP (normal temperature and pressure)) for about 10 minutes

before melting to replace the air in the furnace with the argon gas to prevent oxidation of the metal. The materials were heated to 1773 K. At this temperature, it was held for 30 minutes to make sure the metal completely being melted. Subsequently, the molten alloy was sucked through a silica tube using a syringe. Then, it was put into water to cool it rapidly.

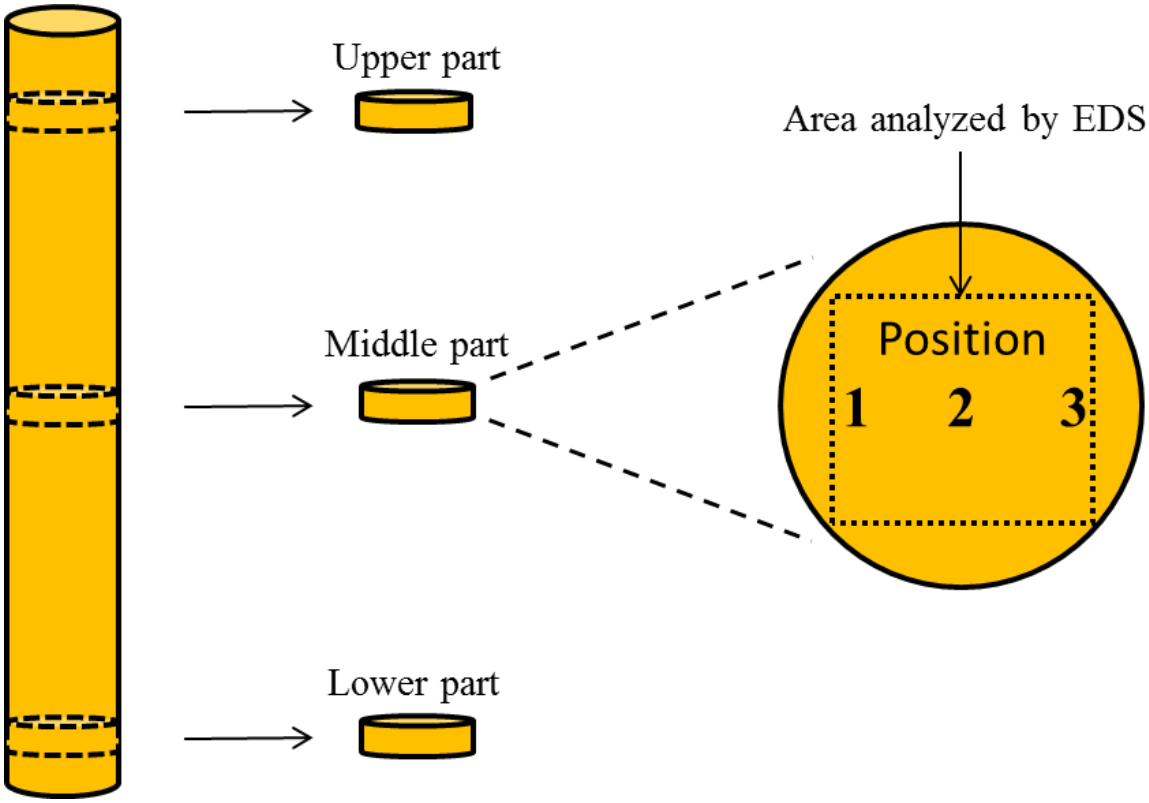

Fig. 2.2 Schematic image explanation for chemical analyzed site of solidified rod

4) Investigation of segregation

The cooled sample was rod in shape. The content of nickel in the solidified rod sample was measured with a spot analysis of an EDS energy dispersive X-ray spectroscopy (EDS-JEOL JSM-6300). Fig. 2.2 showed schematic of the solidified rod. The rod was cut into slices with 3 mm of thickness from the upper, the middle and the

lower part of the rod, as shown in Fig. 2.2. Nickel content in each part was measured in order to investigate the segregation.

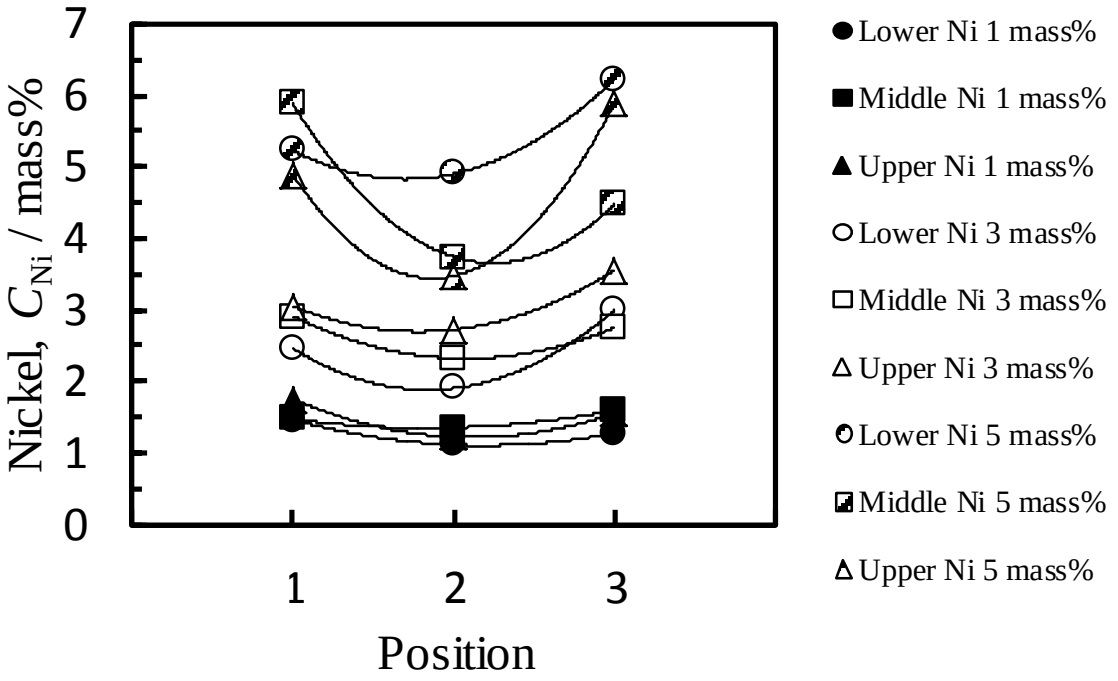

Fig. 2.3 Relation between nickel content and position. The position was shown in Fig. 2.2.

Fig. 2.3 showed the distribution of nickel content using a spot analysis by EDX. Nickel content at the center of the slice was low, and it increased slightly in the direction from the center (position 2) to the side (position 3). However, the nickel content at each radial distance from the center did not changed much with the position in the longitudinal direction of the rod-like sample. This meant that central segregation occurred in the solidified sample. Fig.2.4 showed the dependency of the nickel content measured with the area analysis on the longitudinal direction of the rod-like sample. Here, the nickel content at seven different places were measured with an area analysis of the EDX. The measured

area size was approximately 0.04 mm^2. The nickel content was evaluated with the mean of seven measured values. The maximum scattering of the nickel content was approximately ± 10% for the mean value. As shown in Fig. 2.4, the total composition of the sample cut in round slice from the rod-like sample was not influenced by the position in the longitudinal direction. Therefore, the sample for measurement of solubility of carbon was prepared in such slice.

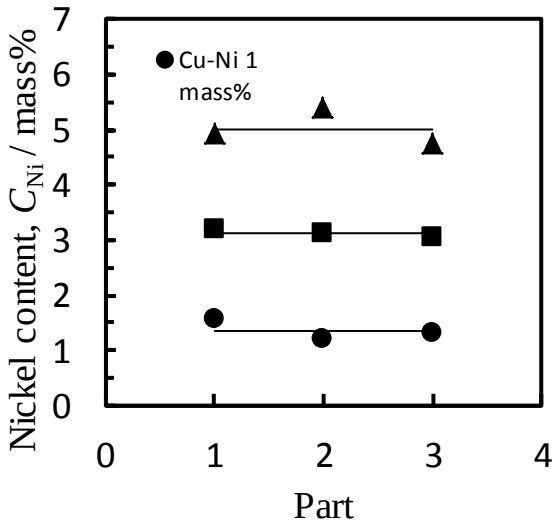

Fig. 2.4 Nickel content in each part of solidified Cu-Ni alloy. Each part was shown in Fig. 2.2.

5) Preparation of sample for measurement of solubility of carbon.

The sliced sample was approximately 1.24 g in weight. Based on the average nickel content in Fig. 2.4, the nickel contents in the sliced sample were 1.35 ± 0.10 mass%, 3.13 ± 0.11 mass% and 5.02 ± 0.10 mass% respectively. Nickel content was measured with an ICP-OES and an area analysis of EDS. The area analysis was performed at the randomly chosen ten places of a sample. Both two analytical values almost accorded in the range of scattering of the analytical values. Therefore, the value of nickel which was measured

with an EDS was mainly used.

2.2.2 Experiment for measuring saturated carbon content

1) Graphite crucible and lid

Graphite was cut from a graphite rod (purity 99.99 mass%) into a custom designed graphite crucible shown in Fig. 2.5. This figure showed the drawing of the graphite crucible including the graphite lid. The bottom of the graphite lid was designed to be as nearest to the surface of a molten Cu-Ni alloy. The small graphite crucible in which the sample was placed was concealed with the graphite lid.

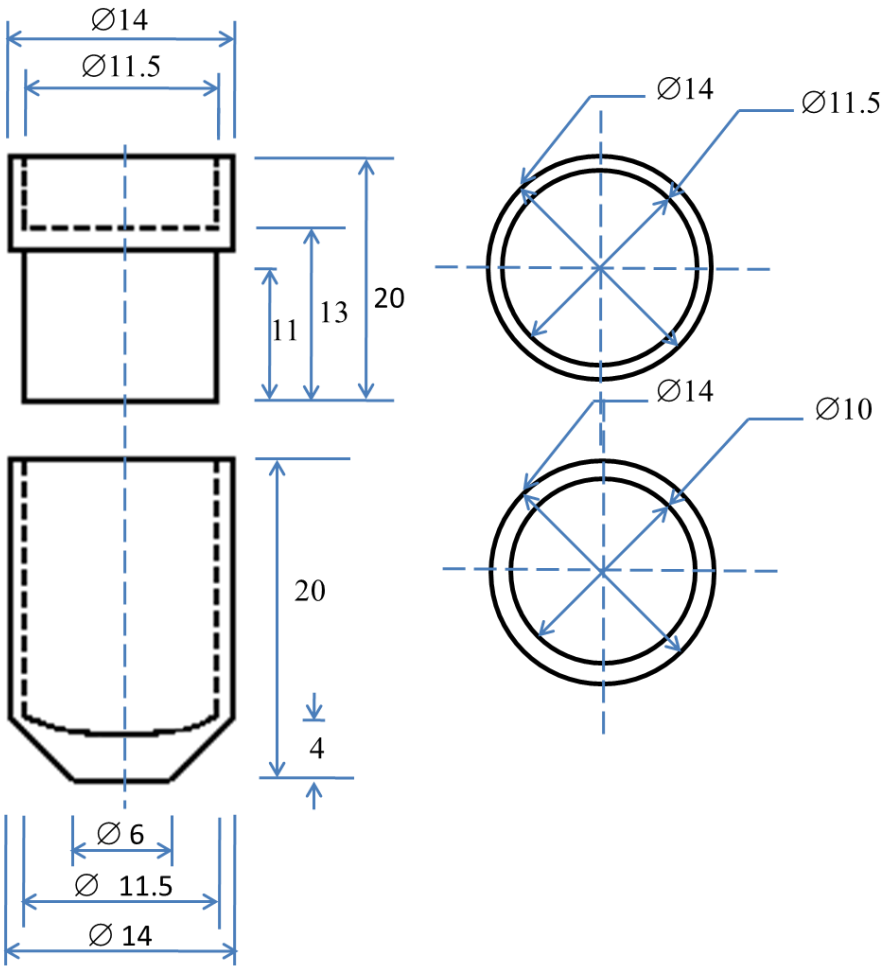

Fig. 2.5 Drawing of graphite crucible and graphite lid

2) High frequency induction furnace

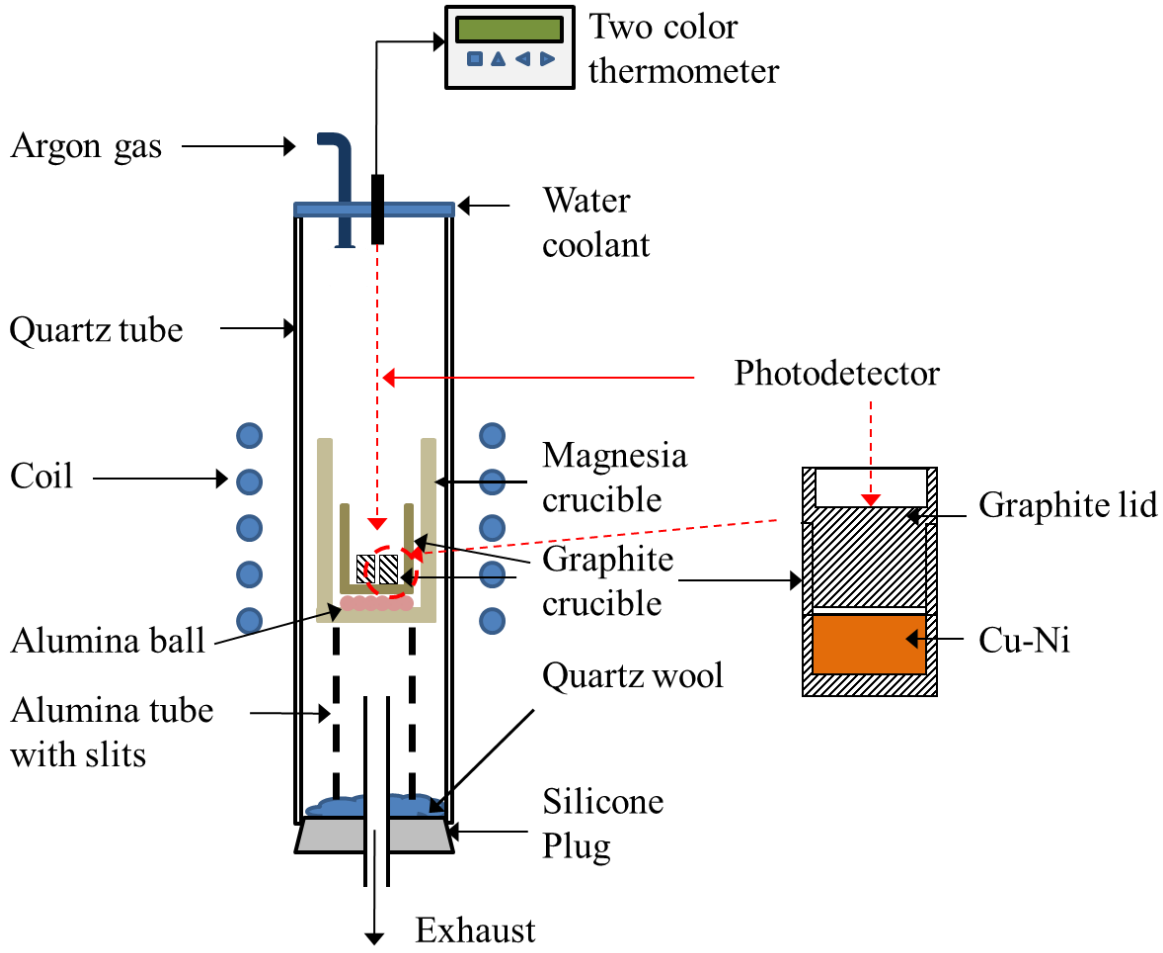

Fig. 2.6 Experimental apparatus for measurement solubility of carbon in molten Cu-Ni alloy.

Fig. 2.6 showed the experimental apparatus. A high frequency induction furnace (130 kHz, 30 kW) was used to melt the Cu-Ni alloy inside graphite crucible. The outer large graphite crucible was heated by the induction furnace. The crucible was heated by heat transfer from the outer graphite crucible. The two color thermometer (CHINO series IR-FL2AH04) which equipped with a laser pointing system was used for measurement of

the crucible temperature. The temperature at the laser pointed place could be measured with this thermometer. When the temperature of the surface of the molten metal in the crucible was measured, it was differed with the measuring spot. Then, the temperature of the graphite lid was measured, because the graphite could be estimated to be black body. The three samples were heated in one time inside the larger graphite crucible.

3) Experiment procedure

The sliced Cu-Ni alloy was placed in the graphite crucible. Subsequently, argon gas with a flow rate of $2.0 \times 10^{-5} m^3 s^{-1}$(293 K, 101.3 kPa (NTP)) was introduced into the furnace to displace the air and prevent oxidation during experiment. Then, the alloy was heated under argon gas flow. It took around one hour to heat the crucible at the desired temperature. The temperature was controlled at desired temperature with ± 10 K manually. Fig. 2.7 showed the example for time dependency of the temperature when the sample was heated to the temperature of 2143 K. Usually, it took 15 minutes that the temperature for all specimens increased to 1300 K. the time when the temperature arrived at the desired temperature was choose to the starting point. After keeping the temperature of the crucible constant for 0.5, 1.0 or 2.0 hours, the alloy was cooled in the furnace.

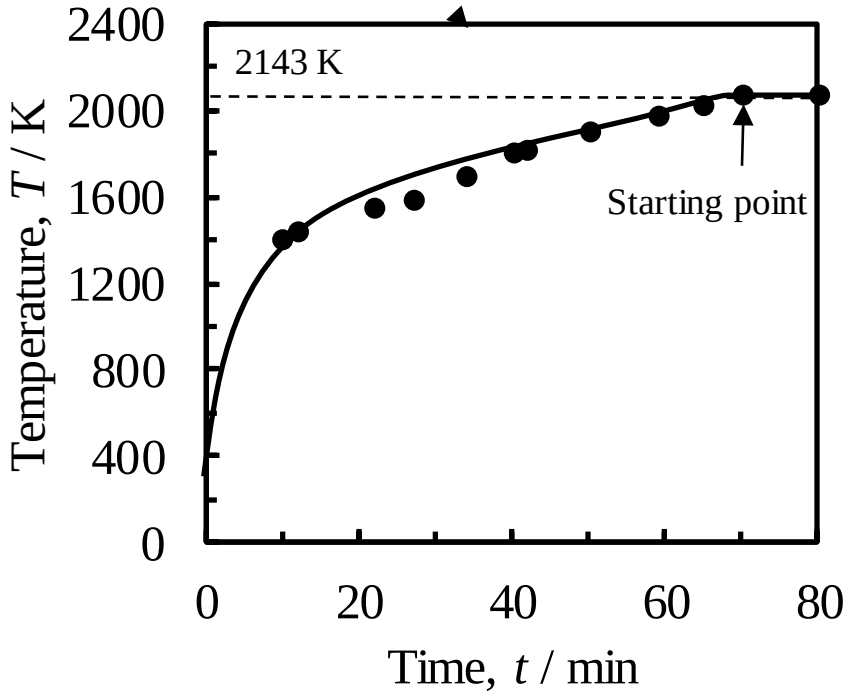

Fig. 2.7 Example of change in temperature with time.

4) After melting process

Fig. 2.8 showed an example of the samples Cu-Ni 5.02 mass% which were heated for 1 hour at the temperature of 2073 K. The lower side, which contacted with graphite crucible, adhered to graphite. Some alloys did not adhere to the crucible, but other alloys adhered strongly to the graphite crucible. This strong adhesion was observed for the sample whose nickel content was around 1.35 mass%, 3.13 mass % and 5.02 mass% which were prepared over the temperature of 1973 K, 2073 K and 2143 K respectively. The shape of the sample changed from a disk shape to a button shape after heated. Sample interface which contacted the graphite crucible was ground with emery paper carefully to eliminate the fragment of the graphite crucible. Then the sample was cleaned using ultrasonic bath.

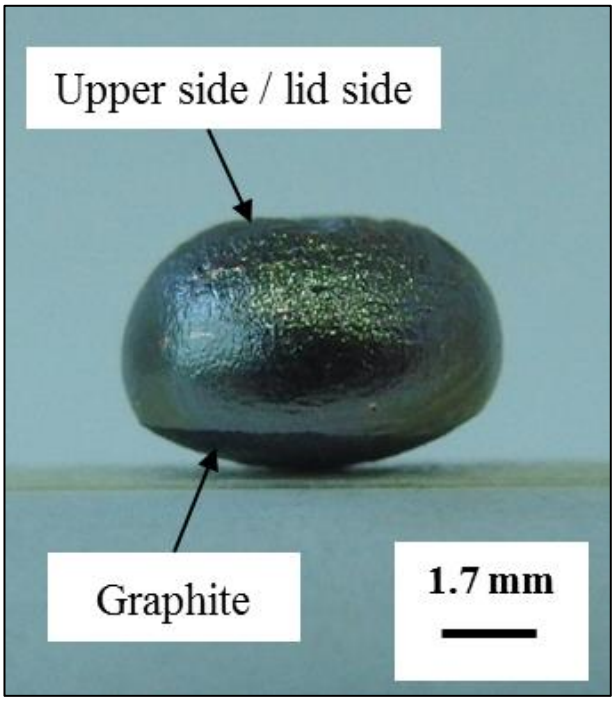

Fig. 2.8 Shape of alloy in which nickel content was 5.02 mass% after heated for 1 hour at 2073 K.

5) Measurement of content and Vickers hardness, and observation

5-1) Carbon/sulfur content

Carbon content was very important to study the solubility of carbon in molten Cu-Ni alloy. Combustion–infrared absorbing method (HORIBA, EMIA-EF-510) was used to measure the carbon content. This analyzer could measure sulfur content as well as carbon content simultaneously. As described later, graphite particles which were precipitated from carbon saturated molten alloy under cooling were unevenly distributed in samples. Then, the sample was cut into two parts by a wire cutter. The carbon content was determined by the analysis of both two parts. The principle of this combustion method was as follows: First, a sample was burned in an oxygen gas stream. Then CO_2 and SO_2 were formed as a result of the combustion. They were analyzed with infrared

detectors.

5-2) Observation of surface and cross-section.

The samples for observation and analysis of nickel composition were also prepared in the same way as the samples for analysis of carbon and sulfur contents. The sample was cut along the center axes of the samples for observation of the cross section. The sample was put in liquid resin, and was held for a day to harden the resin. The sample was polished by an emery papers, abrasive of alumina and colloidal silica in this order, and was observed by a laser microscope (Keyence VK8500) and a SEM (scanning electron microscope) (JEOL JSM-6300) equipped with an EDS. For SEM observation, the samples were coated with platinum of around 20 nm in thickness. It was important to coat the sample with platinum, otherwise the sample will be charged up.

5-3) Vickers hardness

Micro hardness tester (Shimadzu HMV Micro Hardness Tester) was used to investigate the Vickers hardness of the alloy. Vickers hardness of the alloy was measured with the test force of 980 mN and holding time of 10 s.

Specimens which were prepared at 1673 K, 1873 K and 2073 K were heat-treated at the temperature of 973 K for 2 hours. The hardness of the annealed sample was also measured. The hardness was measured for the lower, center and upper part of the specimen. The hardness was measured for 7 different locations of each part. The highest and lowest measured hardness were eliminated, and the average of the remaining 5 points was used as actual hardness. The scattering of the measured hardness was ± 50 MPa.

2.3 Results and discussion

2.3.1 Solubility of carbon in Cu-Ni alloy

1) Saturated carbon content

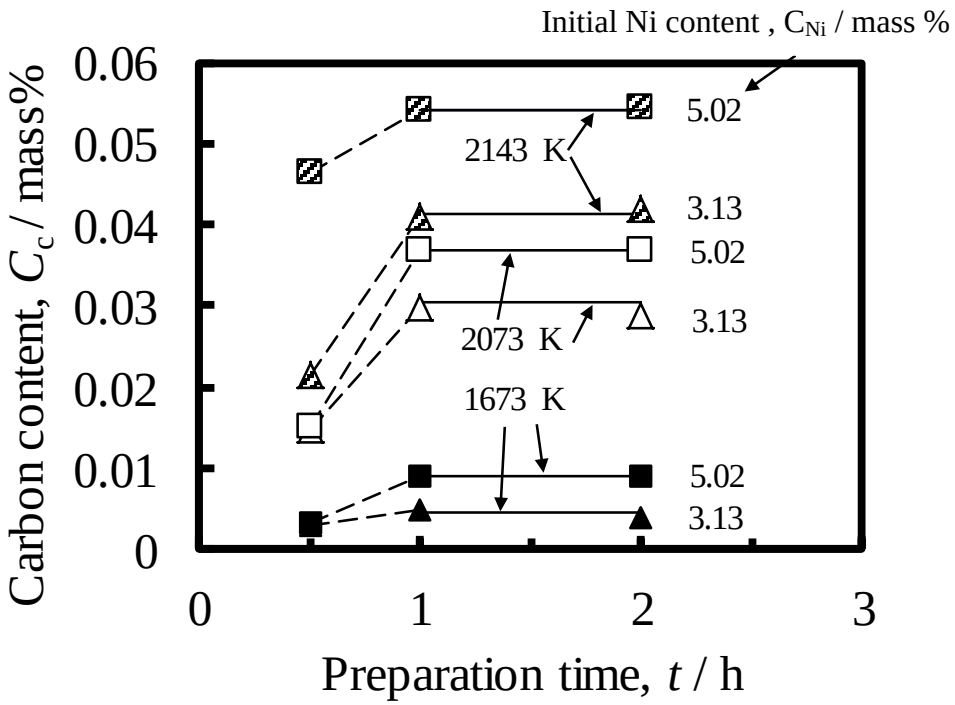

Fig. 2.9 Example of change in carbon content in molten Cu-Ni alloy with time.

Change of carbon content with holding time was investigated to measure the time needed for carbon to be completely saturated in molten Cu-Ni alloy. Fig. 2.9 showed an example of change in carbon content in molten Cu-Ni alloy with time. The carbon content in the molten Cu-Ni alloy became constant one hour later from keeping the temperature at desired temperature, irrespective to nickel content and temperature. In addition, as described later, any reaction product and any nickel rich phase except graphite were not observed and detected at the interface between molten alloy and graphite crucible. Therefore, the carbon was saturated and equilibrated with graphite.

Fig. 2.10 showed the example of change in sulfur content with time. The sulfur

contents in the alloys were below approximately 0.005 mass% (50 mass ppm) were almost constant irrespective to time.

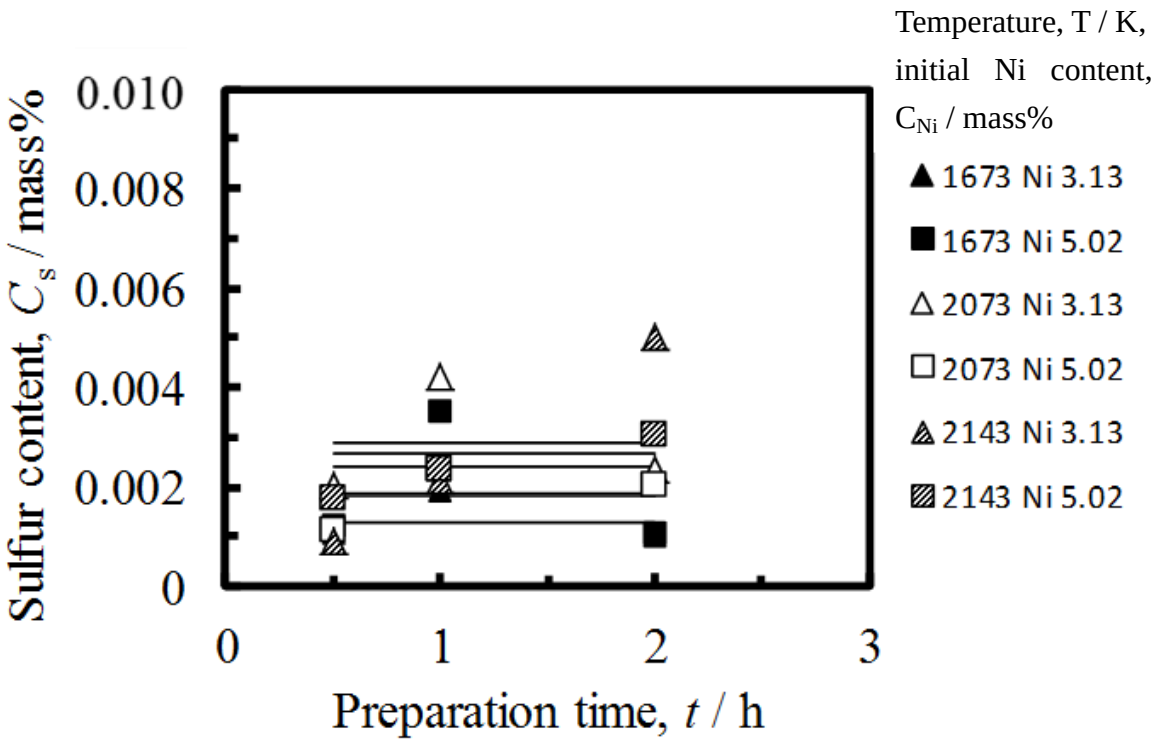

Fig. 2.10 Example of change in sulfur content with time.

The carbon content was plotted on a phase diagram, as shown in Fig. 2.11. The solubility of carbon in pure copper was also shown in Fig. 2.11. The saturated carbon content for each nickel content in the molten alloy increased with an increase in the temperature. In addition, the saturated carbon content for each temperature increased with an increase in nickel content. Anderson and Bever [10] studied the carbon solubility of molten Cu-Ni alloy with the nickel content up 90.672 mass% at 1748 K. Their solubility was also shown in Fig. 2.11. The relation between the saturated carbon content and the nickel content which was predicted from this work agreed well to their work.

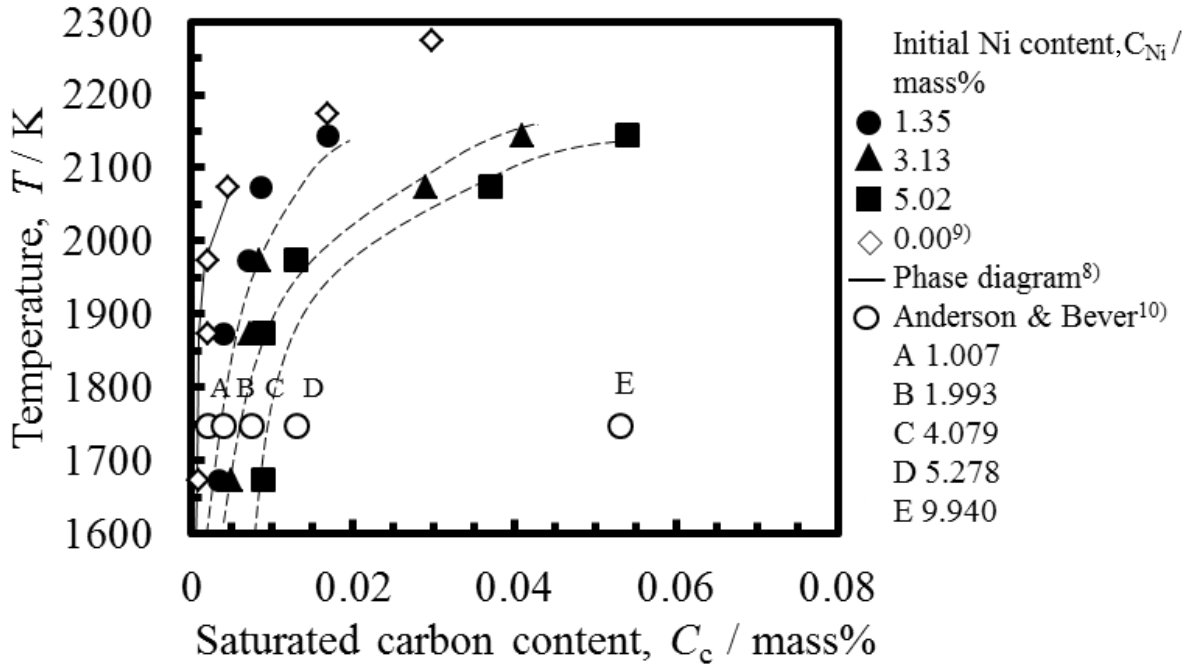

Fig. 2.11 Example of change in carbon content in molten Cu-Ni alloy with temperature and nickel content.

It was convenient to express the solubility as a function of thermodynamic temperature, T [K]. The solubility could be expressed by the following expression:

Nickel content, C_{Ni} : 1.54 mass% ~ 1.69 mass%

$$\ln[\text{mass\%C}] = 2.6878 \times 10^{-9}T^3 - 1.2885 \times 10^{-5}T^2 + 0.0245T - 23.728 \quad (2\text{-}1)$$

C_{Ni} : 3.51 mass% ~ 3.72 mass%

$$\ln[\text{mass\%C}] = -1.1636 \times 10^{-8}T^3 + 7.0623 \times 10^{-5}T^2 - 0.1371T + 80.6944 \quad (2\text{-}2)$$

C_{Ni} : 5.18 mass% ~ 5.39 mass%

$$\ln[\text{mass\%C}] = 9.4479 \times 10^{-9}T^3 - 4.5006 \times 10^{-5}T^2 + 0.0724T - 44.2706 \quad (2\text{-}3)$$

C_{Ni} : 0.00 mass% [9]

$$\ln[\text{mass\%C}] = 4.4683 \times 10^{-9}T^3 - 1.7962 \times 10^{-5}T^2 + 0.0242T - 18.104 \quad (2\text{-}4)$$

Solubility values calculated using the above expression was shown in Fig. 2.11. The values calculated using Eqs. (2-1)-(2-3) and Eq. (2-4) agreed well to the experimentally obtained values.

2) Activity coefficient of carbon

Activity of carbon, a_c, which based on pure substance as standard state could be expressed with using activity coefficient of carbon, γ_c, and molar fraction of carbon, x_c, as:

$$a_c = \gamma_c x_c \quad (2\text{-}5)$$

Because the molten Cu-Ni alloy was equilibrated with graphite, the carbon activity was equal to one. Therefore, the activity coefficient of carbon could be calculated from the following equation:

$$\gamma_c = 1/x_c \quad (2\text{-}6)$$

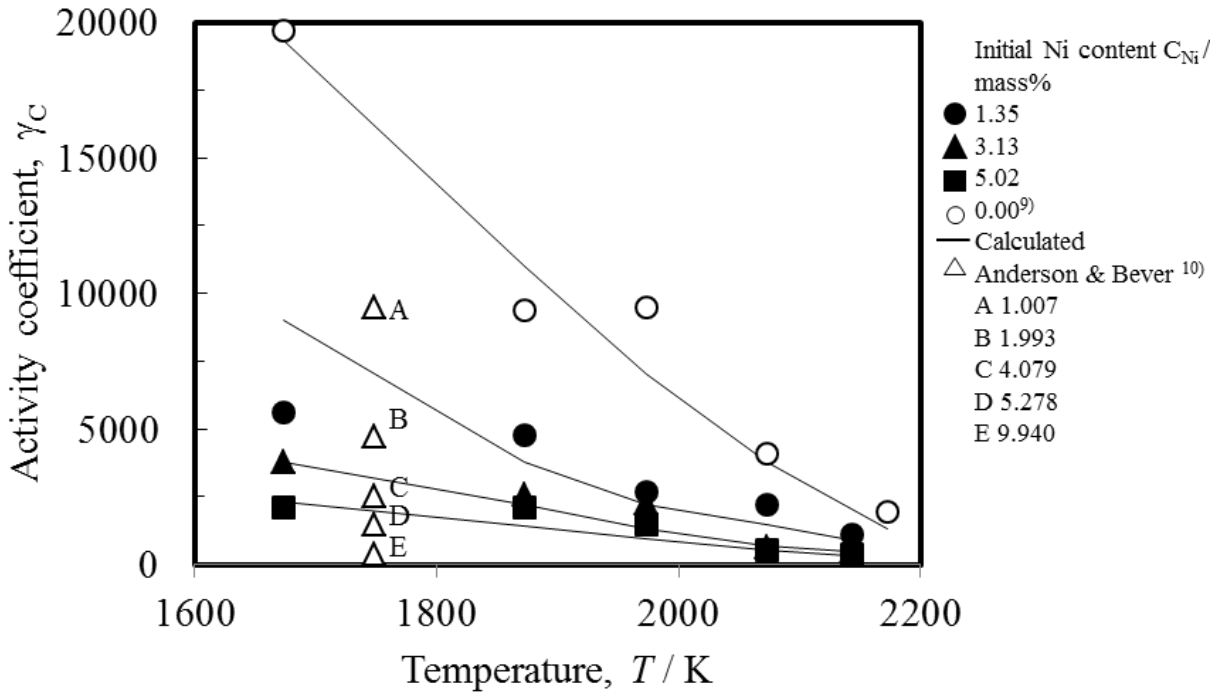

Fig. 2.12 Relation between activity coefficient of carbon and temperature.

The activity coefficient was calculated from eq. (2-6). Fig. 2.12 showed the relation between the activity coefficient of carbon and the temperature. The activity coefficient decreased with the temperature rise, and with an increase in the nickel content. In this figure, the data given by Anderson & Bever [10] were also shown. It was shown that their activity coefficients, agreed qualitatively with the data given by this work. The curved lines were obtained from eqs. (2-1) ~ (2-4) and eq. (2-6). The calculated lines fitted well the experimental values.

Interaction parameter, ω_C^{Ni}, of Cu-Ni-C_{sat} system could be given as:

$$\omega_C^{Ni} = \partial \ln \gamma_C / \partial x_{Ni} \tag{2-7}$$

Fig. 2.13 showed the relation between natural logarithm of the activity coefficient of carbon and molar fraction of nickel. The solid lines were given by the regression

analysis. There was the good linear relation between them for each temperature. The data by Anderson and Bever [10] were also shown as a dotted line in this figure. There was also good linear relation between them. These linear relations indicated adaptability of eq. (2-7). The gradient of each line gave the interaction parameter, ω_C^{Ni} according to eq. (2-7). The interaction parameters were listed in Table 2.2. The interaction parameters obtained in this work were larger than the parameter given by Anderson and Bever [10]. There was no clear dependency of the interaction parameter on the temperature. Then, the interaction parameter was determined by averaging the experimentally obtained interaction parameters. The averaged interaction parameter was -17.1, as listed in Table 2.2. The broken lines in Fig. 2.13 were drawn by using the averaged interaction parameter. These broken lines could also express the data.

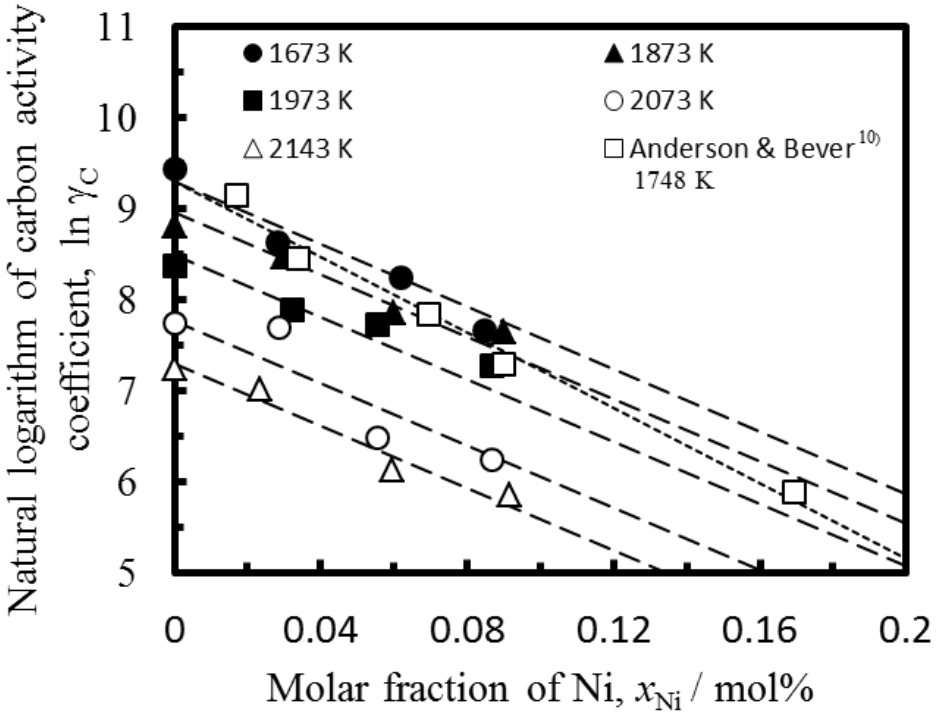

Fig. 2.13 Relation between natural logarithm of carbon activity coefficient and nickel molar fraction. Broken line was a calculated line with using the average interaction parameter, ω_C^{Ni}, which is listed in Table 2.3.

As listed in Table 2.2, the nickel content in the sample after experiment was larger than that before experiment. This originated from that the vapor pressure of pure copper was approximately 20 times larger than that of pure nickel [12]. Furthermore, in consideration of activity of nickel in cu-Ni alloy, the vapor pressure of copper in the alloy was around 400 times larger than that of nickel.

Table 2.2 Nickel and carbon contents before and after experiment (two hours later), activity coefficient γ_C and interaction parameter ω_C^{Ni}.

Temp. T / K	Ni content, C_{Ni} / mass%		Carbon content after experiment, C_C / mass%	γ_C	ω_C^{Ni}
	Before	After			
1673 K	1.35	1.66	3.38×10^{-3}	5.60×10^{3}	-19.7
1673 K	3.13	3.64	5.00×10^{-3}	3.79×10^{3}	
1673 K	5.02	5.18	8.93×10^{-3}	2.10×10^{3}	
1873 K	1.35	1.76	3.98×10^{-3}	4.76×10^{3}	-13.7
1873 K	3.13	3.51	7.33×10^{-3}	2.59×10^{3}	
1873 K	5.02	5.28	9.07×10^{-3}	2.10×10^{3}	
1973 K	1.35	1.54	7.07×10^{-3}	2.68×10^{3}	-12.3
1973 K	3.13	3.72	8.33×10^{-3}	2.28×10^{3}	
1973 K	5.02	5.39	1.31×10^{-2}	1.45×10^{3}	
2073 K	1.35	1.69	8.54×10^{-3}	2.22×10^{3}	-19.9
2073 K	3.13	3.25	2.89×10^{-2}	0.66×10^{3}	
2073 K	5.02	5.09	3.70×10^{-2}	0.51×10^{3}	
2143 K	1.35	1.37	1.68×10^{-2}	1.13×10^{3}	-16.4
2143 K	3.13	3.49	4.09×10^{-2}	0.46×10^{3}	
2143 K	5.02	5.37	5.41×10^{-2}	0.35×10^{3}	
Interaction parameter, $\omega_{C\ average}^{Ni}$					-17.1
1748 K[10)]	1.01	-	2.00×10^{-3}	9.46×10^{3}	-20.7
1748 K[10)]	1.99	-	4.00×10^{-3}	4.73×10^{3}	
1748 K[10)]	4.08	-	7.50×10^{-3}	2.53×10^{3}	
1748 K[10)]	5.28	-	1.30×10^{-2}	1.46×10^{3}	
1748 K[10)]	9.94	-	5.30×10^{-2}	0.36×10^{3}	

2.3.2 Observation of alloy

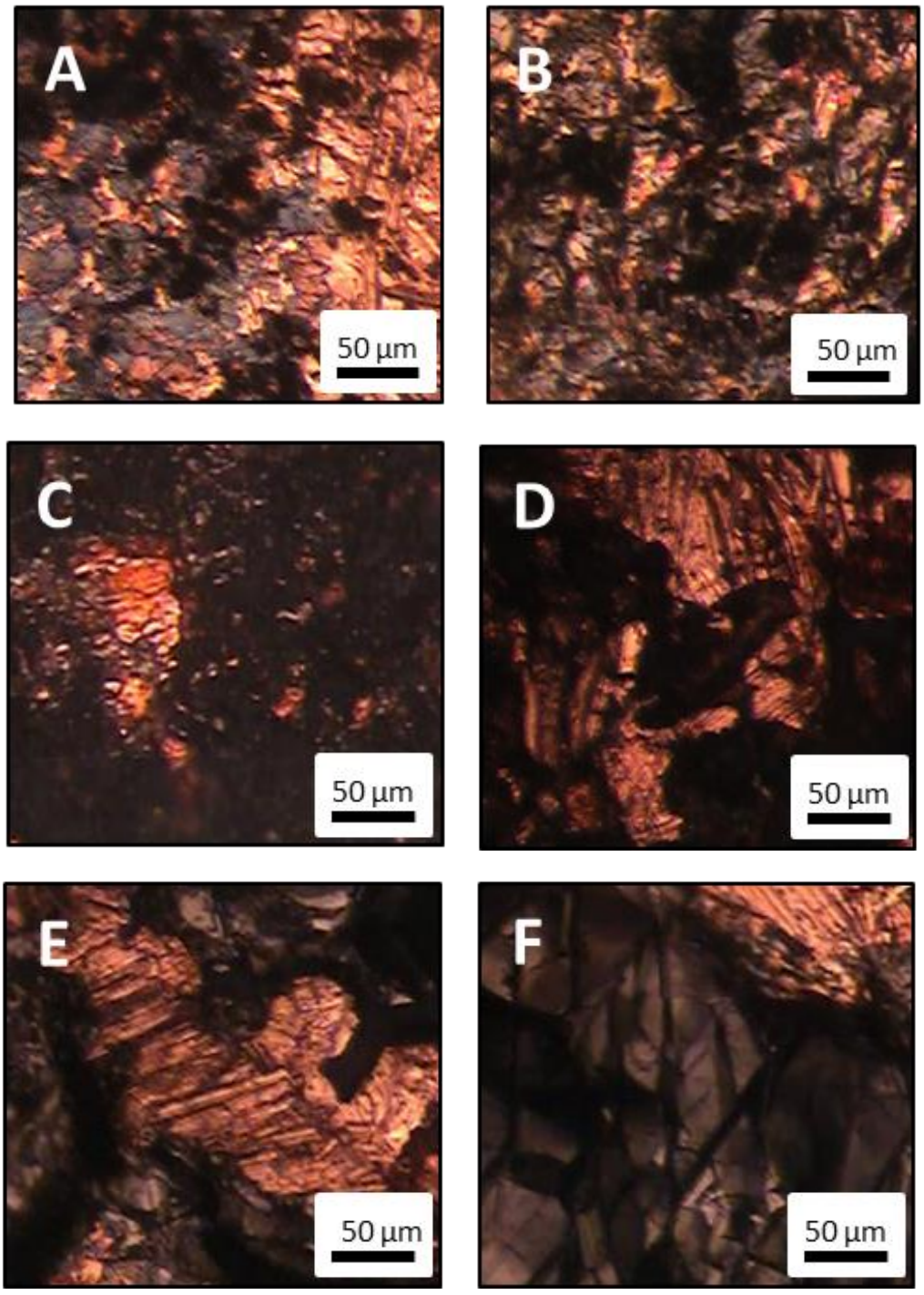

Fig. 2.14 Surface of the Cu-Ni alloys after holding 2 hours at temperature of 1773 K and 2073 K. A: Cu-Ni 1.35 mass%, 1773 K, B: Cu-Ni 3.03 mass%, 1773 K, C: Cu-Ni 5.02 mass%, 1773 K, D: Cu-Ni 1.35 mass%, 2073 K, E: Cu-Ni 3.13 mass%, 2073 K, F: Cu-Ni 5.02 mass% 2073 K.

The surface and cross section of the alloy after the experiment was observed using both a SEM and a laser microscope. Fig. 2.14 showed example of the surface for composites prepared at 1773 K and 2073 K observed with using the laser microscope. The sample was cleaned with a blower before the observation. From the figures each surface was covered partly with a substance in blackish color. Blackish parts were graphite particles precipitates from the carbon saturated molten alloy. The other parts were metallic alloy.

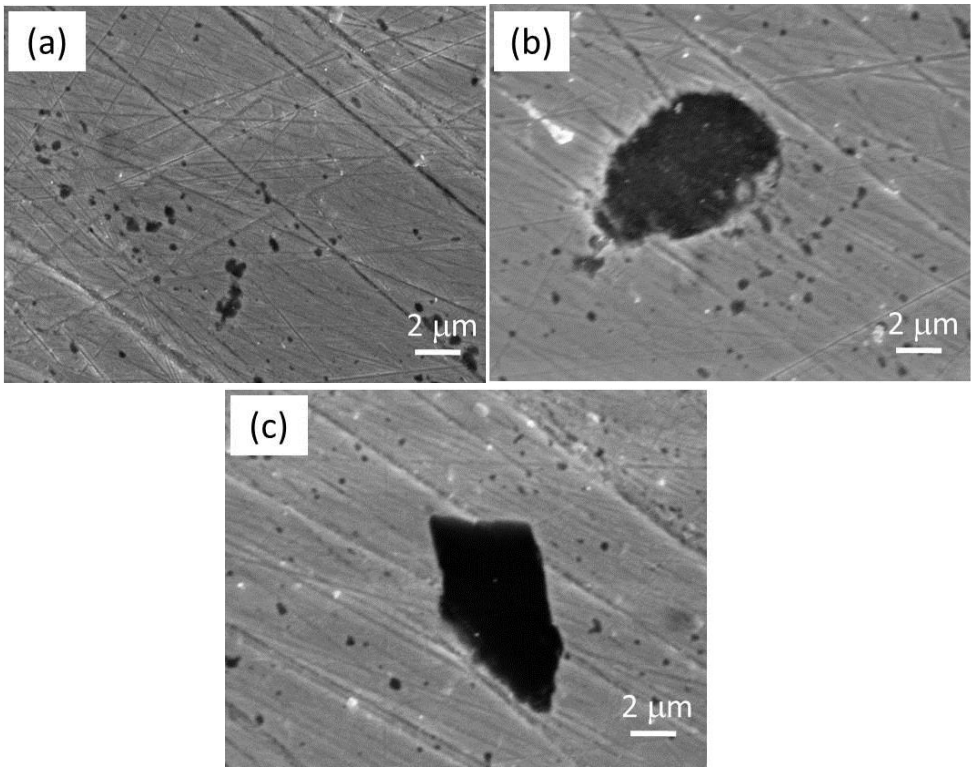

Fig. 2.15 Graphite particles around center of solidified Cu-Ni alloy with initial nickel content of 5.02 mass%. The alloy was fused at 2073 K for two hours.

The morphologies and sizes of the precipitated graphite inside the sample were observed using SEM. Fig. 2.15 showed the cross-section of the upper part of the samples

heated at 2073 K for 2 hours. Fig. 2.15 (a), (b) and (c) represented the cross-section of Ni content of 1.35 mass%, Ni content of 3.03 mass% and Ni content of mass% 5.02 respectively. Small black particles could be observed on the cross-section of the alloys. The black particles were analyzed with the spot analysis of the EDS. As a result, the elements except carbon could hardly be detected. Therefore, these particles were identified to be graphite. The number of the graphite particles increased with the nickel content. These graphite particles distributed in these samples were 0.5 μm to 3 μm in size.

The lower part of the cross section of the alloy was investigated to study the reaction of graphite crucible with the Cu-Ni alloy during melting and cooling. This part always touched the graphite crucible. Figs. 2.16 (a), (b) and (c) represented the cross sections of the lower parts of the alloys with the nickel content of 1.35 mass%, 3.03 mass% and 5.02 mass% respectively. As shown in Fig. 2.16 (a), the graphite crucible hardly adhered to the alloy at the interface between the alloy and the graphite crucible. As shown in Figs. 2.16 (b) and (c), graphite crucible adhered to the interface of the alloy. Therefore, the amount of the adhered graphite increased with an increase in the nickel content. In addition, the shape of the interface changed from a relatively smooth shape to a concave-convex shape. This indicated that dissolution of the graphite crucible did not proceeded on a parallel to the surface of the crucible microscopically.

As shown in Figs. 2.16 (a), (b) and (c), the number of the graphite particles which was shown as black particles in Fig. 2.16 increased with the increase in the nickel content. This thing correspond the dependency of the carbon solubility on the nickel content. Generally, under solidification of the small cooling rate, it was easy that the solute was precipitated in the final solidification place. The temperature dependency of the saturated carbon content of Cu-Ni-C was very large. Even if decline of the temperature was small,

graphite particles were easy to precipitate from the melt. Therefore, graphite particles precipitated at the bottom of the molten alloy.

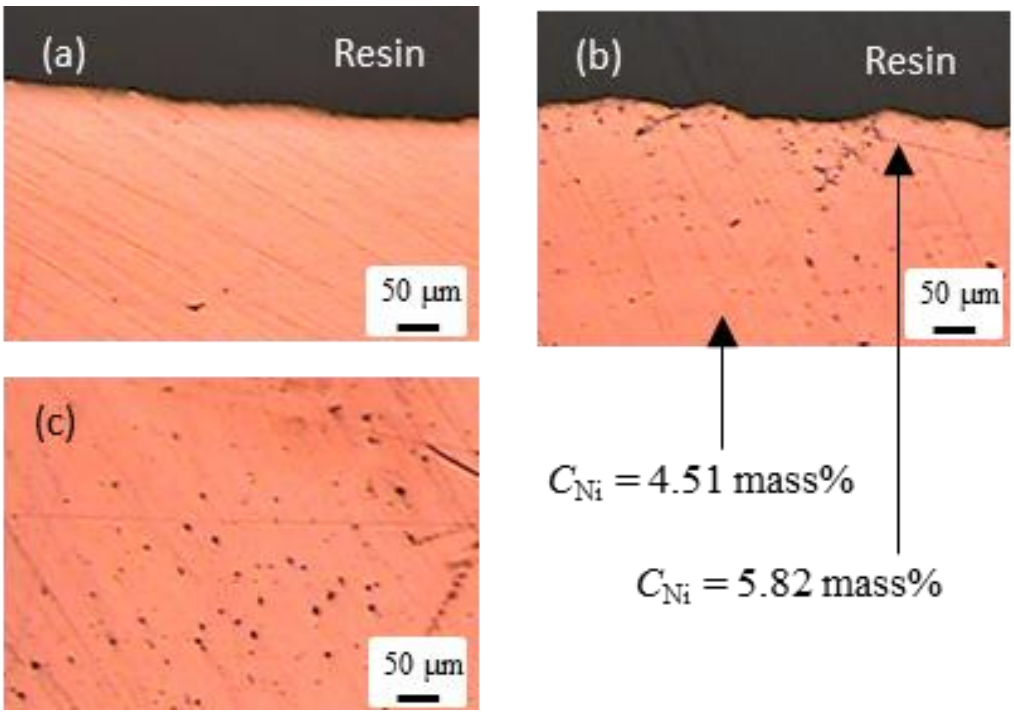

Fig. 2.16 Distribution of graphite particles in carbon saturated Cu-Ni alloy which included initial nickel content of 5.02 mass%. Upper part of the alloy was prepared at 1673 K (a) and 2073 K (b). Center part of the alloy was prepared at 2073 K (c).

The precipitated particles in the solidified Cu-Ni-C_{sat} alloy were shown in Fig. 2.17. In this figure, the particles were classified into the relatively large particles, which were approximately 5 μm and more in size, and the relatively small particles with approximately 0.5 μm in size. Many of the large graphite particles were observed on the alloys which were prepared at a higher temperature, and/or which included high nickel content. These things indicated that the alloys contained the higher dissolved carbon content. In addition, these particles had a variety of shapes, they were more or less

angular in shape.

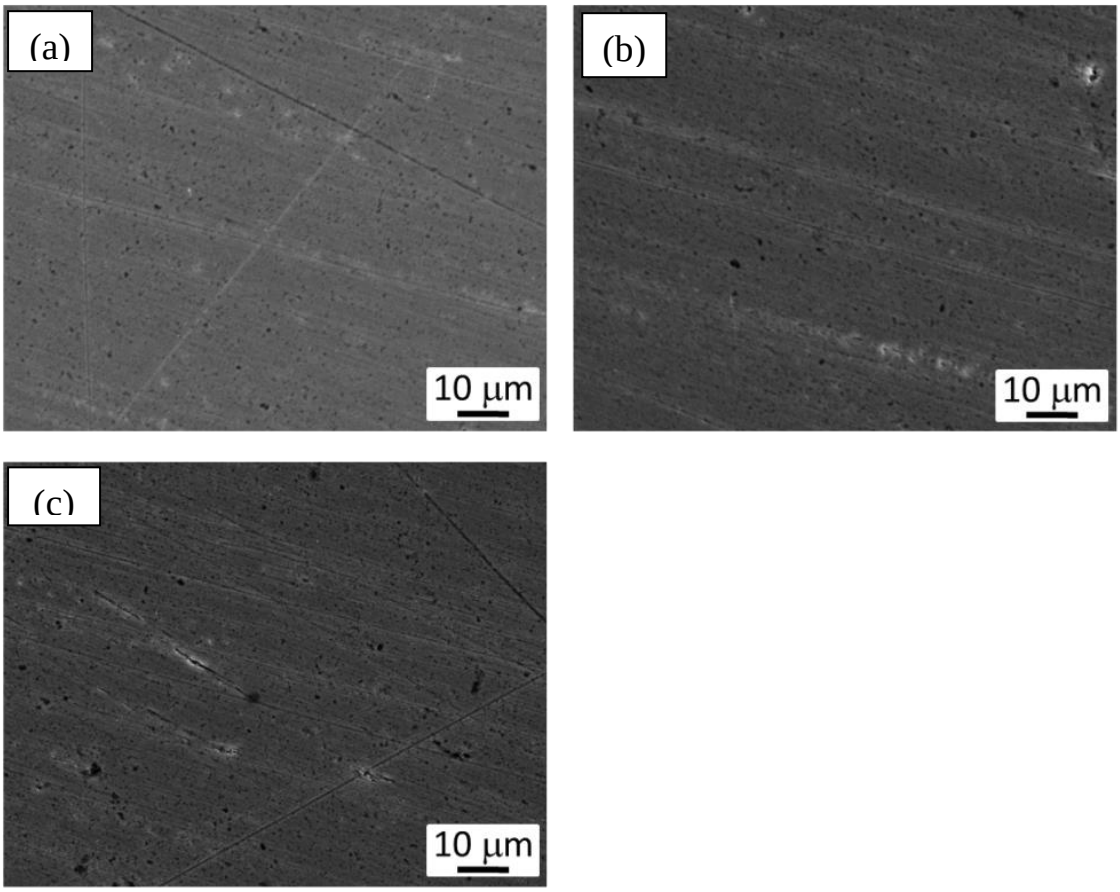

Fig. 2.17 Cross-section of Cu-Ni alloy at center area heated for 2 hours. (a) Cu-Ni 1.35 mass%, 2073 K, (b) Cu-Ni 3.13 mass% , 2073 K and (c) Cu-Ni 5.02 mass%, 2073 K.

Fig. 2.18 showed the distribution of graphite particles. In comparison between Fig. 2.18 (a) and Fig. 2.18 (b), as shown in Fig. 2.18 (b), many graphite particles were observed in the sample which was prepared at higher the temperature, which meant that the saturated carbon content in the sample was higher. The particles were in every place of the whole sample, as shown in Fig. 2.18 (b) and Fig. 2.18 (c). However, the particles did not exist uniformly, but existed unevenly, that is, many graphite particles were at some place and a few particles were at other place in the sample. The large particles with the size of 5 μm or more could be observed in Fig. 2.18. As shown in Fig. 2.18 (b), the

nickel content in the metallic phase near the graphite particle was larger than that apart from the graphite particle. Fig. 2.19 showed the binary phase diagram of Cu-Ni [13]. Cu-Ni alloy system was an all proportional solid solution. When the liquid marked (a), was cooled, Ni rich phase was precipitated as a primary crystal. When the sample was further cooled, and existed in the region of a liquid and solid Ni content in the liquid phase was smaller than that before solidification. Because the saturated carbon content decreased with the decrease in the nickel content, graphite could be easily precipitated near the nickel rich phase.

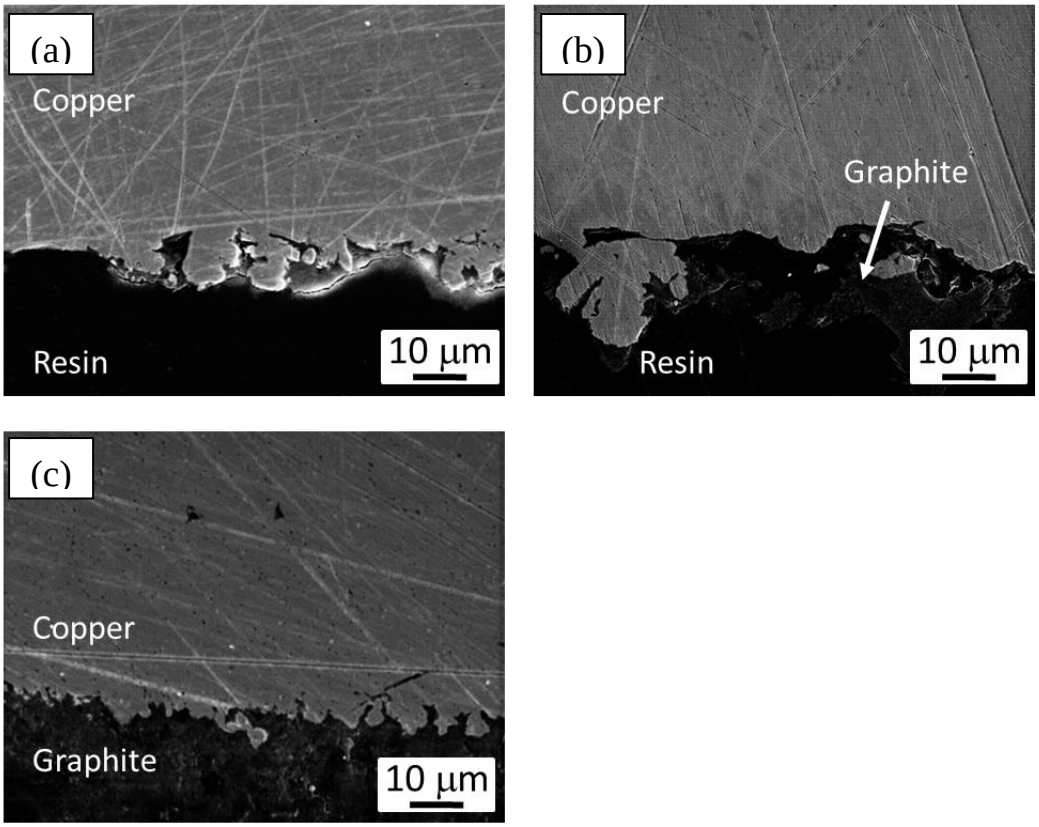

Fig. 2.18 Cross-section of Cu-Ni alloy at lower area heated for 2 hours. (a) Cu-Ni 1.35 2073 K, (b) Cu-Ni 3.13 2073 K and (c) Cu-Ni 5.02 2073 K.

The upper part of the sample was considered to be the final solidification site.

Because the relatively small particles were not observed at the upper part, the relatively large particles precipitated from the liquid. Namely, because carbon dissolved in liquid could diffuse more easily than that in solid, the particles grew more and became large. In contrast to the large particles, the small graphite particles precipitated from the solid. Therefore, the small graphite particles did not grow due to the slow diffusion in a solid phase. The carbon distribution between a solid phase and a liquid phase was unknown. In addition, the carbon diffusivities of a solid and a liquid phase had not been studied. Therefore, the distribution ration and the diffusivity were necessary for more quantitative consideration to the precipitation and growth of the graphite particles.

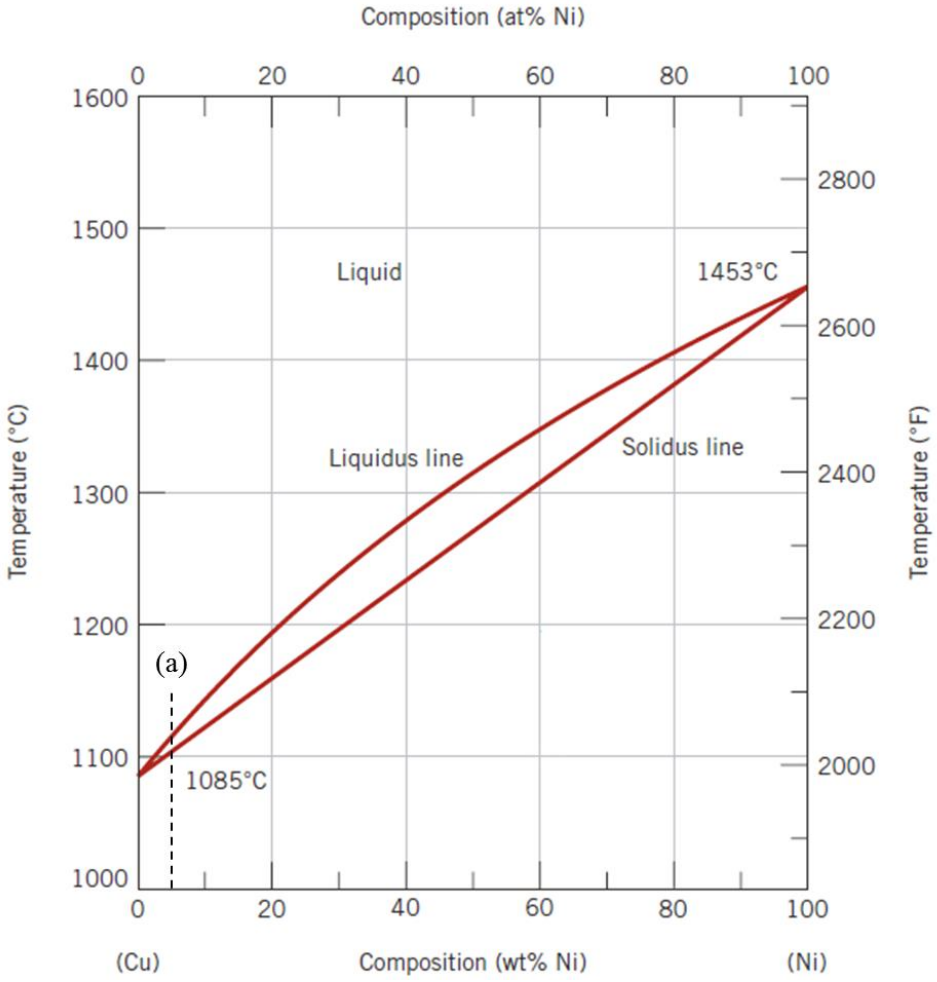

Fig. 2.19 Binary phase diagram of Cu-Ni system. [13]

2.3.3 Vickers hardness.

The Vickers hardness was mainly measured for the annealed samples which were prepared at the temperatures of 1673 K, 1873 K and 2073 K. Table 2.3 and Table 2.4 showed the data for Vickers hardness before and after heat treatment. Fig. 2.20 and Fig. 2.21 showed the relations between the Vickers hardness and fused temperature. As shown in Fig. 2.20, the hardness before heat treatment did not clearly relate with the temperature. However, the hardness after the heat treatment increased linearly with the temperature and nickel content, as showed in Fig. 2.21. Generally, the hardness after heat treatment was smaller than that before heat treatment, as listed in Table 2.3 and Table 2.4 or as shown in Fig. 2.20 and Fig. 2.21. This indicated that as casted copper alloy before heat treatment included dissolved carbon. The as casted alloy was strengthened by the solution hardening of carbon.

Table 2.3 Vickers hardness of each sample part before heat treatment.

T / K	Ni, C_{Ni} /	Position	Vickers hardness, *Hv* / MPa	Vickers hardness, *Hv* / MPa
1673	1.35	Lower	699.2	695.3
1673	3.13	Center	643.3	
1673	5.02	Upper	743.4	
1673	1.35	Lower	540.4	525.7
1673	3.13	Center	536.4	
1673	5.02	Upper	501.1	
1673	1.35	Lower	803.2	674.7
1673	3.13	Center	625.7	
1673	5.02	Upper	594.3	
1873	1.35	Lower	749.3	627.6
1873	3.13	Center	590.4	
1873	5.02	Upper	543.3	
1873	1.35	Lower	522.7	536.4
1873	3.13	Center	543.3	
1873	5.02	Upper	544.3	
1873	1.35	Lower	583.5	573.7
1873	3.13	Center	602.1	
1873	5.02	Upper	534.5	
2073	1.35	Lower	645.3	640.4
2073	3.13	Center	632.6	
2073	5.02	Upper	645.3	
2073	1.35	Lower	564.9	572.7
2073	3.13	Center	585.5	
2073	5.02	Upper	565.9	
2073	1.35	Lower	556.1	560.0
2073	3.13	Center	582.5	
2073	5.02	Upper	542.3	

Table 2.4 Vickers hardness of each sample part after heat treatment.

T / K	Ni C_{Ni} / mass%	Position	Vickers hardness, *Hv* / MPa	Vickers hardness, *Hv* / MPa
1673	1.35	Lower	562.9	520.8
1673	1.35	Center	509.0	
1673	1.35	Upper	492.3	
1673	3.13	Lower	479.6	545.3
1673	3.13	Center	614.9	
1673	3.13	Upper	540.4	
1673	5.02	Lower	551.2	556.1
1673	5.02	Center	581.6	
1673	5.02	Upper	535.5	
1873	1.35	Lower	513.9	542.3
1873	1.35	Center	561.9	
1873	1.35	Upper	552.1	
1873	3.13	Lower	564.9	565.9
1873	3.13	Center	558.0	
1873	3.13	Upper	574.7	
1873	5.02	Lower	596.3	625.7
1873	5.02	Center	619.8	
1873	5.02	Upper	660.0	
2073	1.35	Lower	647.3	593.3
2073	1.35	Center	586.5	
2073	1.35	Upper	547.2	
2073	3.13	Lower	593.3	591.4
2073	3.13	Center	599.2	
2073	3.13	Upper	581.6	
2073	5.02	Lower	664.9	654.1
2073	5.02	Center	607.1	
2073	5.02	Upper	690.4	

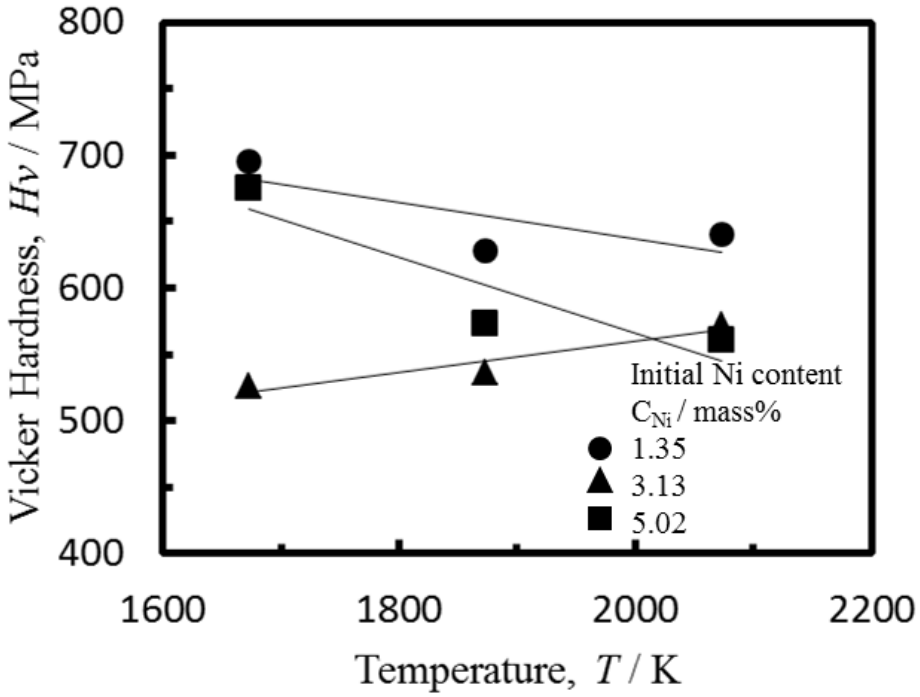

Fig. 2.20 Relation between Vickers hardness before heat treatment and preparation temperature of alloy.

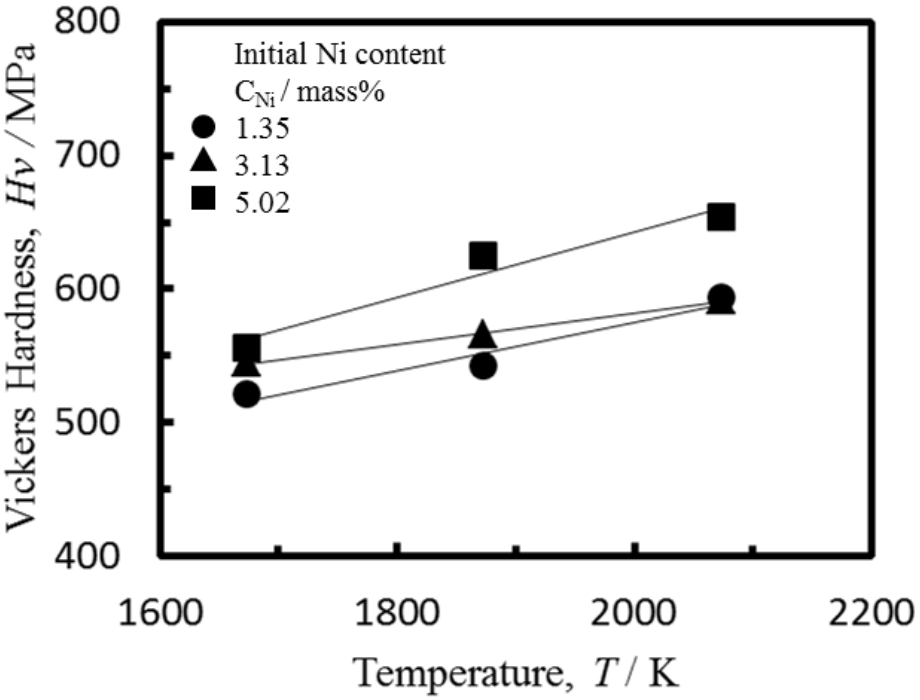

Fig. 2.21 Relation between Vickers hardness after heat treatment and preparation temperature of alloy.

Table 2.5 showed the data of carbon content and their Vickers hardness in each sample, and Fig. 2.22 showed the relation between the Vickers hardness and the saturated carbon content. The Vickers hardness increased linearly with the increase in the saturated carbon content. The phase diagram of Cu-C system indicated that carbon could not dissolve into solid copper. In addition, judging from the carbon solubility in the molten Cu-Ni-C_{sat} in this work, carbon did not dissolve into solid Cu-Ni system. Therefore, this increase in the Vickers hardness with the saturated carbon content did not resulted from dissolved carbon but from the precipitated graphite particles. The hardness also increased with the increase in the nickel content, as shown in Fig. 2.22. Consequently, carbon saturated Cu-Ni alloy which was prepared in this work was hardened by precipitation hardening of the graphite particles and solid-solution hardening of nickel.

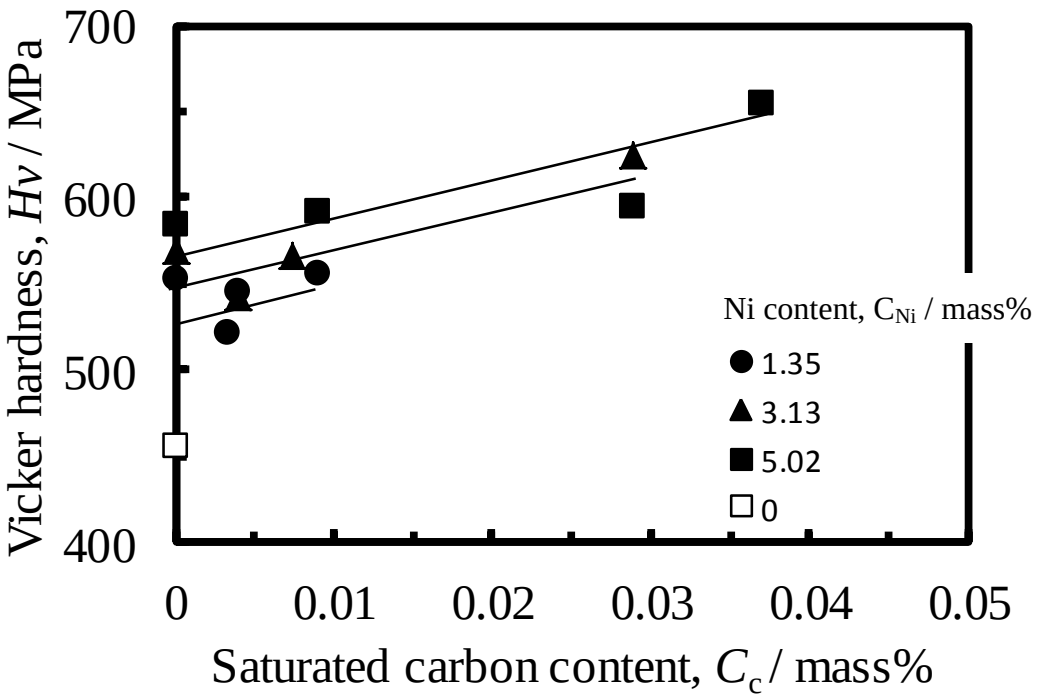

Fig. 2.22 Relation between hardness and saturated carbon content.

Table 2.5 Data of carbon content and their Vickers hardness in each sample.

Ni content, C_{Ni} / mass%	Carbon content, C_c / mass%	Vickers hardness, *Hv* / MPa
1.35	0.0000	553
1.35	0.0034	521
1.35	0.0040	545
1.35	0.0091	556
3.13	0.0000	570
3.13	0.0040	543
3.13	0.0073	566
3.13	0.0289	625
5.02	0.0000	584
5.02	0.0091	591
5.02	0.0289	594
5.02	0.0370	654

2.4. Conclusions

Cu-Ni alloy which included nickel content up to approximately 5 mass% was melted in the graphite crucible to prepare graphite dispersed Cu-Ni alloy. Solubility of carbon in the Cu-Ni alloy and Vickers hardness were measured in this study. Main results and conclusion were summarized as follows:

(1) The solubility of carbon in the molten Cu-Ni alloy increased with the temperature rise and with the nickel content. The relation between solubility of carbon in molten Cu-Ni alloy and temperature, *T* (1673 K ~ 2143 K) could be given by Eqs. (2-1) ~ (2-3).

(2) It was proposed that the interaction parameter, ω_C^{Ni}, for Cu-Ni-C_{sat} (saturated carbon)

was -17.1.

(3) Graphite particles were precipitated from the molten Cu-Ni-C_{sat}. Vickers hardness of Cu-Ni-C_{sat} system increased with saturated carbon content and nickel content. The heat treated Cu-Ni-C_{sat} alloy was hardened by precipitation hardening of the graphite particles and solution hardening of nickel.

It was tried that the graphite dispersed copper alloy composite prepared with dissolution-solidification method. The carbon content in the prepared composite was up to 0.05 mass%. Graphite dispersed copper alloy composite usually demanded carbon content from approximately 20 mass% to 85 mass%. This carbon content was too small in comparison with the carbon content in usual graphite dispersed copper alloy composite.

REFERENCES

1) P. Jenei, J. Gubicza, E. Y. Yoon, H. S. Kim, J. L. Lábár: “High temperature thermal stability of pure copper and copper–carbon nanotube composites consolidated by High Pressure Torsion”, Compos. Part A Appl. Sci. Manuf., vol. 51 (2013) pp. 71–79

2) Y. Feng, S. L. Burkett: “Modeling a copper/carbon nanotube composite for applications in electronic packaging”, Comput. Mater. Sci., vol. 97 (2015) pp. 1–5

3) D. Kuhlmann-Wilsdorf: “Electrical fiber brushes-theory and observations”, Components, Packaging, and Manufacturing Technology: Part A, IEEE Trans., vol. 19 (3) (1996) pp. 360–375

4) Z. L. Hu, Z. H. Chen, J. T. Xia: “Study on surface film in the wear of electrographite brushes against copper commutators for variable current and humidity”, Wear, vol. 264 (2008) pp. 11–17

5) L. Yang, P. Shen, Q. Lin, F. Qiu, and Q. Jiang: “Effect of Cr on the wetting in Cu/graphite system”, Appl. Surf. Sci., vol. 257 (14) (2011) pp. 6276–6281

6) P. B. Abel, A. L. Korenyi-Both, F. S. Honecy, and S. V. Pepper: “Study of copper on graphite with titanium or chromium bond layer”, J. Mater. Res. Vol. 9 (3) (1994) pp. 617–624

[7] J. Zhang, T. Wang, C. Liu and Y. He: “Effect of brazing temperature on microstructure and mechanical properties of graphite/copper joints”, Mater. Sci. Eng, vol. 594 (2014) pp. 26-31

[8] P. R. Subramanian, D. E. Laughlin: “Phase diagrams of binary alloys. Monograph series on alloy phase diagrams”, Materials Park, OH: ASM International, vol. 10 (1994) pp. 109

[9] S. Yokoyama, Y. Takashima, M. Nor, Y. Murata, H. Kanematsu, J. Sasano, M. Izaki:

“Solubility of carbon and Vickers hardness of copper saturated with carbon”, AMPT, Sept. (2012) pp. 1-8

[10] P. B. Anderson and M. B. Bever: “Solubility of carbon in molten copper-manganese and copper-nickel alloys”, Metals Tech., vol. 14 (1947) pp. 2151

[11] E. T. Turkdogan: “Physical chemistry of the high temperature technology”, Academic Press (1980) pp. 17

[12] Y. Kawai and Y. Shiraishi, “Handbook of physico-chemical properties at high temperature”, ISIJ (1988) pp. 74

[13] P. Nash: “Phase Diagrams of Binary Nickel Alloys”, ASM International, Materials Park, OH (1991)

CHAPTER 3

SOLUBILITY OF NITROGEN GAS INTO MOLTEN COPPER AT TEMPERATURE RANGE OF 1993 K TO 2443 K

3.1 Introduction

The various reactions of a molten metal at around smelting temperatures have been studied until now to understand and improve smelting processes. A high temperature process such as a thermal spraying comes to be used recently [1]. Thermodynamic data above a smelting temperature have been needed so as to understand phenomena in a higher temperature process. It is reported that nitrogen gas is insoluble in solid and liquid copper at the temperature of up to 1673 K. In addition, no reaction between metallic copper and nitrogen gas occurs [2, 3]. Accordingly, nitrogen gas has been considered to be an inert gas like argon for example. However, copper nitride is synthesized by the reaction between copper and ammonia and with a RF magnetron sputtering on copper in the gas mixture of argon and nitrogen gas [4-6].

In chapter 2, solubility of carbon (graphite) into molten copper was measured to prepare a graphite dispersed copper composite with casting method [7]. It was found that the solubility of carbon steeply increased with the increase in temperature and/or the nickel content, when the temperature exceeded approximately 2100 K. There is a possibility that nitrogen gas dissolve in molten copper at a higher temperature. However, the carbon solubility was not so large that large quantity of graphite could not precipitate like cast iron. If the solubility of nitrogen in molten copper is large, it is anticipated that copper nitride or nitrides of alloying elements in copper forms in copper alloy. Then, as a

fundamental study, the solubility of nitrogen gas into liquid copper was measured in this study.

3.2 Experimental

3.2.1 Preparation of copper-nitrogen composite

1) Apparatus

Fig. 3.1 showed the schematic of the experimental apparatus. The levitation melting apparatus was used in this study for melting copper. Because this apparatus could melt a copper without a crucible, a copper could be melted without contamination from a crucible.

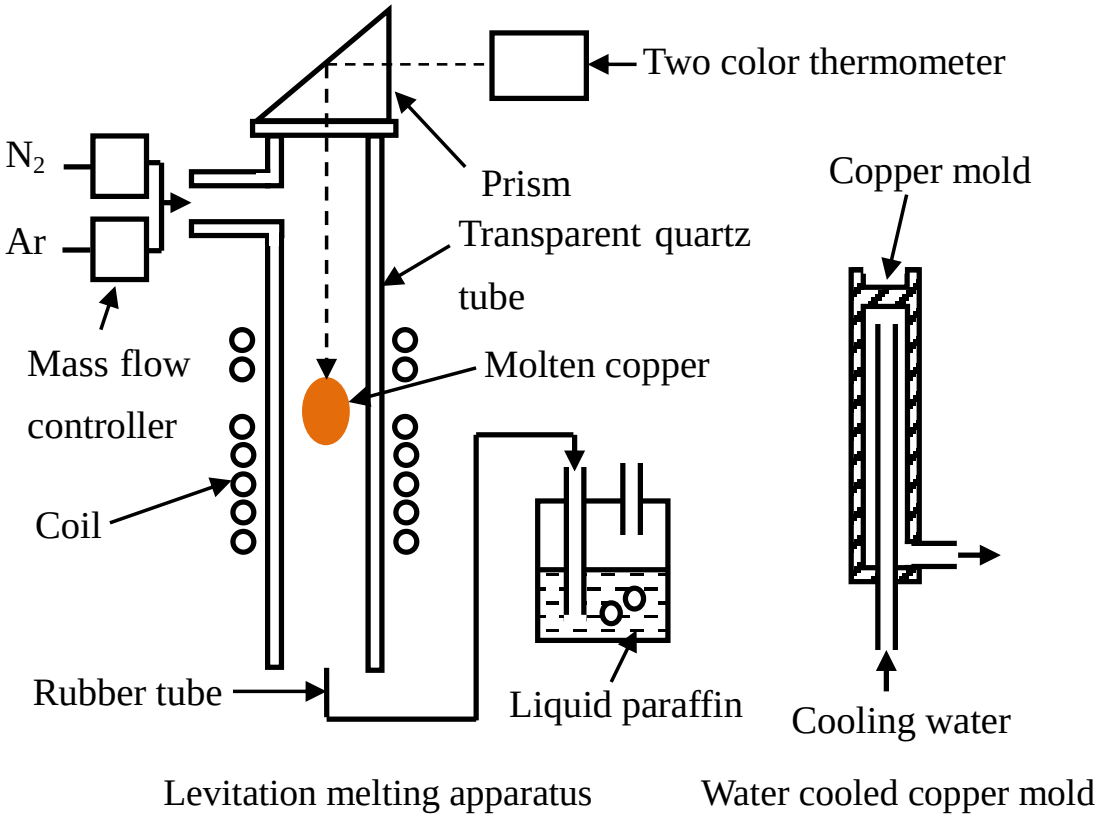

Fig. 3.1 Schematic of experimental apparatus.

2) Sample preparation

The copper sample used in this study was cut from a copper rod with purity of 99.994 mass% to be $2.20 \pm 0.05 \times 10^{-3}$ kg in weight.

3.2.2 Experiment procedure

The copper sample was levitation-melted in the induction furnace (130 kHz, 60 kW) in the gas mixture of nitrogen and argon gas flow with the flow rate of 8.33×10^{-5} $m^3 \cdot s^{-1}$ (293 K, 101.3 kPa (NTP)). Composition of nitrogen gas in the gas mixture was 25 vol%, 50 vol% and 100 vol%. The gas flow rate of the mixed gas was controlled with a mass flow controller. Purities of the nitrogen gas and argon gas were 99.9995 vol% and 99.999 vol% respectively. Temperature of the molten copper was measured with a two color thermometer, and was controlled manually within the range of 10 K. Temperature outputted from the thermometer was lower than that given from the thermocouple due to the emissivity of copper. The temperature was calibrated by measuring the temperature of a molten copper in MgO crucible in a high frequency induction furnace up to approximately 2120 K with the two color thermometer and thermocouple (Pt-20 mass% Rh, Pt-40 mass% Rh). In the case that the temperature of a molten copper exceeded approximately 2120 K, the temperature was corrected by extrapolation of the obtained calibration line.

The sample began to melt approximately 60 s later after it was levitated. The levitated liquid copper reached the predetermined temperature approximately 40 s later after the melting. The time when the melt arrived at the predetermined temperature was used for the start time for the experiment. After the copper sample was held for a predetermined time, the water-cooled copper mold shown in Fig. 3.1 was inserted from

the bottom end of the quarts reaction tube. Immediately after the mold touched the levitated copper, induction furnace was turned off and the copper sample was cooled rapidly on the mold.

The sample was divided into two parts with a wire cutter and measured both nitrogen and oxygen content in the copper sample with an inert gas fusion method (Horiba EMGA 1300). The principle of detection of nitrogen in this apparatus was the same as that in a gas chromatograph. The calibration line for analysis of oxygen and nitrogen was drawn by using the standard sample for iron. As described later, nitrogen content in the molten copper was very small. The copper sample for analysis was taken to be as large as possible. The lower detection limit of nitrogen content could not be reported simply because the product of the weight of a sample and its nitrogen content determined the limit. However the limit was approximately 0.4 massppm. In addition, the scattering of measured value was ± 0.2 massppm.

3.3 Results and discussion

3.3.1 Change in nitrogen concentration with time.

Fig. 3.2 showed the example of the change in nitrogen content in the molten copper with time. The nitrogen contents under nitrogen gas and the mixed gas flows increased with time, and were almost constant at the time of 180 s or more. Taking account of the accuracy of analysis, it could be considered that the nitrogen content was equilibrated with the given pressure of nitrogen approximately 180 s later.

Changes in oxygen content with time were shown in Fig. 3.3. These experimental conditions shown in this figure were the same as those shown in Fig. 3.2. Even after 180 s when nitrogen content became constant, the oxygen content increased with time. This

increase in the oxygen content resulted from oxidizing by impurities which nitrogen and argon gasses included. The measured solubility of nitrogen gas was the one for the copper of which oxygen content was 60 massppm to 120 massppm.

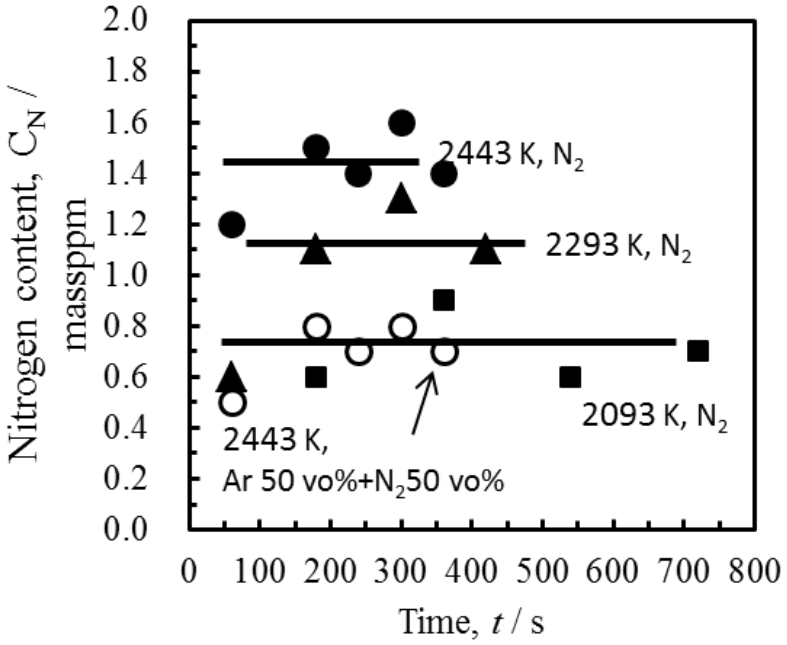

Fig. 3.2 Example of change in nitrogen content with time.

Fig. 3.4 showed the relation between the solubility of nitrogen and the temperature. The calculated line in this figure was described later. Whereas the solubility of nitrogen increased with the temperature rise, the solubility even at 2443 K was approximately 1.6 massppm and not so large. This solubility was approximately one quarter of that reported previously [8].

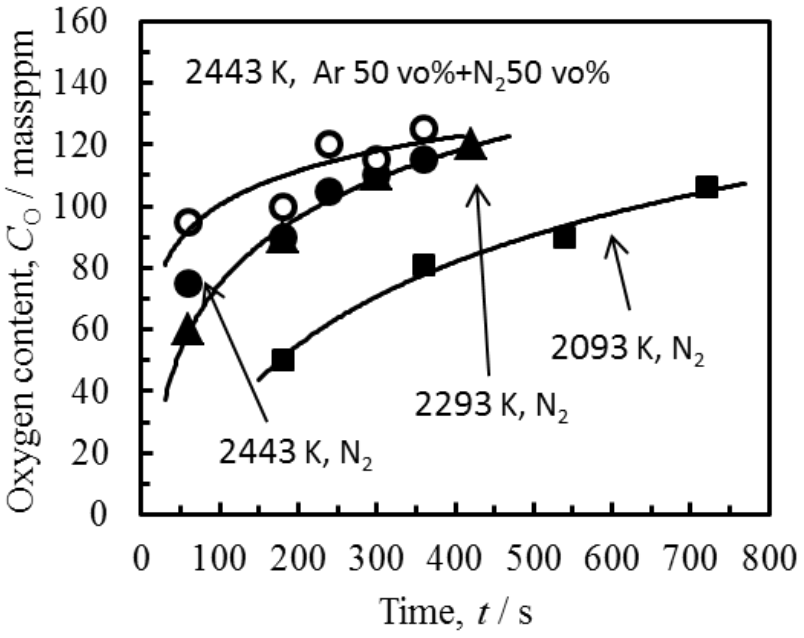

Fig. 3.3 Example of change in oxygen content with time.

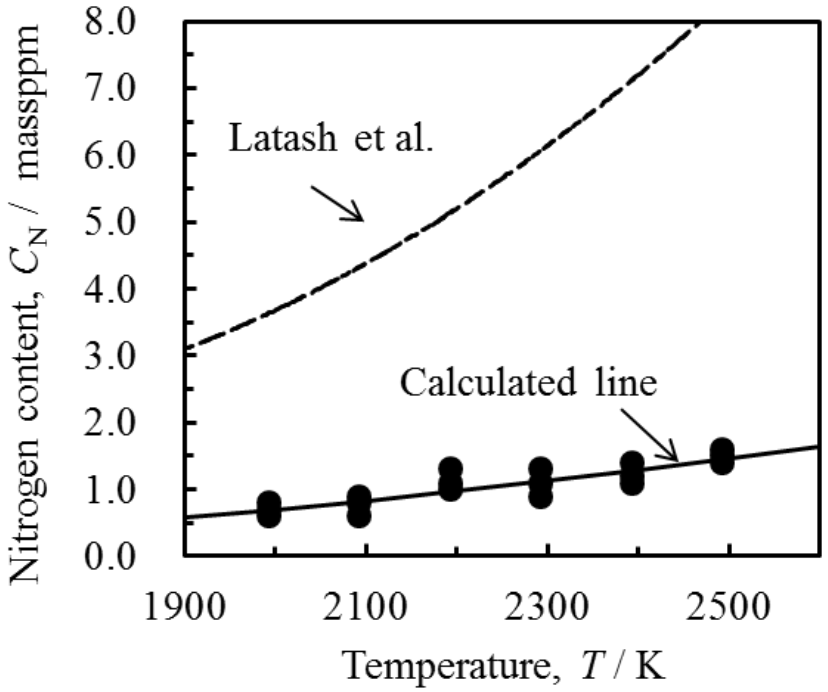

Fig. 3.4 Relation between saturated nitrogen content and temperature.

3.3.2 Activity coefficient of nitrogen

Fig. 3.5 showed the relation between the nitrogen content and square root of the partial pressure of nitrogen in the gas mixture.

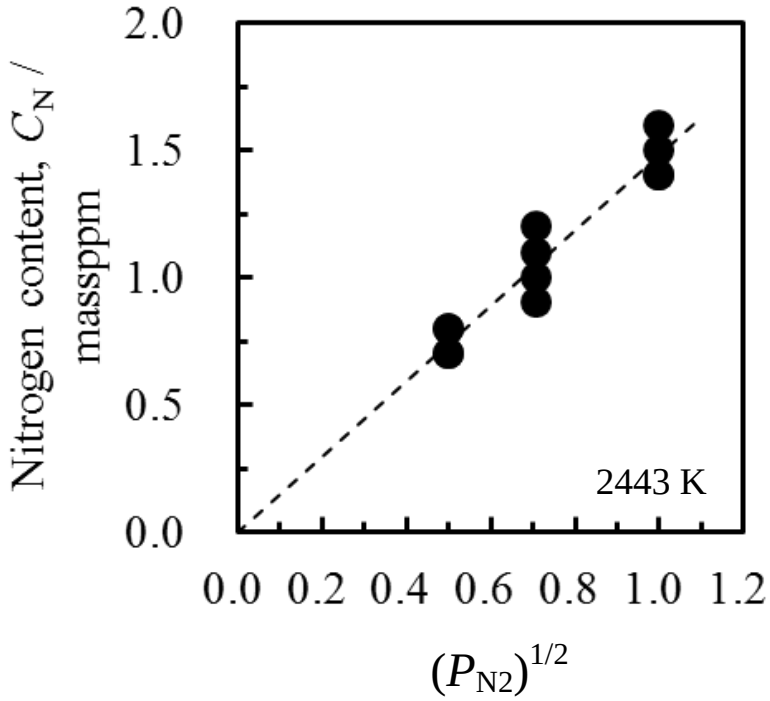

Fig. 3.5 Relation between nitrogen content in molten copper and square root of partial pressure of nitrogen gas.

Here, the pressure was normalized by dividing the pressure expressed in Pa with 100 kPa. Accordingly, the unit of atm could be attached to the value of the normalized pressure. There was a good liner relation between the nitrogen content and square root of the partial pressure of nitrogen. This suggested that the dissolution of nitrogen gas into liquid copper obeyed Sieverts' law. Namely, the dissolution reaction of nitrogen gas into molten copper could be expressed as:

$$\frac{1}{2}\mathrm{N_2(gas)} = \underline{\mathrm{N}} \qquad (3\text{-}1)$$

Here, the underlined element was expressed the element dissolved into a molten copper. The equilibrium constant, *K*, was given as

$$K = \frac{a_{\mathrm{N}}}{\sqrt{p_{\mathrm{N2}}}} \tag{3-2}$$

Here, a_{N} was the activity of nitrogen which was based on the reference state of the infinitely dilute solution of nitrogen in pure molten copper. The p_{N2} was the partial pressure of nitrogen. The activity of nitrogen was expressed as:

$$a_{\mathrm{N}} = \gamma_{\mathrm{N}}[\mathrm{mass\%N}] \tag{3-3}$$

The activity coefficient of nitrogen, γ_{N}, was given as:

$$\log\gamma_{\mathrm{N}} = \log\gamma_{\mathrm{N}}^{\mathrm{N}} = e_{\mathrm{N}}^{\mathrm{N}}[\mathrm{mass\%N}] \tag{3-4}$$

where $\gamma_{\mathrm{N}}^{\mathrm{N}}$ and $e_{\mathrm{N}}^{\mathrm{N}}$ were the interaction coefficient and the interaction parameter of nitrogen respectively [3-9]. Because the dissolution of nitrogen gas into liquid copper obeyed Sieverts' law, the following relations were obtained.

$$\gamma_{\mathrm{N}} = \gamma_{\mathrm{N}}^{\mathrm{N}} = 1 \tag{3-5}$$

$$e_{\mathrm{N}}^{\mathrm{N}} = 0 \tag{3-6}$$

Accordingly, the equilibrium constant was expressed as:

$$K = [\text{mass\%N}] \tag{3-7}$$

The standard reaction Gibbs energy, $\Delta_r G^0$, for the reaction (3-1) was expressed as:

$$\Delta_r G^0 = -RT\ln K \tag{3-8}$$

where R was the gas constant [J/(K·mol)], T was the thermodynamic temperature [K]. This Gibbs energy could also be expressed as:

$$\Delta_r G^0 = \Delta_r H^0 - T\Delta_r S^0 \tag{3-9}$$

where $\Delta_r H^0$ [J/mol] and $\Delta_r S^0$ [J/(K·mol)] were standard reaction enthalpy and entropy respectively. The equations (3-7)~(3-9) gave the following equation.

$$\ln[\text{mass\%N}] = -\frac{\Delta_r H^0}{RT} + \frac{\Delta_r S^0}{R} \tag{3-10}$$

Fig. 3.6 showed the relation between natural logarithm of [mass%N] and the reciprocal of the temperature. There was a good liner relation between them. This suggested that $\Delta_r H^0$ and $\Delta_r S^0$ were considered to be constant irrespective to temperature. $\Delta_r H^0$ and $\Delta_r S^0$ could be calculated from the gradient and the intercept of this straight line respectively. $\Delta_r H^0$ was 61573 J/(molK), and $\Delta_r S^0$ was -48.75 J/mol. Accordingly, equation (3-9) and (3-10) became:

$$\Delta_r G^0 = 61573 + 48.75T \tag{3-11}$$

$$\ln[\text{mass\%N}] = -\frac{7406}{T} - 5.863 \tag{3-12}$$

These equations were used for a molten copper of which oxygen content was 60 massppm to 120 massppm. The solubility of nitrogen calculated from eq. (3-12) was shown in Fig. 3.4. The line calculated from the equation (3-12) fitted the experimental data well.

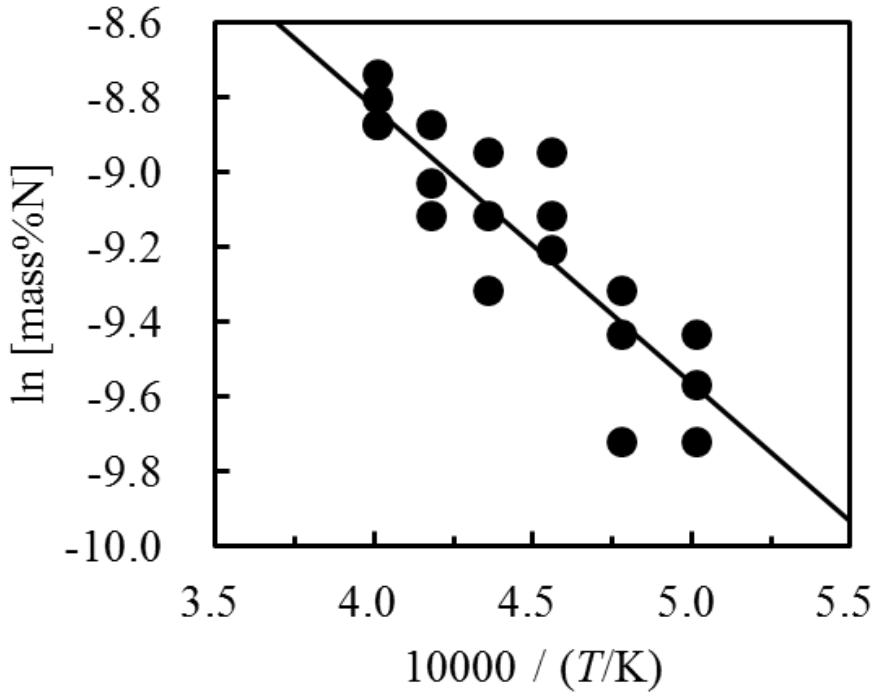

Fig. 3.6 Relation between natural logarithm of [mass%N] and reciprocal of temperature.

Because the value of the standard reaction enthalpy was positive, the nitrogen absorption reaction given by the equation (3-1) was an endothermic reaction. Analysis of the data given by Yatash et. al gave $\Delta_r H^0$ of 63378 J/(molK), and $\Delta_r S^0$ of -33.88 J/mol. The standard reaction enthalpy given by Yatash et al. was almost the same as those

obtained in this work. However, the absolute value of the standard reaction entropy obtained in this work was approximately 1.5 times as large as that of Yatash et al. This difference in the entropy mainly influenced the difference in the solubility of nitrogen.

The standard reaction entropy for dissolution of nitrogen gas into liquid iron was -20.17 J/(mol·K) [10]. Generally, the standard reaction entropy for the reaction between a gas phase and a condensed phase mainly depended on change in the entropy from a gas phase to a condensed phase. Therefore, the value of the standard reaction entropy for liquid copper might become the value similar to the entropy for liquid iron. Therefore, the difference in the standard reaction entropies resulted from the entropy change in condensed phases. The standard reaction entropy for dissolution of nitrogen gas into α- and δ- iron was -19.91 J/(mol·K). This value was almost the same as the one for liquid iron [10]. However, the standard reaction entropy for dissolution of nitrogen gas into γ- iron was -37.42 J/(mol·K) and was different from those for liquid, α- and δ- iron. The standard reaction entropy was different even if the reactions are as similar to each other.

3.4 Conclusion

Solubility of nitrogen gas into a molten copper was measured at the temperature range of 1993 K to 2443 K using a levitation-melting apparatus. The dissolution of nitrogen gas into molten copper obeyed the Sieverts' law, which meant that absorption of nitrogen gas into molten copper was expressed as:

$$\frac{1}{2}\mathrm{N}_2(\mathrm{gas}) = \underline{\mathrm{N}}$$

Solubility of nitrogen gas into a molten copper of which oxygen content was 60

massppm to 120 massppm was expressed as:

$$\ln[\text{mass\%N}] = -\frac{7406}{T} - 5.863 \text{ (T: 1993 K} \sim \text{2443 K)}$$

The standard reaction Gibbs energy was expressed as:

$$\Delta_r G^0 = 61573 + 48.75T \text{ [J/(mol·k)]}$$

The maximum solubility of graphite on this experimental conditions was around 0.05 mass% and was too small, as described in the Chapter 2. In this chapter, the solubility of nitrogen into a molten copper was studied to prepare the nitride dispersed copper composite instead of a graphite dispersed copper alloy composite. Because the solubility of nitrogen was approximately one-tenth of the solubility of graphite, the preparation of nitride dispersed copper composite seemed difficult. However, because the solubility of nitrogen was so small, nitrogen may be use as an inert gas to pure copper like argon.

REFERENCES

[1] R. Kromer, S. Costil, J. Cormier, L. Berthe, P. Peyre, D. Courapied: “Laser patterning pretreatment before thermal spraying: a technique to adapt and control the surface topography to thermomechanical loading and materials”, J. Thermal Spray Tech., vol. 25 (2016) pp. 401–410

[2] M. Hansen: “Constitution of binary alloys”, McGrawhill (1958) pp. 600

[3] J. R. Davis: “Copper and Copper Alloys”, ASM international (2001) pp. 177

[4] T. Nakamura, H. Hayashi, T. Hanaoka, and T. Ebina: “Preparation of copper nitride (Cu3N) nanoparticles in long-chain alcohols at 130-200 °C and nitridation mechanism”, Inorg. Chem., vol. 53 (2014) pp. 710–715

[5] J.F Pierson: “Structure and properties of copper nitride films formed by reactive magnetron sputtering”, Vacuum, vol. 66 (2002) pp. 59–64

[6] C. M. Caskey, R. M. Richards, D. S. Ginleya, A. Zakutayeva: “Thin film synthesis and properties of copper nitride, a metastable semiconductor”, Mater. Horiz., vol. 1 (2014) pp. 424-430

[7] S. Yokoyama, Y. Takashima, M. Nor, Y. Murata, H. Kanematsu, J. Sasano, M. Izaki: “Solubility of carbon and Vickers hardness of copper saturated with carbon”, AMPT, Sept. (2012) pp. 1-8

[8] Y. V. Latash, G. F. Torkhov, Y. I. Kostenko, N. N. Kalinyuk: “Nitrogen solubility in liquid copper, nickel and Cu-Cr, Ni-Cr alloys”, Izvestiya Akademii Nauk SSSR, Metally, 1 (1986) 45-49

[9] E. T. Turkdogan: “Physical chemistry of high temperature technology”, Academic Press (1980) pp. 76

[10] The Japan Society for the Promotion of Science, the 19th Committee on

Steelmaking: “Steelmaking data source book”, Gordon and Branch Science Publishers, (1988) pp. 21 and pp. 27

CHAPTER 4

PREPARATION OF GRAPHITE DISPERSED COPPER COMPOSITE ON COPPER PLATE WITH SPOT WELDING

4.1 Introduction

In previous chapter 2, the solubility of carbon into the molten copper-nickel alloy (nickel content ≤ 5.0 mass%) was measured. It has been found in chapter 2 and previous work [1] that the wetting of molten copper to graphite is improved at temperature above approximately 2073 K. This suggests that the graphite dispersed copper composite can be prepared by holding the mixture of copper and graphite at the temperature of 2073 K or above.

Lumps of graphite dispersed composites are needed in some cases, and the composites prepared only on the surface are demanded in other cases. One of the heating machines which can locally heat materials to high temperature is a spot welder [2]-[6]. Apart of that, spot welding can heat a substance for a short time and is in no need of complex material preparation. Then, graphite particles on a copper plate were spot-welded in order to prepare the copper-graphite composite only on the copper surface. Usually, operation parameters of a spot welding are a compressive load and an electric current flow. The spot welding has been carried out by changing these parameters. In addition, the sequential operation which consisted of placement of the graphite particles on the copper plate and spot welding were repeated because graphite particles did not adhere to the copper plate by a one-time spot welding. Influences of the compressive load, the electric current flow and the repetition number of the operation on

the Vickers hardness as well as the carbon content were studied in this work.

4.2 Experimental

4.2.1 Materials used

Commercially available pure copper plate (the purity: 99.9 mass%) with 1 mm in thickness and graphite particles (SEC-Carbon purity of 99.97 mass%) with 50 μm in average size were used in this study. The copper plate which was cut from the plate was 15 mm width by 50 mm. To remove unnecessary substances such as grease, house dust and so on, the copper plate was cleaned with an ultrasonic washing machine (45 kHz, 300 W) in which acetone was filled. Graphite powder was grounded with an agate mortar and a pestle. The ground particles were passed through the sieve of which opening was 20 μm. SEM image of the graphite particles used for this study was shown in Fig. 4.1. The particles were approximately 5 μm in average size. The relatively large and small particles were flat and angular in shape respectively.

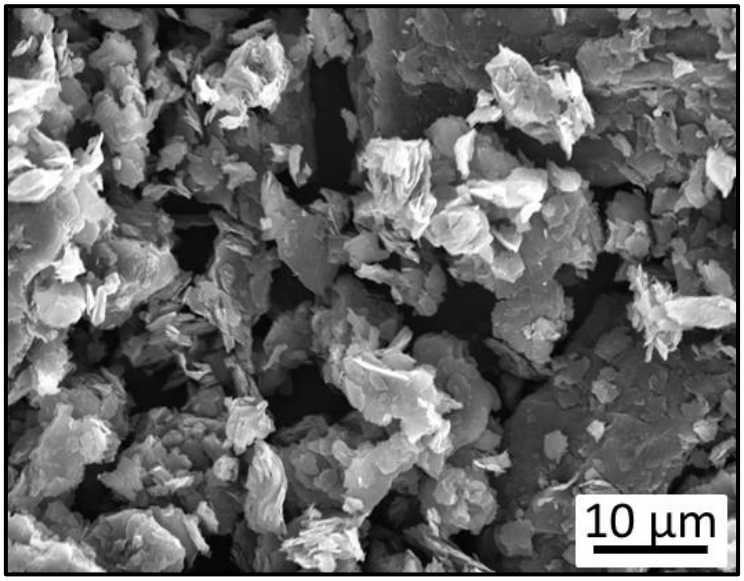

Fig. 4.1 SEM image of ground graphite particles used in this work.

4.2.2 Specimen preparation and apparatus

The graphite particles were placed between the two copper plates, as shown in Fig. 4.2. The layer of graphite particles sandwiched between the two copper plates was approximately 0.8 ~1 mm in height. The sample was fixed by a wooden clip so that the graphite particles did not fall during welding.

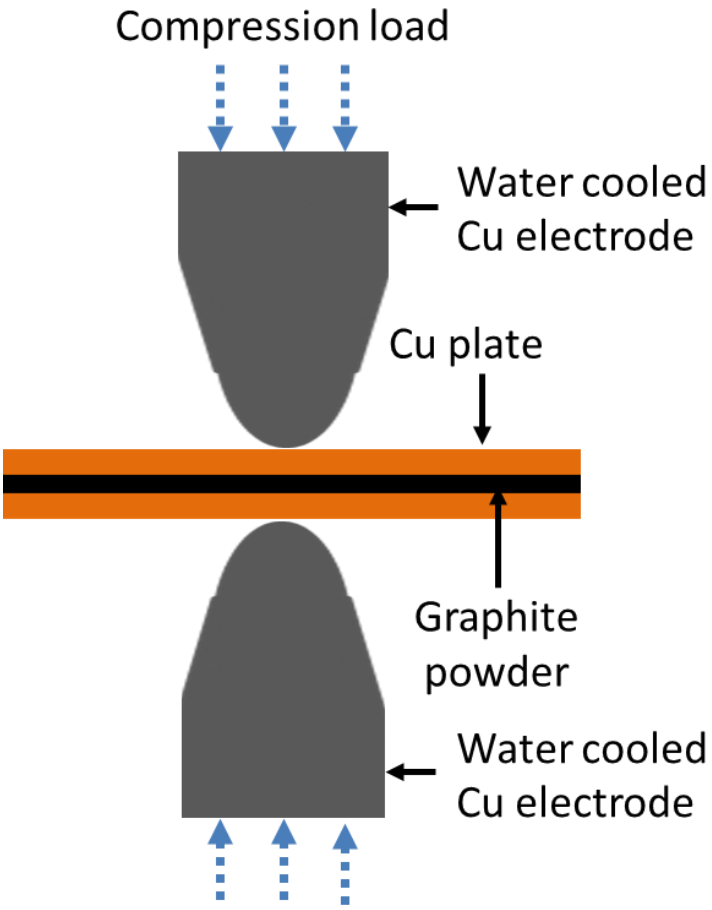

Fig. 4.2 Schematic of main part of apparatus for preparation of graphite dispersed copper composite with resistant spot welder.

The sample was set between the two copper electrodes of the spot welding machine. Subsequently, it was compressed by the electrodes. The compressive loads

were 0.0 kN, 1.3 kN, 3.5 kN and 5.7 kN. Because the deformed area was approximately 100 mm^2, the compressive stresses were 0.0 MPa, 1.3 MPa, 3.5 MPa and 5.7 MPa respectively. Pulsed electric current was energized for 50 ms every pulse 6 times (total 300 ms) by the one spot welding to the sample during the compression. The electric currents were 0 kA, 10 kA and 16 kA.

4.3.3 Analyzation

A series of operations which were consisted of the placement of graphite particles, the spot welding, and the ultrasonic cleaning was performed repeatedly. The surface and the cross section of the copper plate were observed using a SEM (scanning electron microscope) and a laser microscope. Carbon content in the surface was analyzed with an EDX (Energy dispersive X-ray spectroscopy) equipped with the SEM. Therefore, the carbon content was the value for the surface of the plate. The quantity of graphite adhered to the copper plate was evaluated with this carbon content. The carbon content at seven different places were measured with an area analysis of the EDX. The measured area size was approximately 0.02 mm^2. The carbon content was evaluated with the mean of seven measured values. The maximum scattering of the carbon contents was approximately ± 15% for the mean value. Vickers hardness was measured with a micro Vickers hardness tester on the load condition of 0.98 N. The hardness was measured at five positions from the center of the part deformed by the compression, which was the spot welding are, to the periphery of it. The hardness was evaluated with the mean of ten measured values. In addition, the hardness was measured at the matrix of copper except graphite particles in the composite. The maximum scattering of the measured hardness was ± 10% for the average value.

4.3 Results and discussion

4.3.1 Quantity of adhered graphite

After the spot welding, two copper plates prepared without an electric current flow were not attached each other. However, two plates prepared with an electric current flow were attached each other on certain occasions. This suggested that the two copper plates were spot-welded. However, these attached plates could be separated easily by hand. This adhesion was easy to occur when the compressive load and/or the electric current flow were large. Even if the compressive load and the electric current flow were large, this spot welding did not always occur. This meant instability of this preparation method. Furthermore, the electrode and the copper plate were never welded each other. The copper plate was cleaned with the ultrasonic washing machine after the spot welding. The particles which did not come off the plate even with this ultrasonic cleaning were considered to be the particles which stuck firmly to the copper plate.

Fig. 4.3 showed the relation between the carbon content in the copper plate and the repetition number of the compression, in the case that an electrical current was not energized through the sample at compression. Generally, after the carbon content steeply increased with the increase in the repetition number, it slightly increased with the repetition number. In addition, the carbon content increased with an increase in the compressive load. Here, the carbon content in the upper copper plate was almost the same as that in the lower copper plate. There was no systematic difference in both the carbon contents.

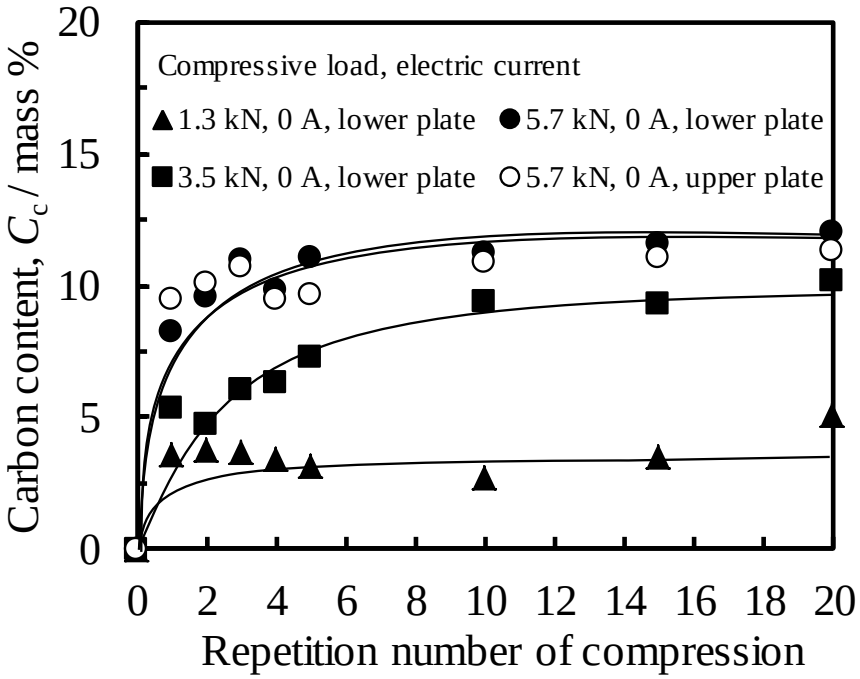

Fig. 4.3 Relation between carbon content and repetition number of compression for composite prepared without electric current flow.

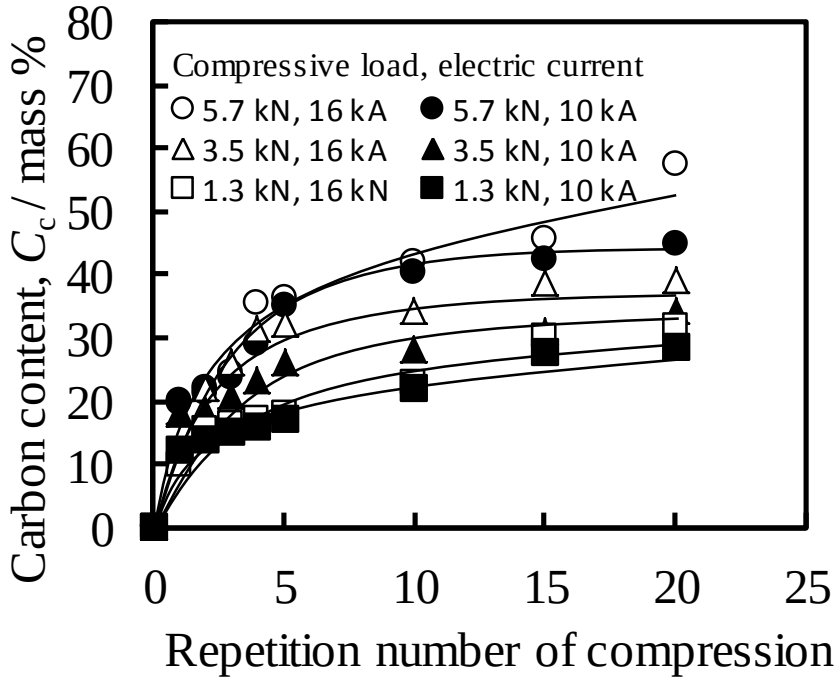

Fig. 4.4 Relation between carbon content and repetition number of compression for composite prepared with electrical current flow.

Fig. 4.4 showed the relation between carbon content in the copper plate and the repetition number of the compression, in the case that an electrical current was energized through the sample at compression. The carbon content increased with an increase in the compression load as well as the repetition number. These behaviors of the carbon contents were qualitatively the same as those for the composites prepared without an electric current flow. In addition, the carbon content increased with an increase in the electric current flow. In comparison with the carbon content as shown in Fig. 4.3, the carbon content in the composite prepared with an electric current flow was approximately five times larger than that without an electric current flow.

4.3.2 Graphite particles in composite

Fig. 4.5 showed the surface of the composite prepared without an electric current flow. As shown in Fig. 4.5 (a), the graphite particles were hardly observed in the macroscopic image. The particles were observed on the plate before the ultrasonic cleaning, whereas most of them were removed by the ultrasonic cleaning. Microscopically, the graphite particles locally adhered to the copper plate, as shown Fig. 4.5 (b). Because there were a lot of places where the graphite particles distributed as shown Fig. 4.5 (b), it could be said that the graphite particles distributed sparsely. As shown in Fig. 4.5 (b), the hollows like craters were observed on the plate. These showed traces where the particles had been plunged.

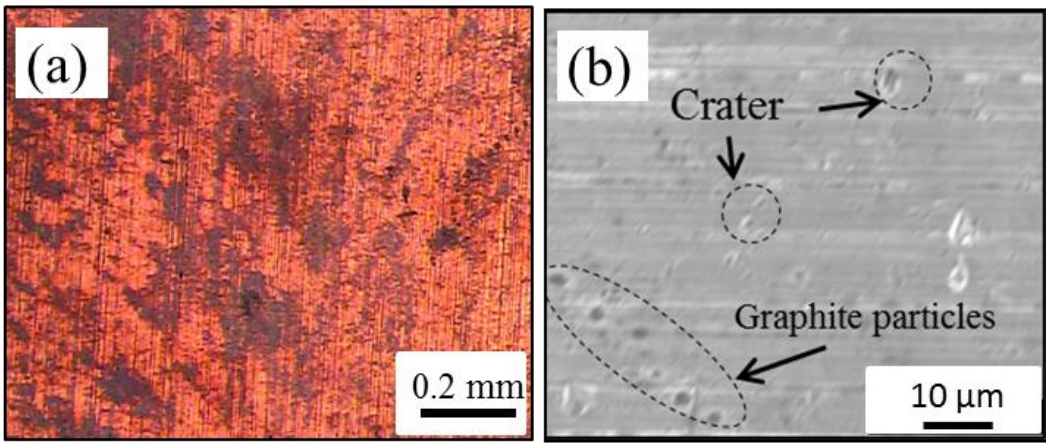

Fig. 4.5 Surface and cross section of composite prepared without an electric current flow. (The repetition number: 20, the compressive load: 5.7 kN,) Figures (a) and (b) macroscopically and microscopically showed the surface of the copper plate respectively.

Therefore, the mechanism of plunging the graphite particles in a copper plate could be explained as follows. When a flat particle, which meant the relatively large particle, was plunged into a copper plate as shown in Fig. 4.6 (a), the pressed particle made a dent on the plate surface. Because this particle was only pressed, particle did not adhere chemically to the copper plate and was easily removed from the plate by the ultrasonic washing. When an angular sharp particle, which meant the relatively small particle, was plunged into a copper plate as shown in Fig. 4.6 (b), the compression made the particle stuck in the plate. This particle did not bond with copper chemically but was fastened by deformation of the copper plate. Therefore, the ultrasonic washing could not remove this plunged particle.

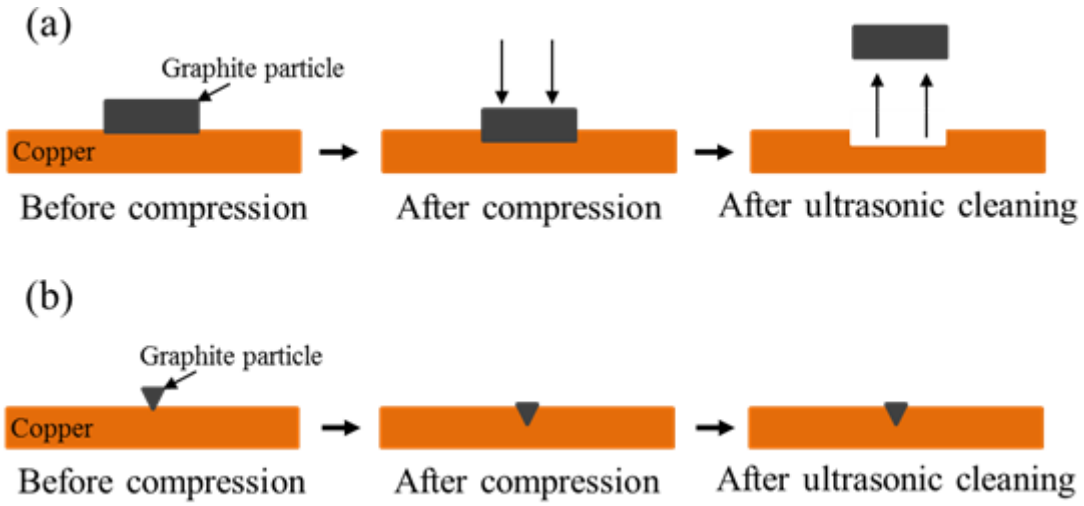

Fig. 4.6 Outline of mechanism for formation of graphite dispersed copper composite prepared without electric current flow. Fig. (a) showed the mechanism for a relatively large and flat particle. Fig. (b) showed the mechanism for a relatively small and angular particle.

Fig. 4.7 showed an example of the composite prepared with an electric current flow. The surfaces and the cross sections of the composites prepared on the different compressive load and electric current were almost the same as those shown in Fig. 4.7. Numerous graphite particles adhered to the copper plate, as shown in Figs. 4.7 (a) and (b). Except for the graphite particles sandwiched between the copper plates, the number of the particles on the plate before the ultrasonic cleaning was almost the same as that after the cleaning. Fig. 4.7 (c) showed the cross section of the plate near the surface. The graphite particles were consolidated into an aggregate form. Its cross section was looked to be the section of a layer. This graphite aggregate was on the copper plate and was composed of graphite particles and copper. In addition, the sizes of them became large, in comparison with those of the graphite particle before the experiment. Fig. 4.7 (d)

showed the cross section of the composite where the copper plates were spot-welded. Many graphite particles were observed not only at the surface of the copper but also in the copper. The graphite particles were polygonal in shape and composed of graphite and metallic copper.

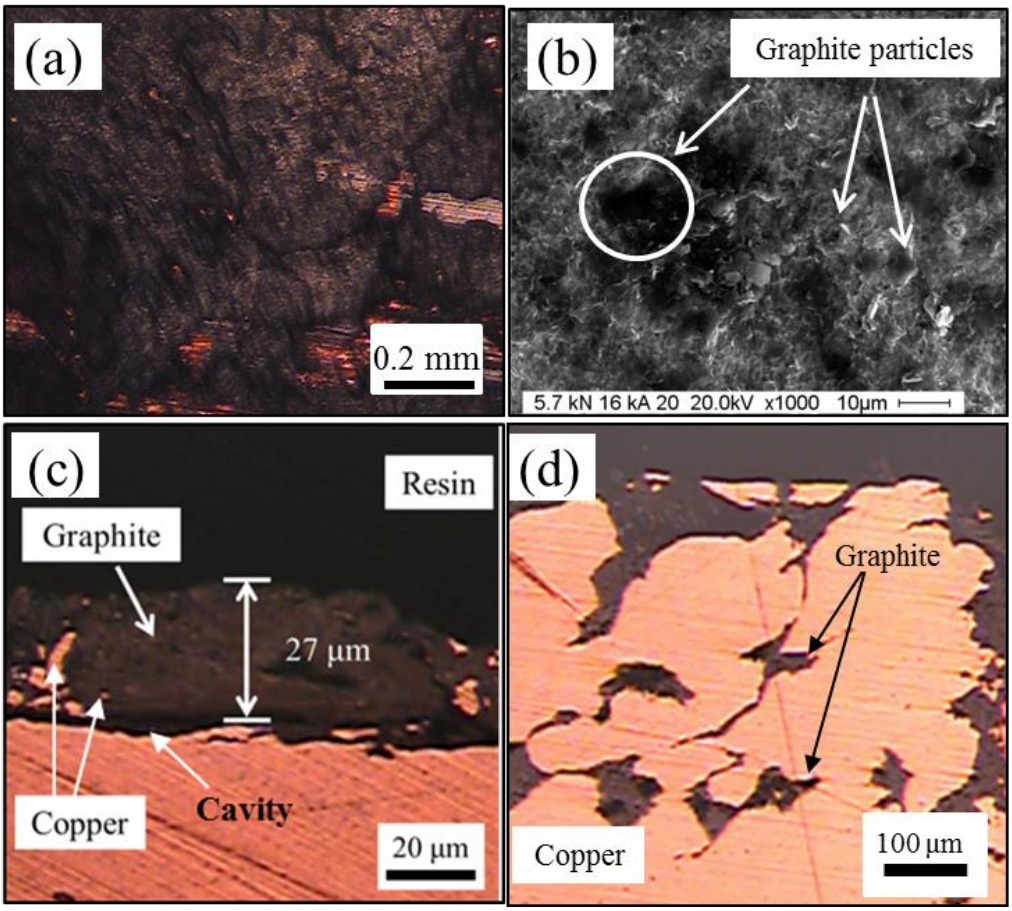

Fig. 4.7 Surface and cross section of composite prepared with an electric current flow (The repetition number: 20, the compressive load: 5.7 kN, the electric current: 16.7 kA). Figures (a) and (b) macroscopically and microscopically showed the surface of the copper plate respectively. Figure (c) showed the cross section of the copper plate. Figure (d) showed the cross section of the copper at the place where the copper plates were welded each other.

Here, it was assumed that electric current flowed through a graphite plate instead of graphite particles layer. When an electric current flowed in the graphite plate, the graphite plate was heated by the Joule's heat as:

$$C_{\mathrm{p}} \frac{ALd}{M_{\mathrm{C}}} (T - T_{298}) = \rho \frac{L}{A} I^2 t \tag{4-1}$$

where A was the cross-sectional area of the plate [m^2], L the thickness of the plate [m], d the density of graphite, M_c the molar mass of graphite [kg/mol], C_p the molar heat capacity of graphite at constant pressure [$J \cdot mol^{-1} \cdot K^{-1}$], I the electric current [A], ρ the electrical resistivity [$\Omega \cdot m$][7], t the time [s] and T_{298} the temperature of 298 K. From this equation, the temperature of the graphite plate, T, was expressed as:

$$T = \frac{\rho I^2 t M_{\mathrm{C}}}{C_{\mathrm{p}} A^2 d} + T_{298} \tag{4-2}$$

Table 4.1 Values used for calculation.

Area, A / m^2	Density,[11] d / $kg \cdot m^{-3}$	Molar mass, M_c / $kg \cdot mol^{-1}$	Electric resistance[7], ρ / Ωm	Heat capacity[8], Cp / $J \cdot mol^{-1} \cdot K^{-1}$	Time, t / s
1×10^{-4}	2.3×10^{3}	12×10^{-3}	0.0138	18.77	0.3

Table 4.1 showed the values used for this calculation. The value of the heat capacity was extrapolated to 10000 K based on the reported values from 298K and 1500 K.[8] Similarly, the molar heat capacity was obtained by averaging the values from 298K to 10000 K. This averaging was used to simplify the calculation.

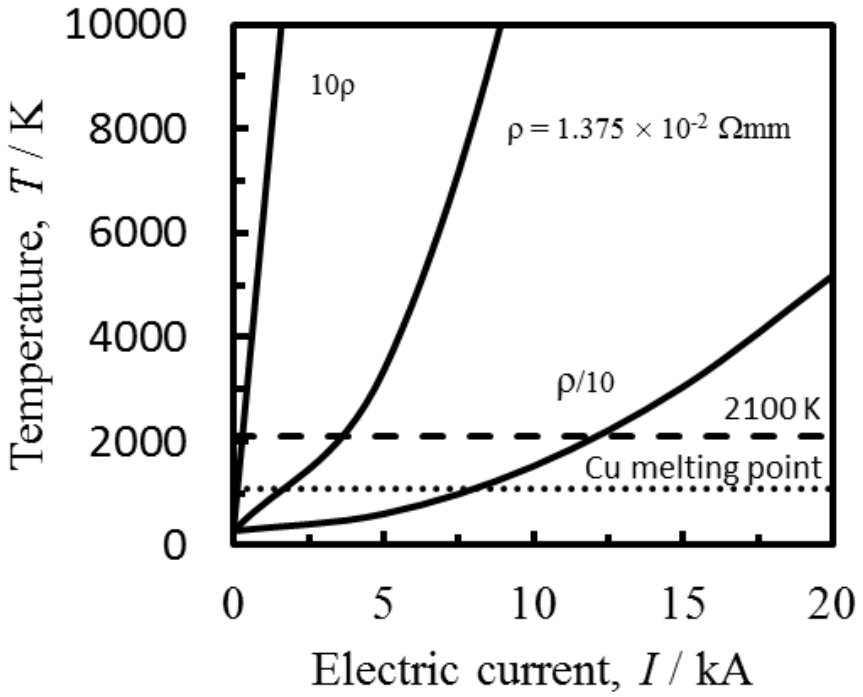

Fig. 4.8 Relation between calculated temperature of graphite plate and electric current.

Fig. 4.8 showed the relation between the temperature and the electric current. Assuming that the electric resistance was ten times (10ρ) or one tenth (ρ/10) as large as the value listed in Table 4.1, the calculated lines were also shown in this figure for reference. The temperature of the graphite plate increased with an increase in the electric current, and increased with an increase in the electric resistance. As shown in Fig. 4.8, the temperature of the graphite plate was higher than a copper melting point and easily arrived beyond 2100 K when the electric current of 10 kA or 16 kA flowed through the graphite plate. This calculation suggested that copper was mainly heated by the heat conduction from the electrically heated graphite.

In our previous study [6], it was found that saturated carbon content in a molten copper steeply increased with the temperature rise of molten copper when it was held at

the temperature above approximately 2100 K. In addition, a molten copper which was held above this temperature could wet to a graphite crucible. In the case that the composite was prepared with an electric current flow, the mechanism of formation of graphite particles to a copper plate could be explained as shown in Fig. 4.9. Namely, when a high electric current was energized through a plunged particle, copper around the graphite particles was melted by the Joule's heat. As described earlier, the graphite particles were different from the particles before the experiment. This suggested that a copper around the graphite particle was heated to temperature above approximately 2100 K.

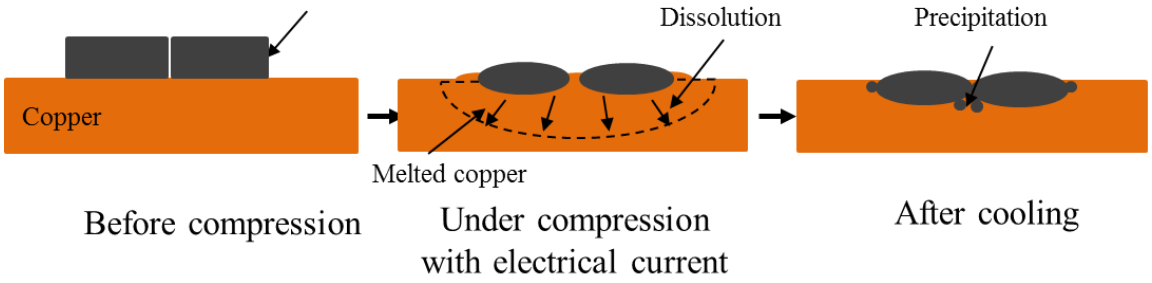

Fig. 4.9 Outline of mechanism for formation of graphite dispersed copper composite prepared with an electric current flow.

Therefore, the graphite particles dissolved into the molten copper entirely or partially. The graphite particles precipitated from the liquid copper under cooling. This dissolution and precipitation caused not only that the particles were consolidated with copper but also that the graphite particles became round. Furthermore, the graphite particles could not be eliminated by the ultrasonic cleaning because the molten copper could wet the graphite particle. Copper was observed between the graphite particles at

the upper part of the copper plate. This suggested that the molten copper rose up by the capillarity. In the case that the adhesion due to the spot welding occurred, the part of melted copper was enlarged deeply in the plate. This meant the temperature of the melt part was higher. During cooling, the graphite precipitated from the melt which the graphite dissolved into.

4.3.3 Vickers hardness

1) Hardness

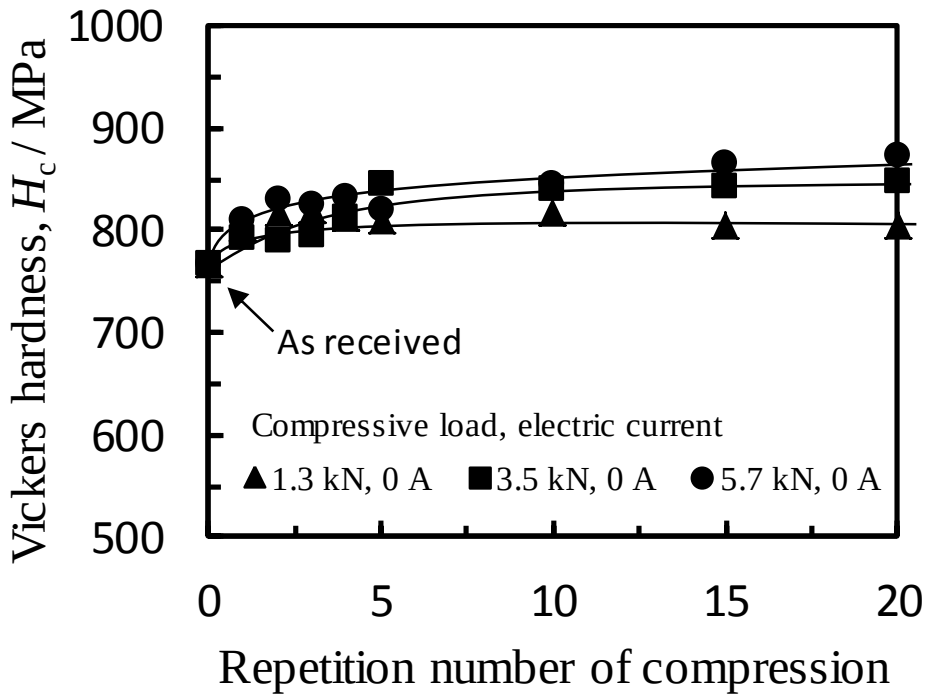

Fig. 4.10 Relation between Vickers hardness and repetition number of compression for composite prepared without an electric current flow.

As described earlier, the hardness was measured from the center of the spot welding to the periphery of it. It was judged from the maximum scattering that the measured

hardness did not depend on the distance from the center. Fig. 4.10 showed the relation between the Vickers hardness and the repetition number of compression, in the case that the composite was prepared without an electric current flow. Generally, the Vickers hardness steeply increased with the increase in the repetition number. Subsequently, it slightly increased with the repetition number. The Vickers hardness increased with an increase in the compressive load. These dependencies of Vickers hardness on the repetition number and compressive load were as similar as the dependencies of the carbon content.

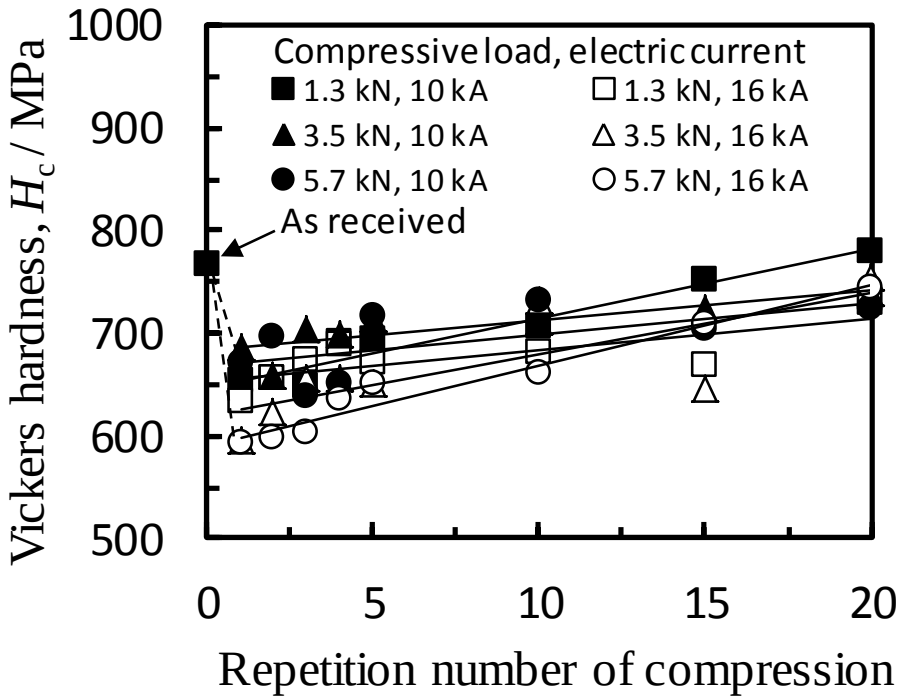

Fig. 4.11 Relation between Vickers hardness and repetition number of compression for composite prepared with electric current flow.

Fig. 4.11 showed the relation between the Vickers hardness and the repetition number of compression, in the case that the composite was prepared with an electric

current flow. Generally, the Vickers hardness decreased at the first compression. This resulted from the annealing, as described later. Subsequently, it increased with an increase in the repetition number of compressive load and the electric current value. The Vickers hardness increased with an increase in the compressive load and an increase in the electric current. In comparison with the hardness as shown in Fig. 4.10, in general, the hardness of the composite prepared with an electric current flow was smaller than that prepared without an electric current flow.

2) Hardness relation with carbon content

Fig. 4.12 showed the relation between the Vickers hardness and the carbon content. Generally, the Vickers hardness linearly increased with an increase in the carbon content. In addition, the hardness for the composite prepared without an electric current flow was larger than that for the composite prepared with an electric current flow. The dependencies of the hardness on the carbon content, which were the gradients of the straight lines given by the regression analysis, were classified into two groups. One group was for the composite which was prepared without an electric current flow. The gradient for them was approximately 9.0 MPa / mass% C. Another group was for the composite which were prepared with an electric current flow. There were two regression lines for the composite which were prepared with an electric current flow. The lower and the upper lines were for the composites with and without the adhesion due to the spot welding respectively. These gradients were approximately 4.1 MPa / mass% C.

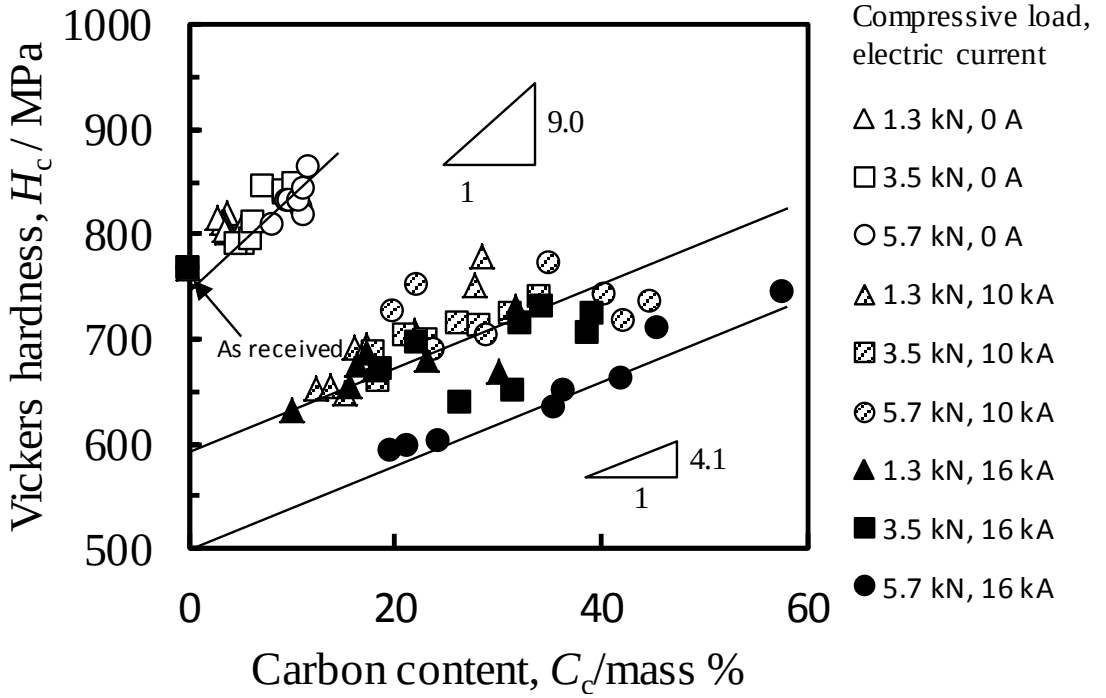

Fig. 4.12 Relation between Vickers hardness and carbon content.

As shown in Fig. 4.12, the intercept which was the hardness at the carbon content of zero mass% expressed the hardness of the copper matrix. The hardness of the copper matrix for the composite prepared without the electric current flow was the highest and was the same as that for as received copper plate. The hardness of the copper matrix for the composite prepared with the electric current flow was lower than that without the current flow because of the annealing due to the Joule's heat. In addition, the hardness of the copper matrix with the adhesion due to the spot welding was smaller than that without the adhesion. As described earlier, the composite with the adhesion was annealed sufficiently because the temperature at the surface of it was higher than that without the adhesion.

3) Hardening mechanism

The dependency of the hardness on the carbon content had made sense if the composite was reinforced only by the solid-solution strengthening. Because most carbon existed as graphite, the relation between the hardness and the carbon content showed only the empirical correlation between them. The rule of mixtures expressed the properties of a bulk composite such as the stress the elastic modulus, the strain and so on. The equations which expressed the upper and the lower bounds for the properties of particle-reinforced composites were known [9]. In this study, the composite material was prepared only on the copper surface. In addition, the hardness was measured at an only copper matrix in the composite. Applying these equations which gave the bounds to the hardness of this composite, the following equations were obtained [10].

$$H_{\mathrm{C}} = H_{\mathrm{Cu}}\left(1 - f_{\mathrm{g}}\right) + H_{\mathrm{g}} f_{\mathrm{g}} \tag{4-3}$$

$$\frac{1}{H_{\mathrm{C}}} = \frac{1 - f_{\mathrm{g}}}{H_{\mathrm{Cu}}} + \frac{f_{\mathrm{g}}}{H_{\mathrm{g}}} \tag{4-4}$$

where H was the hardness [Pa], f the volume fraction, subscript C, Cu and g indicated the composite, copper and graphite respectively. The volume fraction of graphite was calculated from the carbon content, densities of copper and graphite [11, 12].

Fig. 4.13 and Fig. 4.14 showed the adaptability of eq. (4-3) and eq. (4.4) to the relation between the Vickers hardness and the volume fraction of graphite. Good linear relations were identified in both figures, and this meant that the relation between the hardness and the volume fraction of graphite could be expressed by both eq. (4-3) and eq. (4-4). The relation between the hardness and the volume fraction of graphite given

by eq. (4.4) was also shown as broken lines in Fig. 4.13. It could not be judged from the compatibility of the experimental data to the equations which equations expressed the relation between the hardness and the volume fraction.

The following things could be said on the hardness of the copper matrix given from these two expressions. The hardness of the copper matrix for the composite prepared without the electric current flow was the highest. It without the adhesion in case of the electric current flow was second highest. It with the adhesion in case of the electric current flow was the lowest. Here, the value of H_{Cu} given by eq. (4-3) and eq. (4-4) were different each other. Similarly, the value of H_g were different each other. This resulted from that those values obtained from a regression analysis based on eq. (4-3) and eq. (4-4). These things originated in being annealed or not, and annealing temperature, as described earlier. Similarly, the following things could be said on the hardness of the graphite, H_g, given from these two expressions. The hardness of the graphite for the composite prepared without the electric current flow was the highest. It without the adhesion in case of the electric current flow was second highest. It with the adhesion in case of the electric current flow was the lowest. However, the hardness of the graphite for the composite should not be changed by the preparation conditions, because the graphite particle was solid.

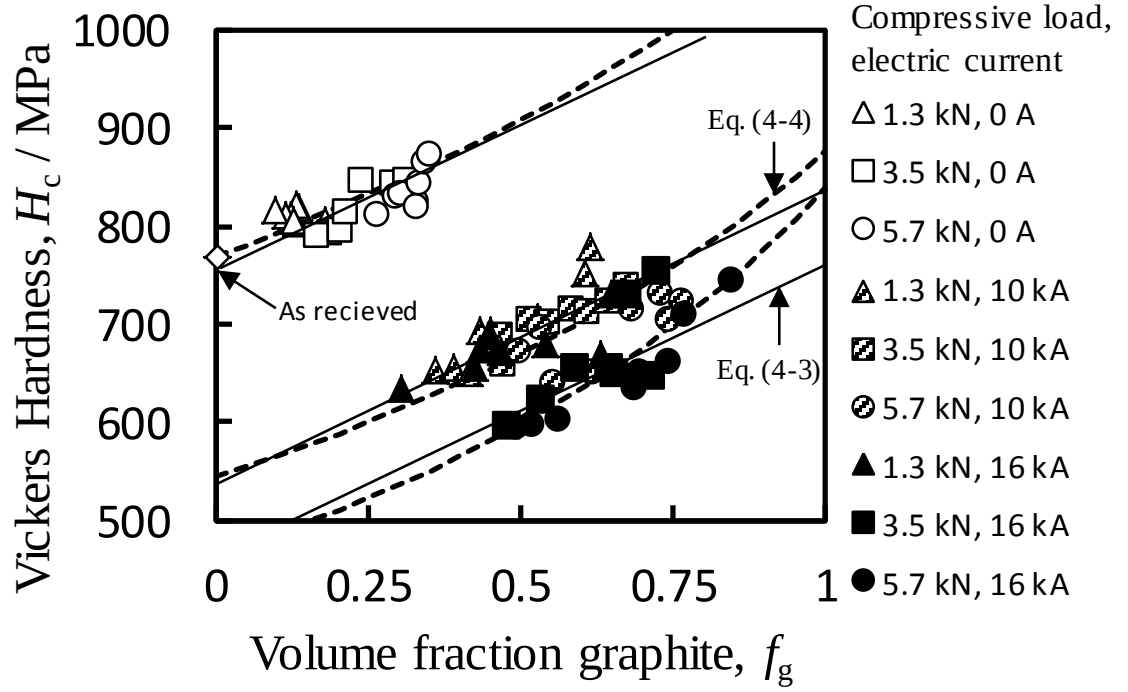

Fig. 4.13 Relation between Vickers hardness and volume fraction of graphite.

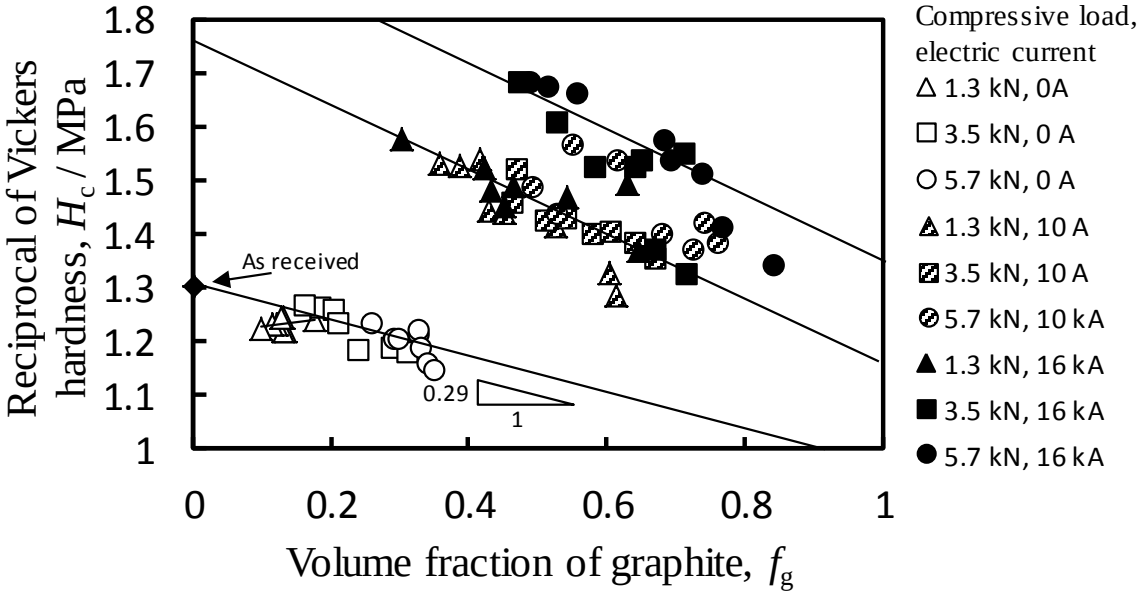

Fig. 4.14 Relation between reciprocal of Vickers hardness and volume fraction of graphite. (Adaptability of eq. 4.4 for the relation)

In this study, the hardness measurement was performed for a copper matrix in the composite. Therefore, the hardness of graphite did not directly influence the measured hardness. An indenter was pushed into a material in the indentation hardness test like a Vickers hardness test, Brinell hardness test and so on. The indenter deformed a materials plastically. This lead to the work hardening. In this study, because graphite particles were pushed into a copper plate, copper in the vicinity of the graphite particle was deformed and work hardened. Fig. 4.15 showed the schematic explanation of hardening method after graphite particles were pushed into copper. Because the hardness of the deformed copper was considered to be influenced by the preparation conditions, the hardness of graphite, H_g, could be changed by the conditions. As a practical matter, the hardness of graphite, H_g, in the expressions was really the hardness of the copper around the particle. Here, a spot welding was composed of compression, energization under compression and removal of compression. Even if the copper in the vicinity of the graphite particle was fused, the copper near the graphite particle was deformed. It could not be determined which eq. (4-3) and eq. (4-4) more expressed the experimental data. Because the rule of mixture given by eq. (4-3) and (4-4) could be applicable to the properties of bulk composite, the further study was needed to clear the mechanism of the reinforcement of the composite prepared in this study.

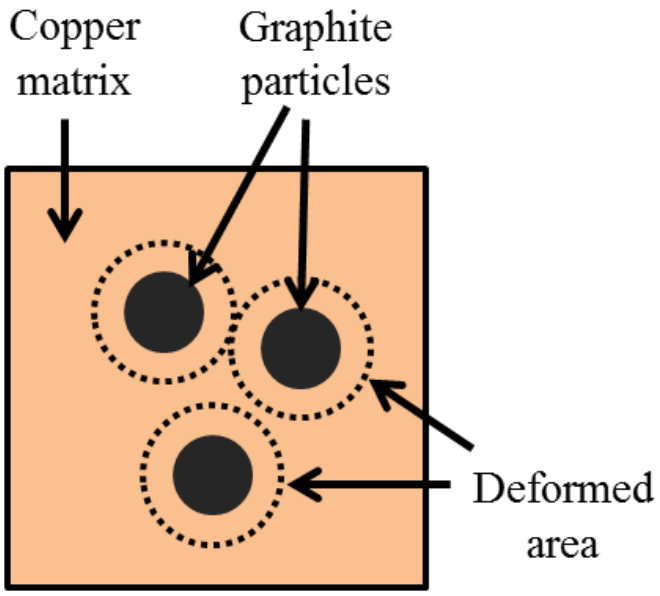

Fig. 4.15 Schematic explanation of hardening of composite

Fig. 4.16 showed the relation between the Vickers hardness and the depth from the surface of the plate. In the case of the composite prepared without an electric current flow, the Vickers hardness at the depth of 0.05 mm became larger than that at the surface. Subsequently, the hardness decreased with an increase in the depth. The spot welding contained the compression process. This compression caused the deformation of the surface, and made the surface hardened. The graphite particles which were pushed into the surface transformed the copper plate. The deformation on the surface was easily relaxed by the change in volume of the copper plate surface, but the volume could not change freely inside of the copper plate. Therefore, the hardness at the depth of 0.05 mm became larger than that at the surface due to the work hardening. In addition, the hardness gradually decreased because the work hardening did not influence deeply.

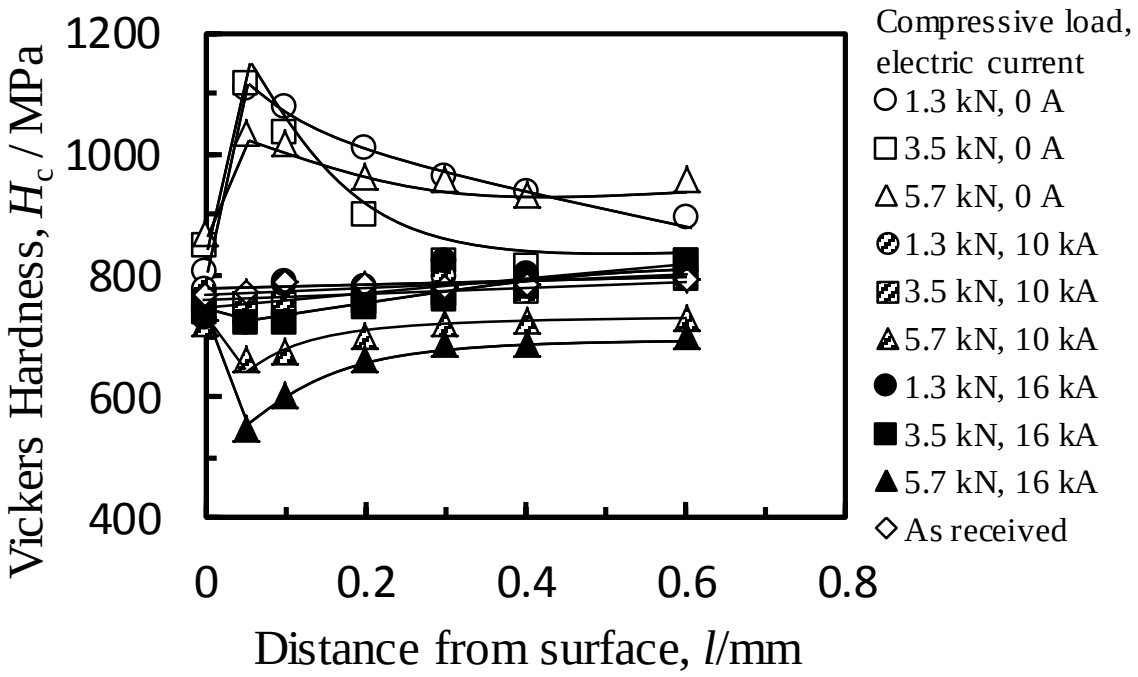

Fig. 4.16 Relation between Vickers hardness and depth from surface.

In the case of the composite prepared with an electric current flow, generally, the Vickers hardness at the depth of 0.05 mm became smaller than that at the surface. Subsequently, the hardness increased with an increase in the depth. The drop of the hardness tended to become large with increases in the compressive load and electric current. The graphite particles were scarcely observed at the depth of 0.05 mm. The copper plate was softened by the annealing. In addition, the hardness gradually increased, because the annealing did not influence deeply. From the view point of heat conduction, the temperature at the copper surface which contacted with the graphite particles was the highest, the temperature in a copper plate decreased with an increase in the depth. Therefore, it was anticipated that the hardness decreased with an increase in the depth.

4.4 Conclusion.

The copper plates which contained graphite particles between them were spot-welded to prepare the graphite dispersed copper composite on a copper plate. The results obtained were summarized as follows:

(1) The composite which was prepared only by the compression of graphite particles without an electric current flow was produced by plunging the relatively small graphite particles. The carbon content in the composite increased with the repetition number of the compression and the compressive load.

(2) When an electric current was energized through the sample at the compression, the copper around the graphite particle melted locally. The graphite particles partially or wholly dissolved into copper melt. Undissolved graphite particles adhered to the copper by the melting. The graphite particles were precipitated from the molten copper under cooling. The carbon content in the composite became higher than that prepared without an electric current flow.

(3) The Vickers hardness of the copper matrix in the composite and the volume fraction of graphite were expressed by the rule of mixtures given by eq. (4-3) and eq. (4-4).

It was tried that the graphite dispersed copper alloy composite prepared only on a copper surface with the spot welding method. The carbon content in prepared composite was approximately 50 mass%. This composite satisfied the carbon content of usual composite which demanded carbon content from approximately 20 mass% to 85 mass%.

REFERENCES

[1] S. Yokoyama, Y. Takashima, M. Nor, Y. Murata, H. Kanematsu, J. Sasano, M. Izaki: “Solubility of carbon and Vickers hardness of copper saturated with carbon”, AMPT Sept (2012) pp. 1-8

[2] P. Rogeona, P. Carrea, J. Costaa, G. Sibilia, G. Saindrenan: “Characterization of electrical contact conditions in spot welding assemblies”, J. Mater. Process Tech., vol. 195 (2008) pp. 117–124

[3] G. Pardala, S. Meco, A. Dunn, S. Williams, S. Gangulya, D. P. Hand, K. L. Wlodarczyk: “Laser spot welding of laser textured steel to aluminium”, J. Mater. Process Tech., vol. 241 (2017) pp. 24–35

[4] G. Pardal, S. Meco, S. Ganguly, S. Williams, P. Prangnell: “Dissimilar metal laser spot joining of steel to aluminium in conduction mode”, Int. J. Adv. Manuf. Technol., vol. 73 (2014) pp. 365–373

[5] R. B. Gou, W. J. Dan, W. G. Zhang: “Influence of Spot Welding on Welding Fatigue Properties of CR340 Steel Joints”, J. Iron Steel Res. Int., vol. 23 (2016) pp. 822-827

[6] C. Liu, X. Zheng, H. He, W. Wang, X. Wei: “Effect of work hardening on mechanical behavior of resistance spot welding joint during tension shear test”, Materials & Design, vol. 100 (2016) pp. 188–197

[7] The Chemical Society of Japan: Kagaku Binran Kiso Hem. Edit. 3, Maruzen, Tokyo, (1984) pp. II-494

[8] The Chemical Society of Japan: Kagaku Binran Kiso Hem. Edit. 3, Maruzen, Tokyo, (1984) pp. II-239

[9] W. D. Callister, Jr., D. G. Rethwisch: Materials Science and Engineering 9th edit., John Wiley and Sons, Asia (2011) pp. 276

[10] H. S. Kim: “On the rule of mixtures for the hardness of particle reinforced composites”, Mater. Sci. Eng., A **289** (2000) pp. 30–33.

[11] David R. Lide, CRC Handbook of Chemistry and Physics, 88th Edition, Taylor & Francis (2007) 4-56

[12] David R. Lide, CRC Handbook of Chemistry and Physics, 88th Edition, Taylor & Francis (2007) 4-61

CHAPTER 5

PREPARATION OF GRAPHITE DISPERSED COPPER COMPOSITE ON SURFACE OF COPPER PLATE WITH CARBON DIOXIDE LASER

5.1 Introduction

Laser processing is well known to be useful in many fields. Laser processing has been used for materials development as one of applications. Many researchers have employed laser beam to synthesis or coating metals. Laser can produce fine structures in surface region of the metallic substrate coated with ceramics [1]. Laser provides a concentrated heat source, which allows us to perform processing precisely and fast. The heat source from laser can lead to partially melting of substrate, which results in metallurgical bond between two materials. In addition, appropriate control of the laser beam can fabricate composite with desirable properties. A laser has been used for the preparation of substances by Nedyalkov et al. [2], the surface treatments by Garbacz et al. [3] and cutting by Yilbas et al. [4]. Al-Nimr et al. [5] reported that a laser could heat the materials locally to higher temperature for a short time. Liu et al. [6] mentioned that laser could be used for a small part such as the brush materials of a small DC motor. Tribological performance could also be improved by laser treatment [7-13]. Kang et al. [1] used laser remelting process to refine microstructure and decrease surface roughness of hypoeutectic Al-Si coating.

In the previous work [14], it was found that the solubility of graphite into molten copper steeply increased at the temperature above approximately 2100 K. In addition,

the molten copper adhered on graphite crucible when it was held at approximately 2100 K and over. This indicated that the molten copper could wet to graphite at a higher temperature.

Bulk of graphite dispersed copper composite has been demanded for sliding contact such as the pantograph. However, there are cases where surfaces of materials are covered with this composite. Then, in Chapter 4 [15], a spot welding was used for preparation of this composite on a copper surface. The carbon content in the composite prepared on the copper plate arrived up to approximately 60 mass%. In addition to a spot welder, a laser can heat the materials locally to a higher temperature for a short time. Then, the laser processing was applied in this study to prepare the graphite dispersed copper composite at the surface of a copper plate.

5.2. Experimental

5.2.1 Preparation of copper plate

A commercially available pure copper plate (purity 99.9 mass%) with 1 mm in thickness and graphite powder (99.97 mass%) with the average size of 50 μm were used in this study. The copper plate was cut into a rectangular with 15 mm width and 50 mm long by a shearing machine. The copper plate was cleaned in an ultrasonic washing machine filled with acetone to remove unnecessary substances such as grease, laboratory dust and so on. The graphite powder was ground with an agate mortar and pestle to reduce size of the graphite particle. Fig. 5.1 showed the ground graphite particles. Most of the particles were flake-like in shape with an average size of ca. 5 μm. The other particles were angular in shape with an average size of ca. 2 μm.

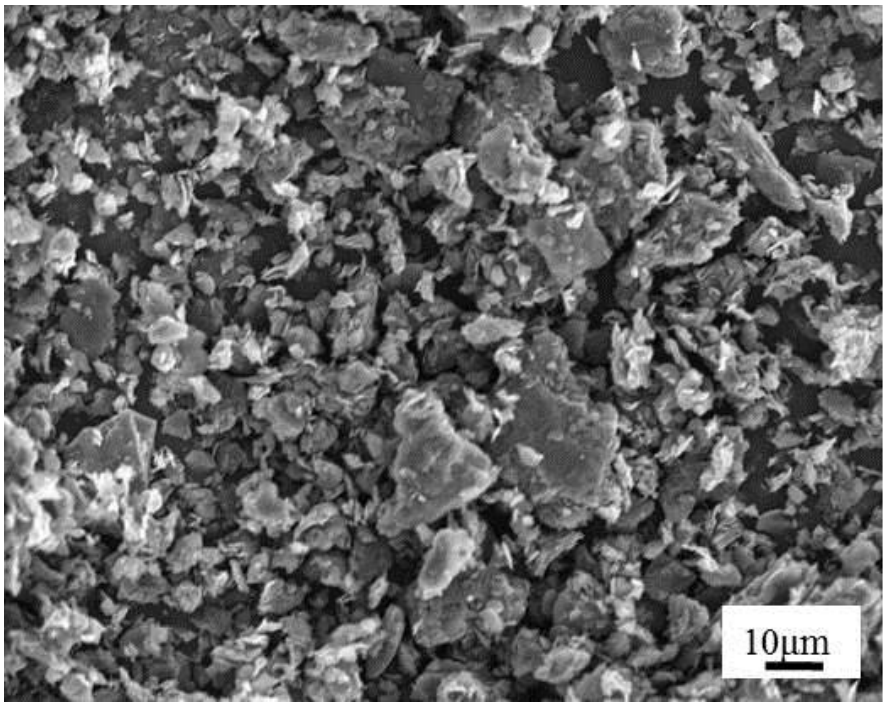

Fig. 5.1 Ground graphite particles used for experiment.

The following methods were attempted to fix graphite particles to a copper plate before laser irradiation. When a laser was irradiated to the copper plate on which graphite powder was laid simply, the graphite powder was eliminated from argon gas introduced flow introduced with laser beam. Therefore, it was needed that the graphite powder was fixed to a copper plate to prevent them from being blown off by argon gas flow. Then, it was attempted that the graphite powder was plunged into a copper plate by rolling. The copper plate with graphite powder was rolled using the rolling mill (Yoshida Kinen Co.) at room temperature with the rolling reduction ratio of 20 %. Here, the reduction ratio was given as dividing the difference between the thicknesses of the plate before rolling and the gap between the rolls with the thickness of the plate before rolling.

However, when the copper plate on which the graphite particles were put was

rolled, the roll swept out the particles from the surface of the plate. So as to deal with this removal by the rolls, an aqueous solution which was prepared with starch glue and water was painted on the copper plate. The graphite particles were put evenly on the plate surface before drying the solution. After naturally drying it, the plate with graphite particles was rolled. The graphite particles were pushed into the copper plate, but most particles were removed from the surface when the plate was tapped with a finger. When such plate was irradiated by a laser, the graphite particles on the copper plate were also removed. This indicated that the particles were not plunged into the copper plate deeply.

It was considered that the copper plate was so hard that graphite particles could not be plunged into the plate. Because the copper plate was work-hardened on its production, the copper plate was annealed to soften it. The anneal was performed under argon (purity: 99.9995 vol.%) gas flow in an electric resistance furnace at 873 K for one hour. Fig. 5.2 showed the procedure of the sample preparation used for laser irradiation.

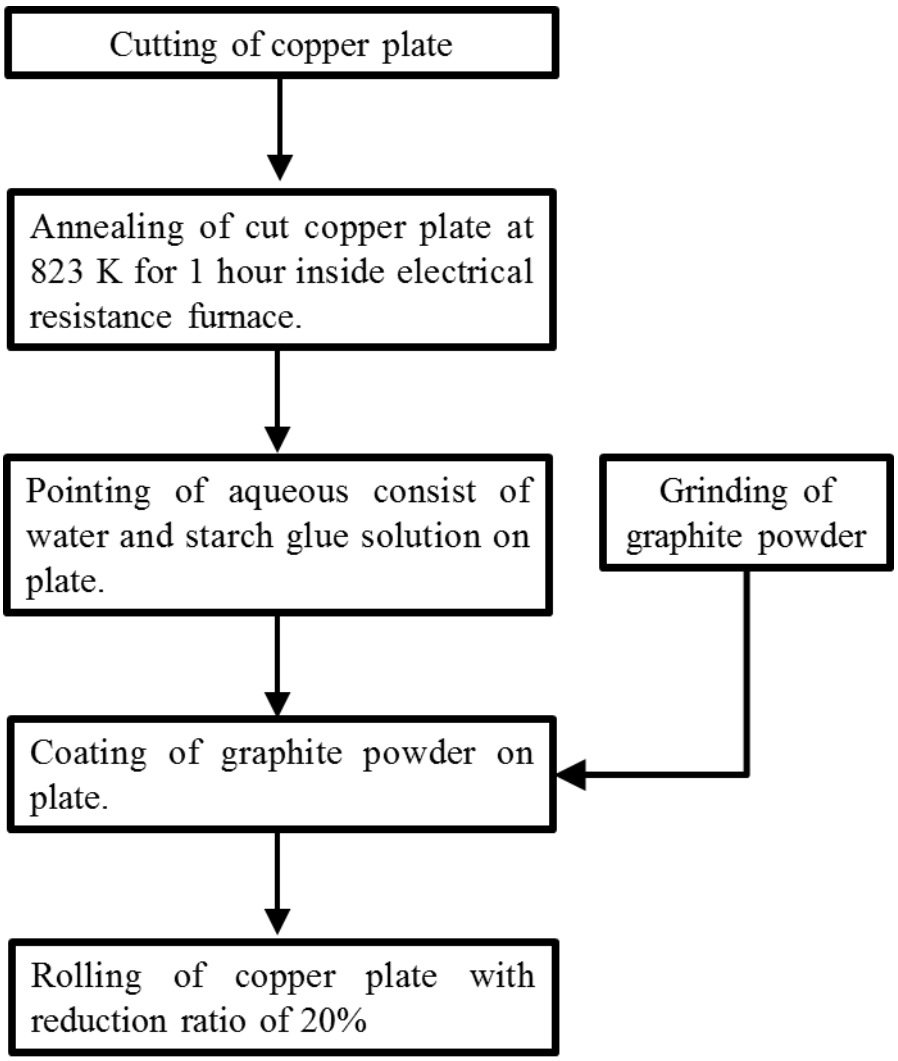

Fig. 5.2 Summarization for preparation of sample used for laser irradiation

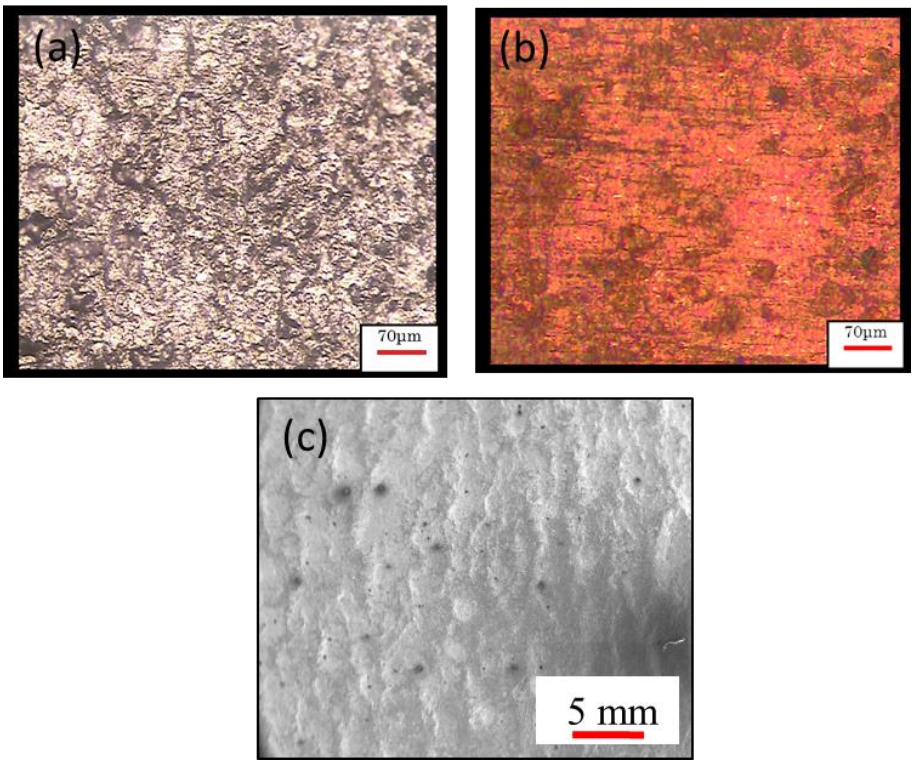

Fig. 5.3 Surfaces of copper plate rolled with graphite particle (as-rolled sample), (a), and ultrasonically washed as-rolled sample (ultrasonic-cleaned sample), (b). Fig. 5.3 (c) was the microscopic image of Fig. 5.3 (b).

Fig. 5.3 (a) showed the copper plate which was rolled with the graphite particles. The particles covered the copper plate. When the copper plate with graphite particles was rolled, the particles were plunged into the copper plate. The relatively large flat particles were shallowly pushed into the copper plate, whereas the relatively small angular particles were stuck into the copper plate by the rolling. Both particles were mechanically fixed by the deformation of the copper plate. The graphite particles which were plunged into the copper plate by rolling did not fall with a finger tapping. Afterwards, this sample was called “as-rolled sample”. However, the relatively large flat particles on the as-rolled sample were removed after the ultrasonic-washing, as shown

in Fig. 5.3 (b). As shown in Fig. 5.3 (c), the relatively small angular particles were fixed so firmly that they were not eliminated even by the ultrasonic cleaning. Afterwards, the sample which was ultrasonic-washed after the rolling was called “ultrasonic-cleaned sample”.

5.2.2 Procedure

Fig. 5.4 showed the schematic of main part of experimental apparatus. Carbon dioxide gas laser (Mitsubishi Electric ML806T3+3016C) was irradiated to the as-rolled sample. The laser was operated at a single mode with power of 3 kW per one pulse and 10 pulses per laser irradiation time of one second, and spot diameter of ca. 12 mm. The irradiation time was changed from 2 s (200 pulses) to 24 s (240 pulses). Argon gas (99.9995 vol%) was introduced through a nozzle before, during and after the laser irradiation to prevent both the copper plate and the graphite particles from being oxidized. In addition, a paper circular tube was placed around the copper plate to prevent the argon from being mixed by the air. After the laser irradiation, the copper plate was cooled to the room temperature under an argon gas flow.

After the laser irradiation, the copper plate was immersed in an ultrasonic washing machine to remove unnecessary graphite particles from the plate. The graphite particles which were not removed by this ultrasonic cleaning was considered to be the particles firmly adhered to the copper plate. The surface of the copper plate was observed using laser microscope (KEYENCE VK 8510) and SEM (scanning electron microscope, JEOL JSM6300). Similarly, the cross section of the plate in a resin was also observed with them. Carbon content of the surface was analyzed with an EDX (Energy dispersive X-ray spectroscopy) equipped with the SEM. Area with approximately 100 μm square

was analyzed with the EDX. The EDX gave the total carbon content which was sum of carbon as graphite particles and dissolved carbon into a copper plate. However, because the carbon content dissolved into a copper plate was not so large [14], the carbon content given with an EDX mainly represented the amount of the graphite particles on the surface. Naturally, carbon content in the as received copper plate was zero mass%. The carbon content in the as-rolled sample and the ultrasonic-cleaned sample this was approximately 22 mass% and 1.1 mass% respectively. The difference in carbon content between the as-rolled sample and the ultrasonic-cleaned sample expressed the quantity of the graphite particles which was removed by the ultrasonic cleaning. In addition, the difference in carbon content between the ultrasonic-cleaned sample and the as received copper showed the quantity of the angular particles which were fixed so firmly.

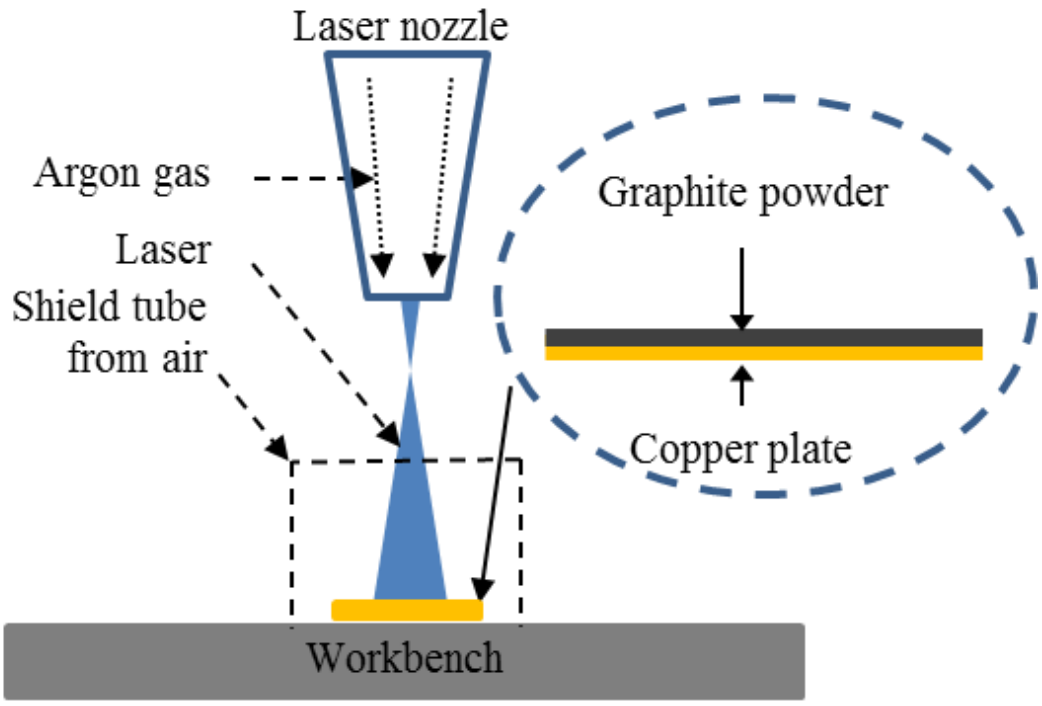

Fig. 5.4 Main part of apparatus with laser emission.

Micro Vickers hardness of the copper matrix of the composite was measured with the Micro Hardness Tester (HMV Shimadzu) on the load condition of 0.98 N. The hardness was measured at five positions which were the same radial distance from the center of the laser spot. The hardness was evaluated with the mean of ten measured values. The maximum scattering was ± 10% for the average value.

5.3. Results and discussion

5.3.1 Fixation and elimination of graphite particles

1) Carbon content

Fig. 5.5 showed the relation between the carbon content on the copper surface and the radial distance from the center of the laser spot. The carbon content which was laser-irradiated for 6 s was almost constant below the distance of approximately 5.5 mm. This carbon content was smaller than that in the as-rolled sample, and larger than that in the ultrasonic-cleaned sample. This meant that some of the graphite particles which should be removed by the ultrasonic cleaning were fixed in the copper plate. This distance of approximately 5.5 mm was almost the same as the radius of the laser spot. Subsequently, the carbon content decreased with an increase in the distance, and became constant. This constant value was the same as the content in the ultrasonic-cleaned sample. In the case that the copper plates were irradiated for 12 s, the carbon contents in the region of the laser spot were almost the constant irrespective to the distance. This carbon content was somewhat larger than that in the ultrasonic-cleaned sample. Subsequently, the carbon content increased with an increase in the distance. After the carbon content at the distance of 7 mm showed the maximum, it decreased to the content in the ultrasonic-cleaned sample. In the case that the copper plates were

irradiated by the laser for 24 s, the carbon contents in the region of the laser spot were zero mass%, and were lower than that in the ultrasonic-cleaned sample. These carbon contents were almost the constant irrespective to the distance. Subsequently, the carbon content increased around the periphery of the laser spot to the carbon content in the as-rolled sample, as the distance increased. After the carbon content was constant below the distance of approximately 10 mm, it decreased with an increase in the distance. The mechanism of the behavior of the carbon content was described later.

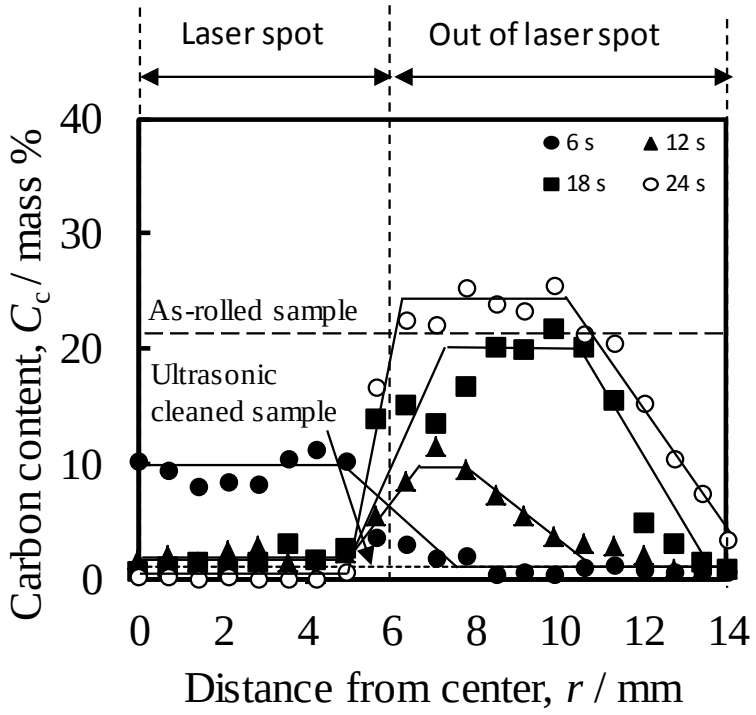

Fig. 5.5 Change in carbon content with radial distance from center of laser spot.

Fig. 5.6 showed the relation between the carbon content and the laser irradiation time. The carbon content at the center of the laser spot steeply decreased from the content of the as-rolled sample until 11 s of the laser irradiation time. Subsequently, it decreased gradually and finally reached the carbon content of ultrasonic cleaned sample.

The carbon content at 7 mm of the distance from the center of the laser spot, the position was the outside of the laser spot, increased from the carbon content which was larger than that in the ultrasonic-cleaned sample to the carbon content in the as-rolled sample.

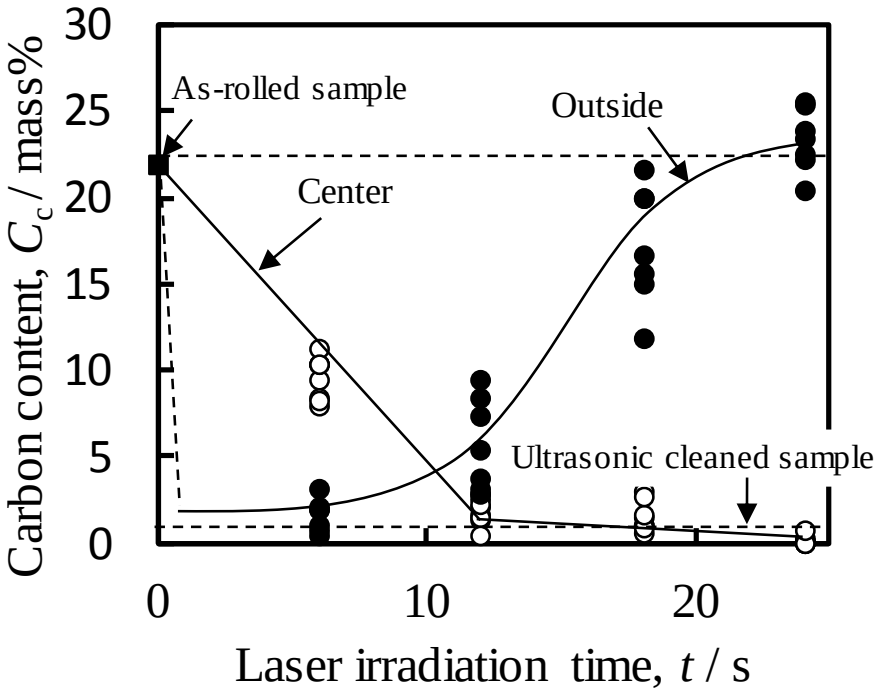

Fig. 5.6 Change in carbon content with laser irradiation time. Center and outside in this figure indicated the center of the laser spot and the position which was 7 mm from the center of the laser spot respectively.

2) Observation of surface of copper plate

Fig. 5.7 showed the center area of the surface of the copper plate irradiated with the laser. First, the black particles were identified to be graphite by the EDS. In addition, dark and light gray domains which were observed in Figs. 5.7 (b), (c) and (d) were indifferent each other in chemical composition by the EDS. Second, the relatively large

particles which were more than approximately 8 μm were not observed in these figures. Instead, some hollows like craters were observed. Judging from the sizes and shapes of the hollows, the hollows were traces where the particles were pushed in by rolling.

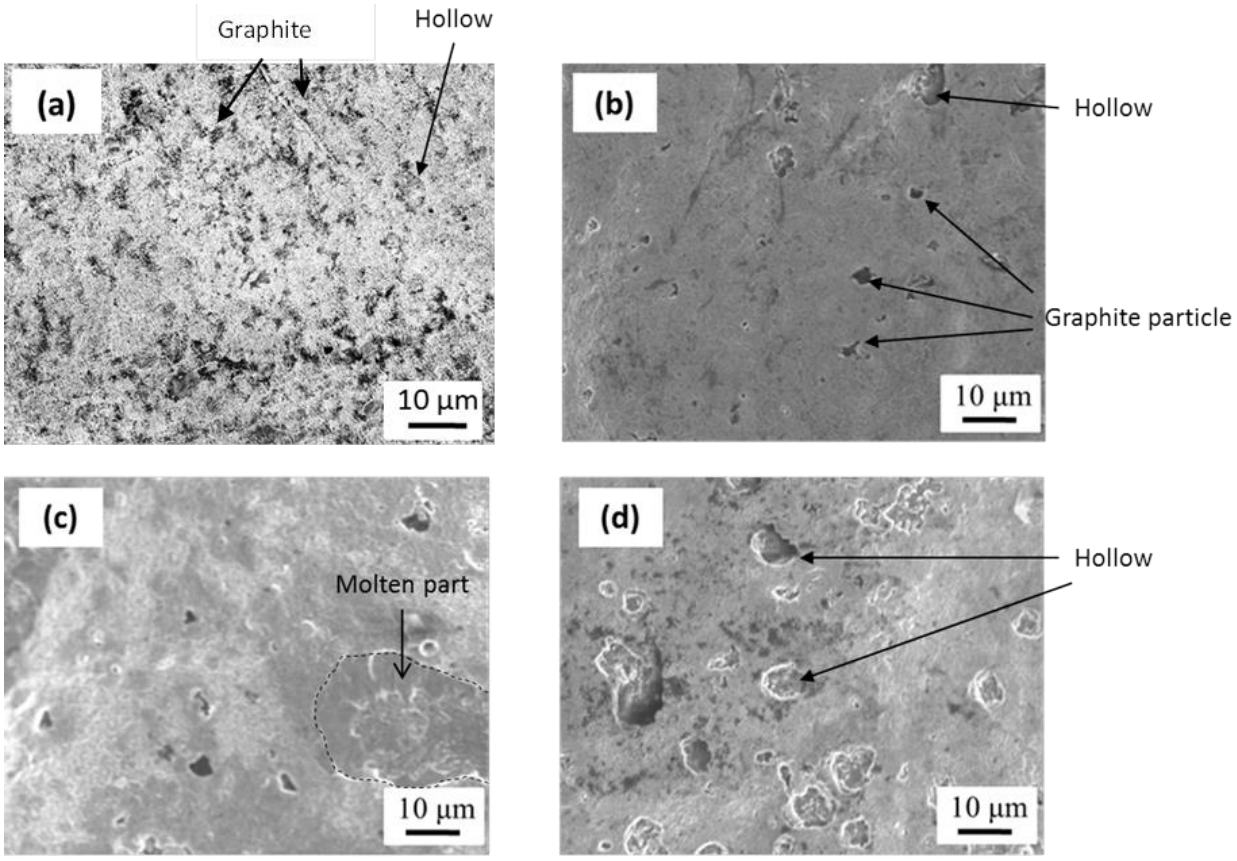

Fig. 5.7 Center of copper plate irradiated with laser for (a) 6 s, (b) 12 s, (c) 18 s and (d) 24 s. The position was the center of the laser spot.

The number of relatively small particles which were less than approximately 5 μm decreased with the increase in the laser irradiation time. The particles of under around 2 μm in size were observed in Fig. 5.7 (a). These small particles disappeared at and after the laser irradiation time of 12 s, as shown in Figs. 5.7 (b) ~ (d). Finally, the surfaces of the part except the hollows, as shown in Figs. 5.7 (b) ~ (d), became flatter than the

surface shown in Fig. 5.7 (a). This flattering depended on the fusion of the copper. Fig. 5.7 (c) showed molten part as an example. This molten part was observed everywhere on the sample. The change in the number of the graphite particles with time corresponded with the change in the carbon content with time as shown in Fig. 5.6.

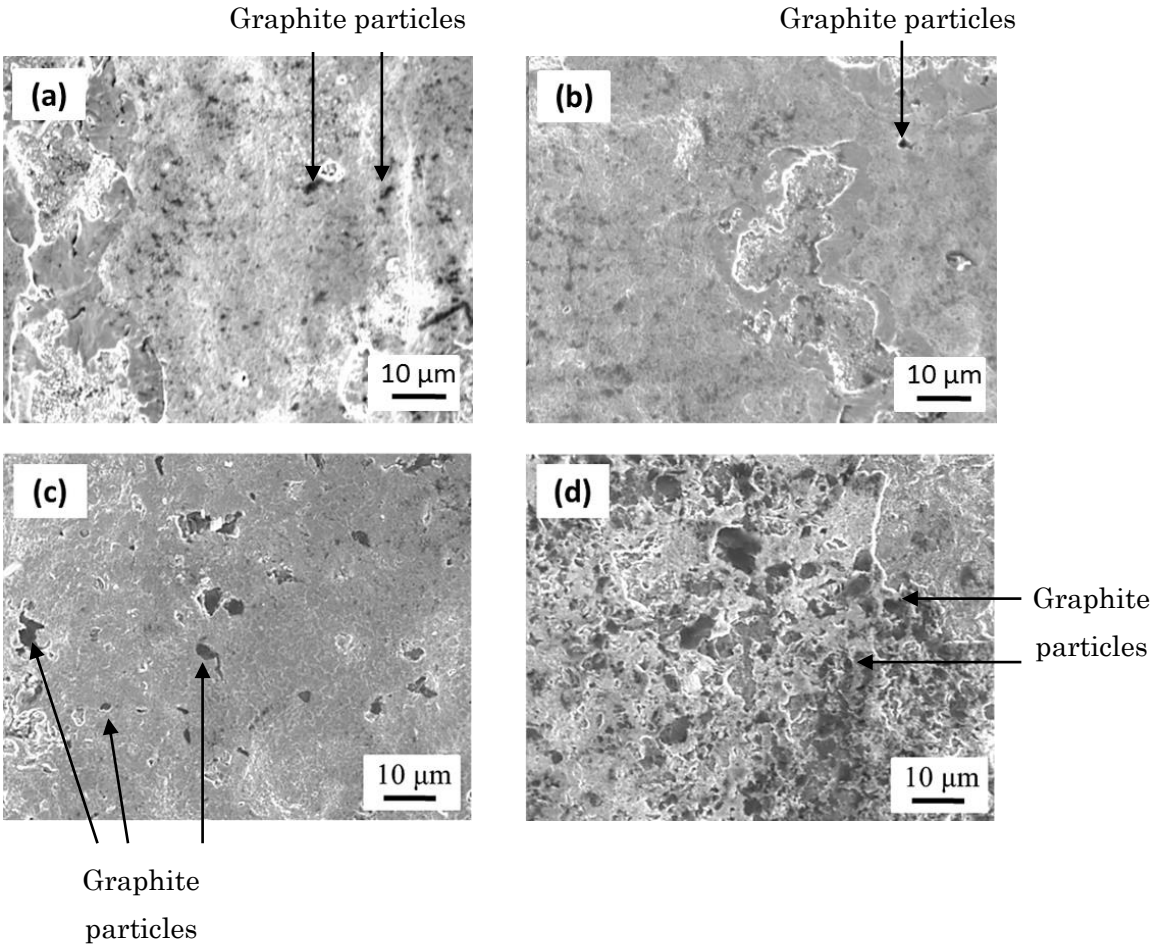

Fig. 5.8 Outside of laser spot of copper plate irradiated with laser for (a) 6 s, (b) 12 s, (c) 18 s and (d) 24 s. The position was approximately 7 mm apart from the center of the laser spot.

Fig. 5.8 showed the surface at the outside of the laser spot. This position was

approximately 7 mm from the center of the laser spot. First, the relatively large particles which were more than approximately 8 μm were not observed on the sample after the laser irradiation of 6 s, and the number of them increased with the increase in the laser-emission time. Therefore, the hollows which were traces of plunged the relatively large particles decreased with the laser irradiation time. The number of relatively small particles which were less than approximately 5 μm was unchanged with the increase in the laser irradiation time. Accordingly, quantity of the graphite particles increased with the increased in the laser irradiation time. This behavior of the quantity of graphite particles was almost the same as that of the carbon content as shown in Fig. 5.6.

Fig. 5.9 showed the cross section of copper plate after the of laser irradiation of 24 s. First, some graphite particles were observed at the cross section. These particles were observed even at the place where was apart from the laser spot, and this meant that these particles were caught in the copper from the surface at the time of polishing. In addition, any graphite particles did not appeared at this cross section even if the sample was annealed at 2073 K for one hour. Therefore, graphite particles did not dissolve in molten copper. Second, the surface of the copper plate was not flat but concave. This resulted from graphite particles thickness on the copper plate was not uniform at the rolling. In addition, this uneven surface suggested that entire surface was not melted.

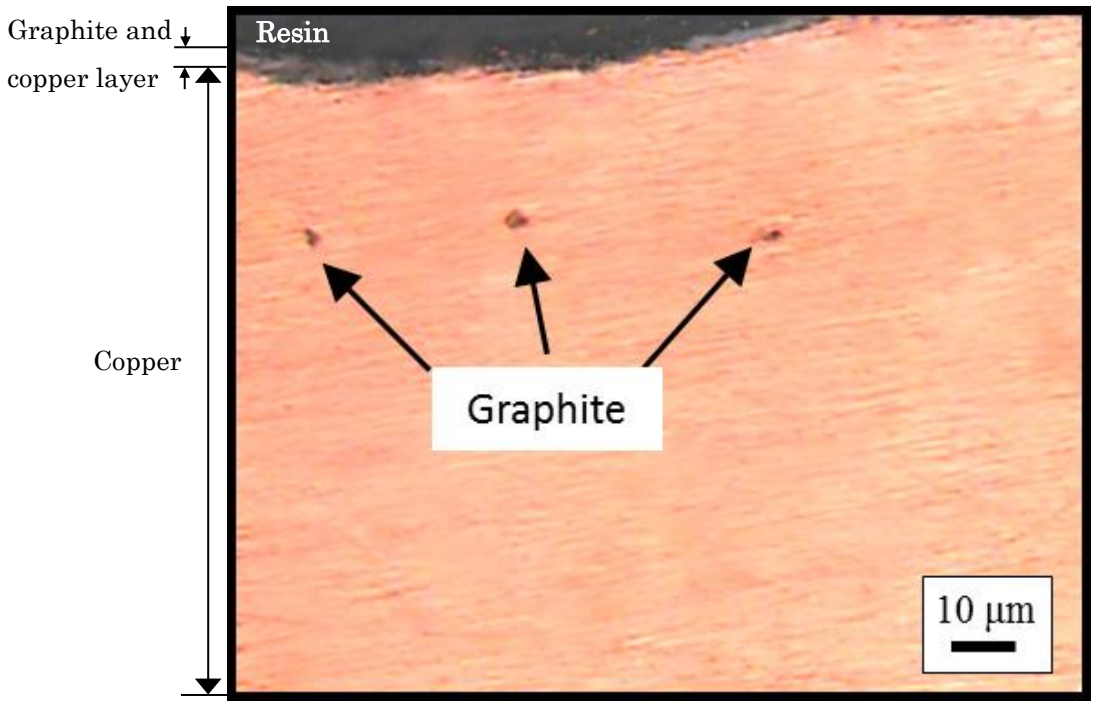

Fig. 5.9 Cross section of copper surface after laser irradiation of 24 s.

Figs. 5.10 showed the upper part of the cross section after the laser irradiation of 24 s. Here, figs. 5.10 (b) and (d) were schematics for Figs. 5.10 (a) and (c) respectively. As shown in Figs. 5.10 (a) and (b), the surface of the copper at the left hand side of the graphite particle showed the convex in the downward direction, whereas the surface of the copper at the right hand side of the graphite particle was obscure. The contact angle was approximately 80 degrees, and this indicated that the molten copper wetted the graphite particle. Similarly, as shown in Figs. 5.7 (c) and (d), the surfaces of the copper at the left and the right hand side of the graphite particle showed that the molten copper wetted the graphite particle because of the contact angle of approximately 80 degrees. The contact angles could not be measured for the melt during the laser radiation. The measured contact angles were for the solidified samples. However, it could be said that the molten copper wetted well graphite particle. In our previous work [14], the molten

copper which was held at approximately 2100 K or over could wet graphite. This wetting also indicated that temperature of copper around the graphite particle arrived at the temperature beyond approximately 2100 K.

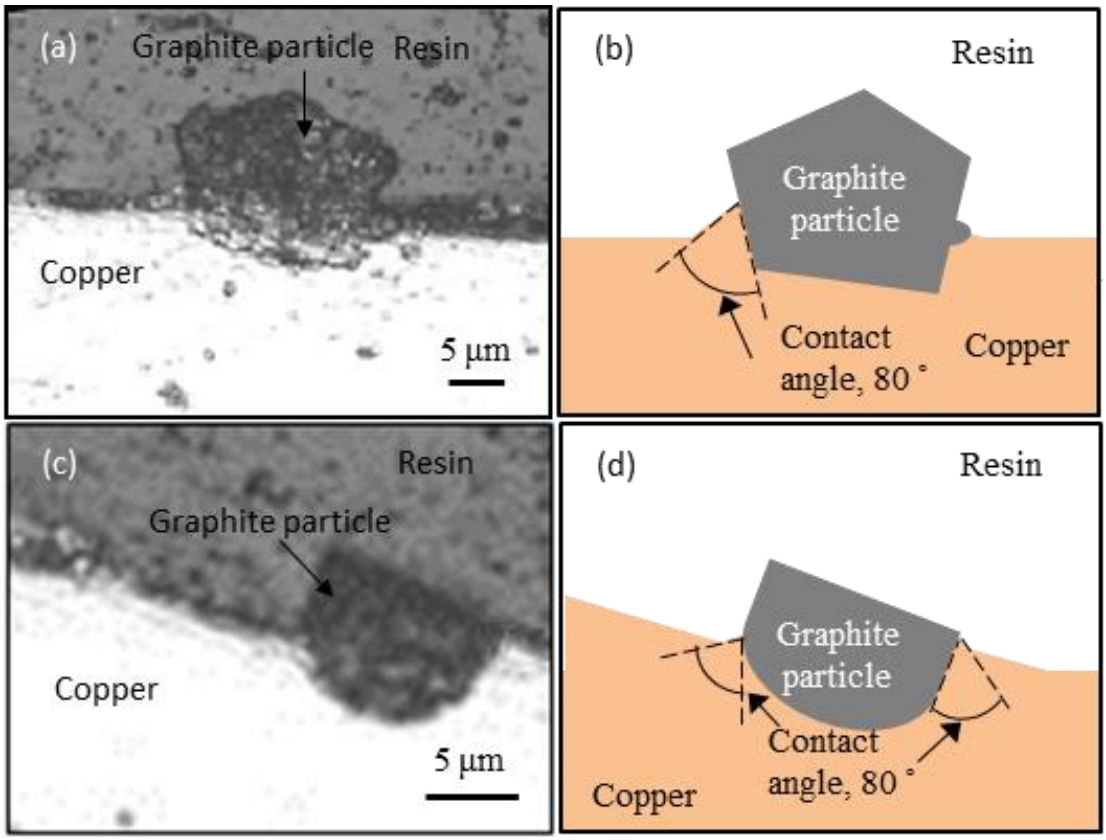

Fig. 5.10 Upper part of cross section of copper plate at radial distance of 8 mm from center of laser spot after laser irradiation of 18 s. Figs. (b) and (d) were schematic of Figs. (a) and (c) respectively.

3) Mechanism of composite

It was assumed that the surface of the copper plate with surface area, A [m^2], was suddenly supplied by the heat, Q_0 [$J \cdot s^{-1}$] from the laser. Unsteady heat conduction for a semi-infinite body was given by the following equation, and initial and boundary

conditions:

$$\frac{\partial^2 T}{\partial x^2} = \frac{1}{\alpha}\frac{\partial T}{\partial t} \quad \left(\alpha = \frac{\lambda}{\rho C_p}\right) \tag{5-1}$$

$$t = 0, x \geq 0 \rightarrow T = T_0$$
$$t > 0, x = 0 \rightarrow \frac{Q_0}{A} = -\lambda\frac{\partial T}{\partial x} \tag{5-2}$$

where T was the temperature [K], x the depth from the surface [m], t the time [s], α the thermal diffusivity [$m^2 \cdot s^{-1}$], C_p the specific heat capacity at constant pressure [$J \cdot kg^{-1} \cdot K^{-1}$], ρ the density [$kg \cdot m^{-3}$], and λ the thermal conductivity [$W \cdot m^{-1} \cdot K^{-1}$]. From eq. (5-1) and eq. (5-2), the temperature distribution was given as:

$$T - T_0 = \frac{2Q_0\sqrt{\alpha t/\pi}}{\lambda A}\exp\left(-\frac{x^2}{4\alpha t}\right) - \frac{Q_0 x}{\lambda A}\left\{1 - \mathrm{erf}\left(\frac{x}{2\sqrt{\alpha t}}\right)\right\} \tag{5-3}$$

Here, the following values were used for the calculation of eq. (5-3). A was 1.13×10^{-4} m^2 from diameter of the laser spot. In addition, Q_0 was set to be 3000 $J \cdot s^{-1}$ which was the input energy for the laser, whereas the all input energy was not used for heat.

Fig. 5.11 showed the temperature distribution. In the case that the laser irradiation time was constant, the temperature at the surface was high and decreased gradually with the increase in the depth. Generally, the temperature became high with the increase in the laser irradiation time. The difference in temperature between the surface and the backside of the copper plate was small because of the high heat conductivity of copper. Whereas the one-directional heat conduction model expressed by eq. (5-1) and eq. (5-2) could not be applied to the phenomena with three-dimensional heat conduction, this

calculated results also indicated that heat easily conduct from the laser spot to the radial direction. The temperature at the surface exceeded the melting point of copper after the laser irradiation time of approximately 1.7 s. Similarly, the temperature at backside of the copper plate exceeded the melting point after the irradiation time of approximately 1.8 s. However, in this work, the backside of the copper plate did not melt even if the laser was emitted to the copper plate for 24 s.

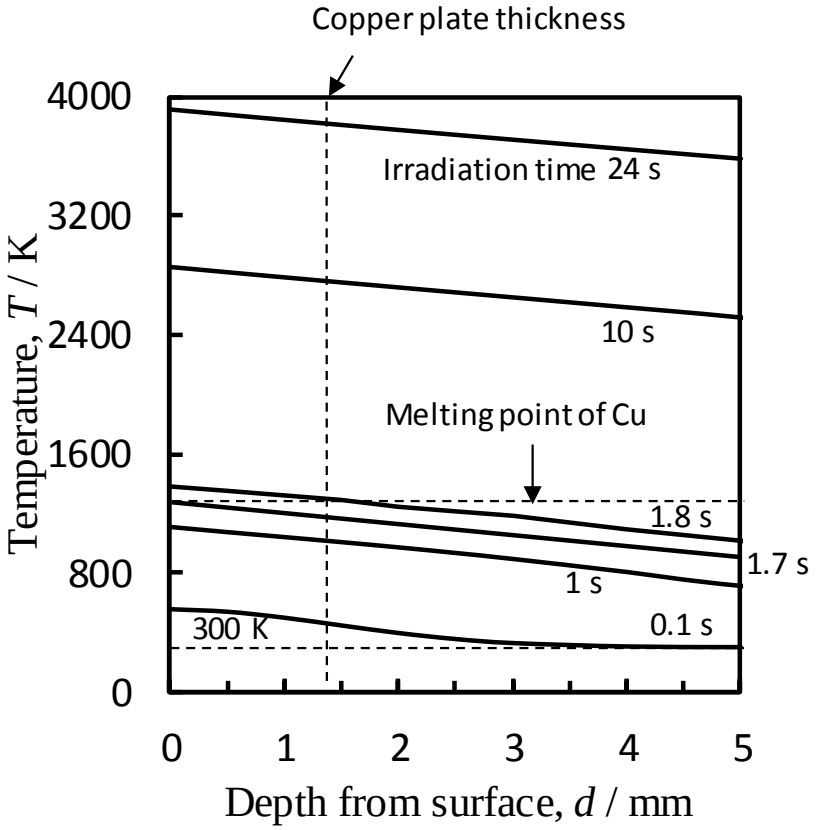

Fig. 5.11 Temperature distribution in the copper plate given by heat conduction in case of constant heat supply.

Usually, a metal was not so heated by the laser, because it reflected most laser [16]. Therefore, absorption agent like carbonaceous material was painted on a metal

before a laser cutting for example. The graphite was mainly absorbed the laser, and was heated. As another of the characteristics, a laser could catch a particle, which was called “laser trapping”. When the laser was irradiated to the copper plate with the graphite particles, the graphite particles which were relatively large and flat in shape were eliminated by the laser trapping.

Fig. 5.12 showed the schematic explanation for the phenomena occurred under the laser-irradiation. The phenomena occurred in the area of the laser spot were as follows: When graphite particles on the copper plate were irradiated with a laser for 6 s, the relatively large particles which were shallowly pushed into the copper plate were removed by the laser trapping. Hence, the traces in which the particles were pushed remained. However, the particles which were plunged into the copper plate deeply remained and heated. Copper around the graphite particles was heated and melted partly. This heating enhanced the adhesion between the graphite particles and the copper plate. Therefore, the graphite particles adhered on the copper plate could not be eliminated by the ultrasonic cleaning. When the sample was laser-irradiated furthermore, the copper around the remained graphite melted more. The remained particles were eliminated by the laser trapping. Here, fixation of the graphite particles indicated that the temperature of copper around the particles was beyond approximately 2100 K. The graphite particles might dissolve into molten copper because the solubility of carbon steeply increased beyond this temperature [14]. As mentioned earlier, no graphite precipitated from the copper. It was considered that the amount of dissolution was small.

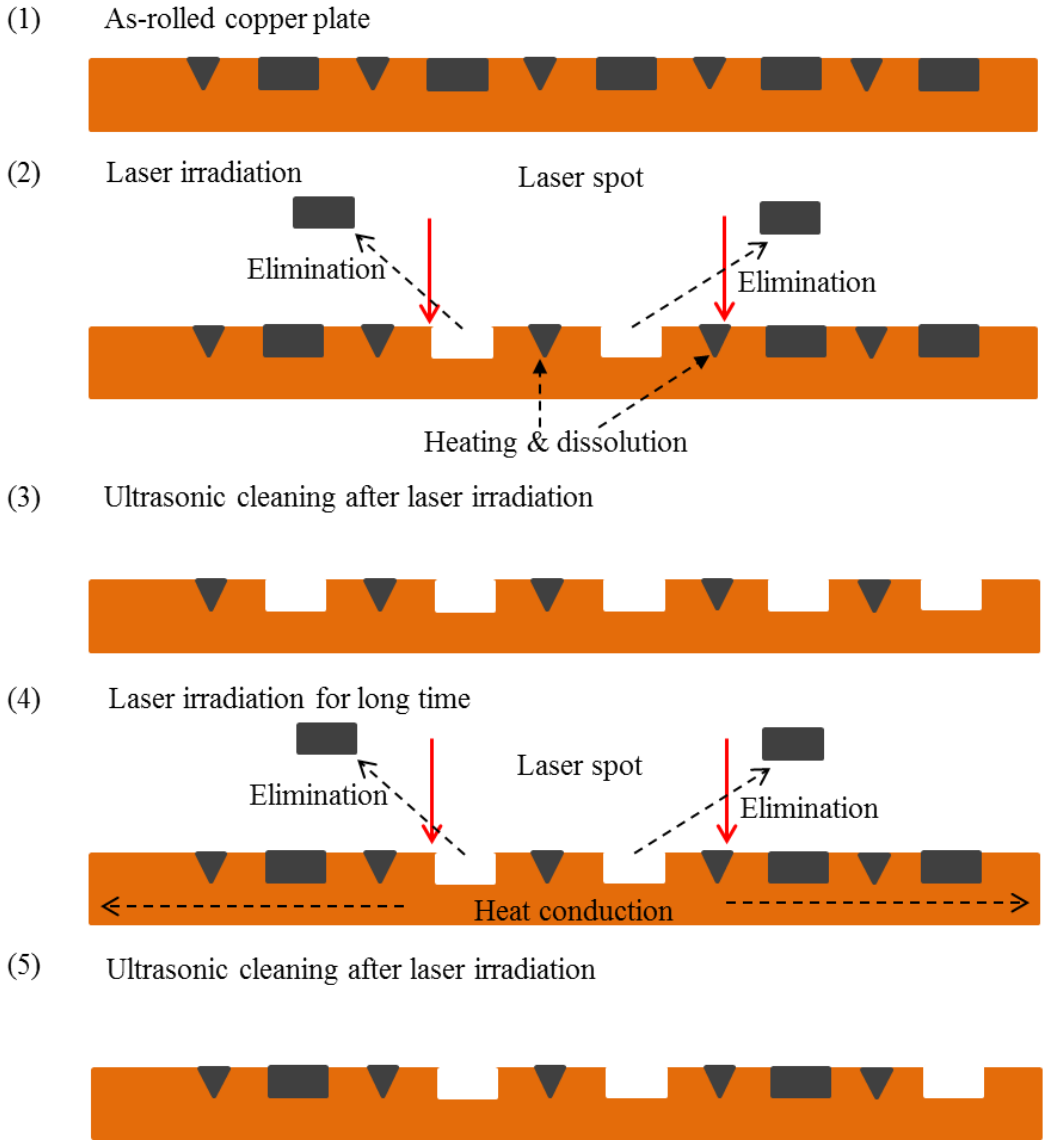

Fig. 5.12 Schematic explanation of fixation and elimination of graphite particles by laser irradiation.

The outside of the laser spot was not laser-heated and not laser-trapped. This are could be heated by the conduction from the laser spot. Therefore, the particles at outside of the laser spot were fixed by the wetting. This thing indicated that the temperature of the molten copper was beyond approximately 2100 K. The fixed particles increased with the increase in the laser irradiation time. The region of the fixation of the particles

became wider with the increase in the laser irradiation time. The particles were not fixed at the area so far from the laser spot.

This consideration suggested the following things so as to prepare locally the graphite dispersed copper composite on a copper plate with a laser: The graphite particles must be plunged into a copper plate. In the case that a laser was irradiated at the place where the particles were wanted to adhere, a laser irradiation time should be shortened. As another method, a laser was irradiated around the place where the particles were wanted to adhere.

5.3.2 Vickers hardness

Fig. 5.13 showed the relation between the Vickers hardness and the time of laser irradiation. The hardness of as rolled copper plate and copper plate annealed under argon gas flow at 1073 K were also shown in this figure. The Vickers hardness of the copper plate irradiated by a laser for 2 s was almost the same as the hardness of as rolled copper. The Vickers hardness decreased to the hardness of the annealed copper with the increase in the laser irradiation time, and the hardness for the sample laser-irradiated for 18 s or over was almost constant. The copper plate was sufficiently annealed because of the constant hardness. The surface composite of the copper plate was work-hardened by rolling. The temperature rise of the copper plate by the laser irradiation annealed the copper plate, and this decreased the hardness. Therefore, this indicated that the laser irradiation could anneal metal locally. As shown in Fig. 5.13, the Vickers hardness at the center of the laser spot was lower than that at outside of the spot by approximately 100 MPa. It could be said that the hardness at the outside where many graphite particles existed was larger than that at the center where a few graphite particles existed.

However, contribution of graphite particles to the hardness was small.

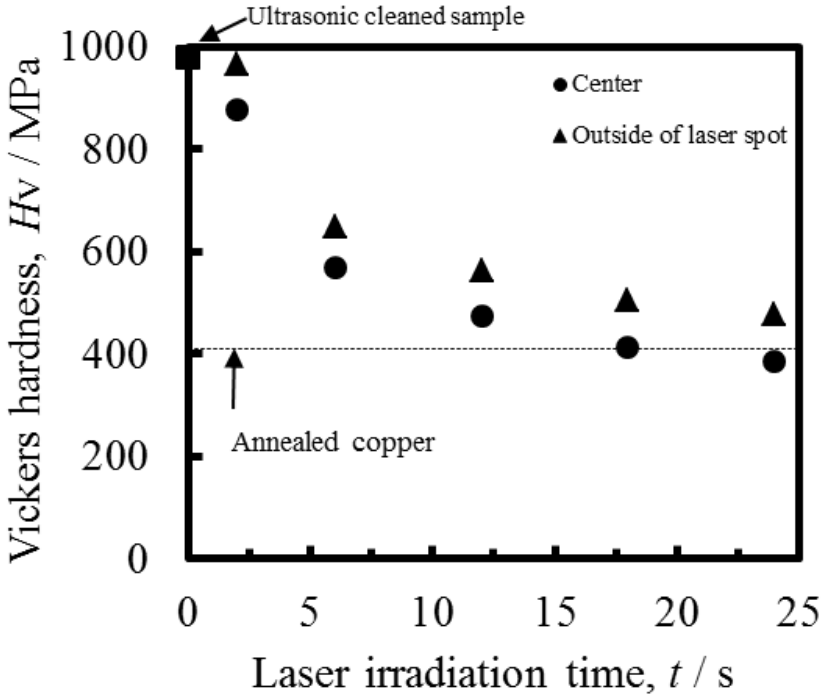

Fig. 5.13 Relation between Vickers hardness and laser irradiation time.

Fig. 5.14 showed the relation between the Vickers hardness and the carbon content. There was not distinctive relation between them. The relation between the hardness of the composite and the carbon content for the sample which was prepared with the spot welding was also shown in this figure. The sample with relatively high Vickers hardness was prepared with relatively shorter laser irradiation time. Therefore, these hardness were almost the same as that prepared by a spot welding the sample without an electric current flow. The hardness of the sample prepared with relatively longer laser irradiation time was almost the same as those prepared by a spot welding the sample with an electric current flow. The composite prepared by a spot welding with compressive load of 5.7 kN and electric current of 16 kA was most annealed in the

composite prepared by a spot welding with loading of 1.3 kN -5.7 kN and electric current of 10 kA and 16 kA. The hardness of the composite prepared by a laser irradiation was smaller than that prepared by a spot welding on such conditions. This indicated the heat by the laser heat annealed the composite sufficiently.

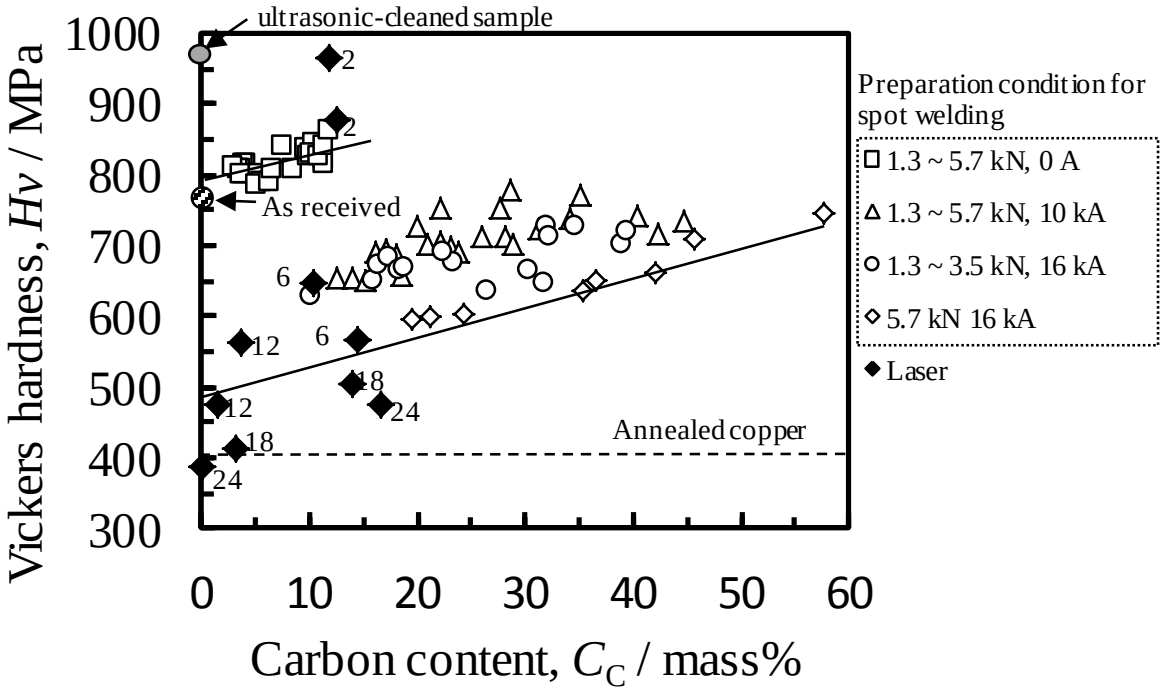

Fig. 5.14 Relation between Vickers hardness and carbon content. Labeled number expressed the laser irradiation time [s].

The rule of mixtures could express the properties of a bulk composite such as the stress, the elastic modulus, the strain and so on. The two equations which expressed the upper and the lower bounds for the properties of particle-reinforced composites were known [18]. In this study, the composite material was prepared only on the copper surface. In addition, the hardness of an only copper matrix in the composite was measured. Applying these equations which gave the bounds to the hardness of this

composite, the following equations were obtained [19].

$$H_{\mathrm{C}} = H_{\mathrm{Cu}}(1 - f_{\mathrm{g}}) + H_{\mathrm{g}} f_{\mathrm{g}} \qquad (5\text{-}4)\ \text{(reshown, see Chap. 4)}$$

$$\frac{1}{H_{\mathrm{C}}} = \frac{1 - f_{\mathrm{g}}}{H_{\mathrm{Cu}}} + \frac{f_{\mathrm{g}}}{H_{\mathrm{g}}} \qquad (5\text{-}5)\ \text{(reshown, see Chap. 4)}$$

where H was the hardness [Pa], f the volume fraction, subscript C, Cu and g indicated the composite, copper and graphite respectively.

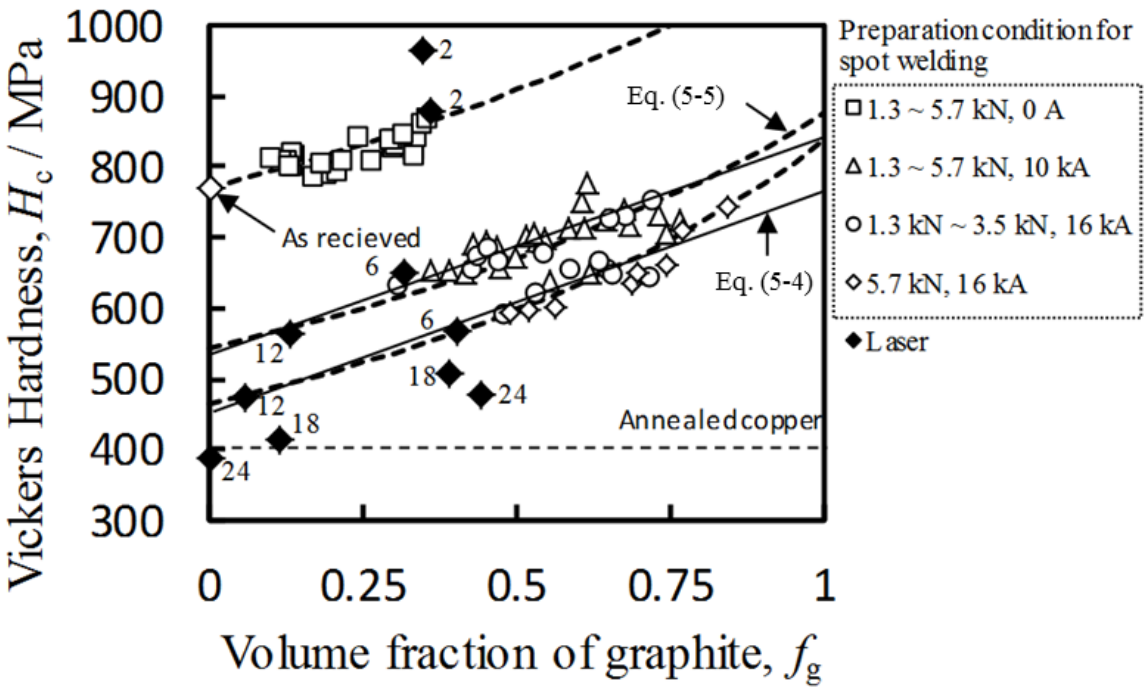

Fig. 5.15 Adaptability of Vickers hardness to composite law. Labeled number expressed the laser irradiation time [s].

Fig. 5.15 showed the relation between the Vickers hardness and the volume fraction of graphite. Here, the volume fraction of graphite was calculated by using mass percentage of carbon, densities of graphite and copper [20][21]. There was no

distinctive relation between them. Accordingly, the hardness of the composite prepared by the laser irradiation could not be expressed by the rule of mixtures. This resulted from that the hardness of copper matrix, H_{Cu}, was influenced by the laser irradiation time, namely the annealing. In addition, the rule of mixtures was adaptable for the properties of a bulk composite such as the stress the elastic modulus, the strain and so on. As described above, relatively high Vickers hardness were almost the same as that prepared by a spot welding the sample without an electric current flow. The hardness of the sample prepared with relatively longer laser irradiation time was almost the same as those prepared by a spot welding the sample with an electric current flow. The hardness of the composite prepared by a laser irradiation was smaller than that sufficiently annealed by a spot welding.

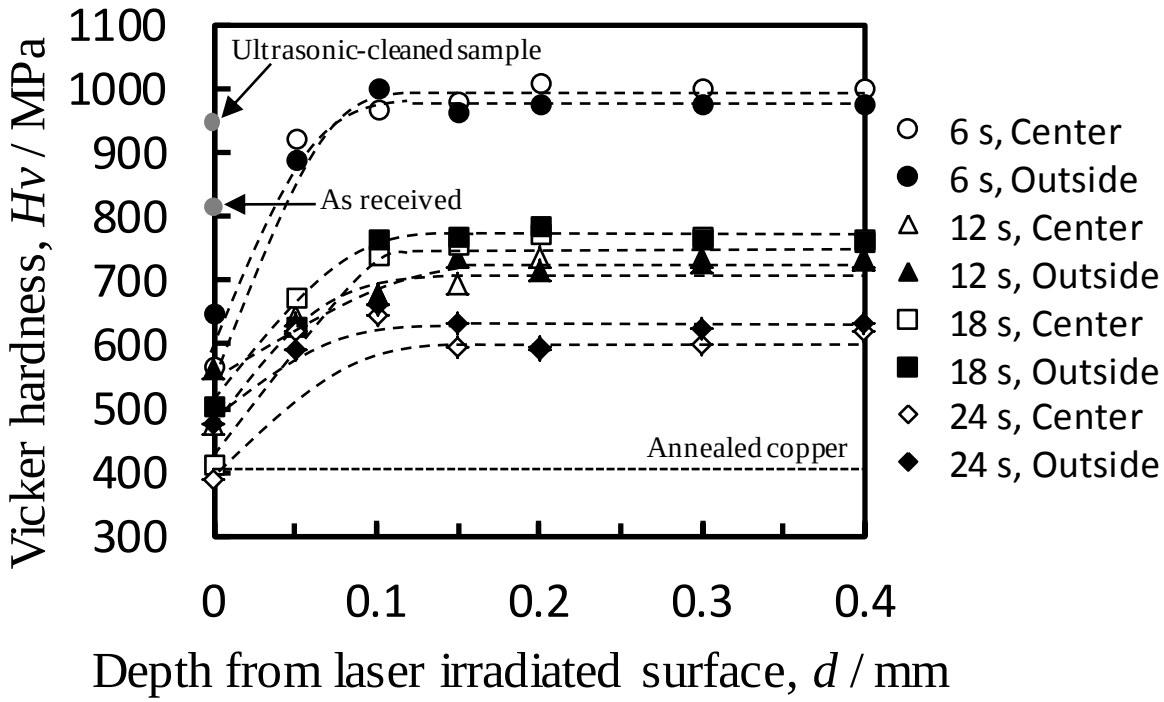

Fig. 5.16 Relation between Vickers hardness and depth from laser irradiated surface.

Fig. 5.16 showed the relation between the Vickers hardness and the depth from surface where the laser was irradiated. In general, the hardness increased with an increase in the depth until the depth of 0.1 mm. Subsequently, it was constant irrespective to the depth. In addition, the hardness decreased with an increase in the laser irradiation time. Whereas the hardness for the center at the surface was smaller than that for the outside of the laser spot, as shown in Fig. 5.13, the hardness of the inner side from the surface of the copper was almost the same irrespective to the position.

5.4. Conclusion

It was tried in this study that graphite dispersed copper composite was prepared locally on the surface of the copper plate with the CO_2 laser. Then, after graphite particles were plunged into a copper plate by rolling, the laser was irradiated on the plate. Obtained results were summarized as follows:

1) Laser could heat a substance and catch a particle. When the laser was irradiated on the graphite particles for a short time, the graphite particles which were pushed into the plate deeply adhered on the surface of the plate, whereas the graphite particles which were pushed shallowly were eliminated by laser trapping. When the laser was irradiated for a longer time, surrounding of the remained graphite particles was melted. Most all graphite particles were eliminated from the surface by the laser trapping.

2) The graphite particles at the outside of the laser spot were easy to remain on the copper plate because the laser trapping did not act there in comparison with the spot. This area was heated by the heat conduction from the laser spot, and the surface melted. The particles was fixed by the wetting. The graphite dispersed copper composite could

be prepared if the laser was irradiated near the place where we want to form the composite However, the graphite particles were half-afloat from the copper plate.

3) Vickers hardness decreased with an increase in the laser irradiation time due to the annealing. The hardness at the outside of the laser spot where the graphite particles more remained was larger by approximately 100 MPa than that at the center.

It was tried that the graphite dispersed copper alloy composite prepared only on a copper surface with CO_2 laser. The carbon content in the prepared composite was up to approximately 20 mass%. This composite satisfied lower level of the carbon content from approximately 20 mass% to 85 mass%.

REFERENCES

[1] N. Kang, C. Verdy, P. Coddet, Y. Xie, Y. Fu, H. Liao, C. Coddet: “Effects of laser remelting process on the microstructure, roughness and microhardness of in-situ cold sprayed hypoeutectic Al-Si coating”, Surf. Coat. Technol., vol. 318 (2017) pp. 355-359

[2] N. N. Nedyalkov, R. Nikov, A. O. Dikovska, P. A. Atasanov, G. Obara, M. Obara: “Laser annealing of bimetal thin films: A route of fabrication of composite nanostructure”, Appl. Surf. Sci., vol. 258 (2012) pp. 9162-9166

[3] H. Garbacz, E. Fortuna-Zalesna, J. Marczak, A. Koss, A. Zatorska, G. Z. Zukowska, T. Onyszczuk, K. J. Kurzydlowski: “Effect of laser treatment on the surface of copper alloys”, Appl. Surf. Sci., vol. 257 (2011) pp. 7369-7374

[4] B. S. Yilbas: “Laser cutting quality assessment and thermal efficiency analysis”, J. Mater. Process. Tech., vol. 155-156 (2004) pp. 2106-2115

[5] M. A. Al-Nimr, M. Alkam, V. Arpad: “Heat transfer mechanisms during short-pulse laser heating of two-layer composite thin films”, Heat Mass Transfer vol. 38 (2002) pp. 609-614

[6] X. Liu, Z. Lu, X. Wang, D. Ba, C. Zhu: “Micrometer accuracy method for small-scale laser focal spot centroid measurement”, Opt. Laser. Technol., vol. 66 (2015) pp. 58-62

[7] M. Pellizzari, M.G. De Flora: “Influence of laser hardening on the tribological properties of forged steel for hot rolls”, Wear, vol. 271, (2011) pp. 2402–2411

[8] J.M. Vázquez-Martíneza,, J. Salguerob, F.J. Botanac, J.P. Contrerasa, S.R. Fernández-Vidala, M. Marcosa: “Metrological Evaluation of the Tribological Behavior of Laser Surface Treated Ti6Al4 V Alloy”, Procedia Engineering, vol. 63 (2013) pp. 752–760

[9] Yongkun Qin, Dangsheng Xiong, , Jianliang Li: “Tribological properties of laser surface textured and plasma electrolytic oxidation duplex-treated Ti6Al4V alloy deposited with MoS2 film”, Surf. Coat. Technol., vol. 269 (2015) pp. 266–272

[10] A. Ashkin: “Optical Trapping and Manipulation of Neutral Particles Using Lasers”, Proc. Natl. Acad. USA, vol. 94 (1997) pp. 4853-4860.

[11] X. Ye, Y. C. Shin: “Synthesis and characterization of Fe-based amorphous composite by laser direct deposition,” Surf. Coat. Technol. vol. 239 (2014) pp. 34-40

[12] A. Singh, W. D. Porter , N. B. Dahotre: “Thermal transitions in Fe–Ti–Cr–C quaternary system used as precursor during laser in situ carbide coating”, Mater. Sci. Eng. A, vol. 399 (2005) pp. 318-325

[13] B. Du, A. N. Samant, S. R. Paital, N. B. Dahotre: “Pulsed laser synthesis of ceramic-metal composite coating on steel”, Appl. Surf. Sci., vol. 255 (2008) pp. 3188-3194

[14] S. Yokoyama, Y. Takashima, M. Nor, Y. Murata, H. Kanematsu, J. Sasano, M. Izaki: “Solubility of carbon and Vickers hardness of copper saturated with carbon”, AMPT Sept (2012) 1-8

[15] Abdul Muizz Mohd Noor, Yoshikazu Ishikawa and Seiji Yokoyama: “Preparation of Graphite Dispersed Copper Composite on Copper Plate with Spot Welding”, Mater. Trans. JIM, vol. 58 (2017) pp. 1138-1144

[16] M. Naeem: “Laser Processing of Reflective Materials”, Laser Technik J., vol. 10 (6) (2013) pp. 18-20

[17] The 140th Committee of Japan Society for Promotion of Science, Handbook of Physico-chemical Properties at High Temperature, The Iron and Steel Institute of Japan 2 (1998)

[18] W. D. Callister, Jr., D. G. Rethwisch: Materials Science and Engineering 9th edit., John Wiley and Sons, Asia (2011) pp. 276

[19] H. S. Kim: “On the rule of mixtures for the hardness of particle reinforced composites”, Mater. Sci. Eng. A, vol. 289 (2000) pp. 30–33

[20] David R. Lide, CRC Handbook of Chemistry and Physics, 88th Edition, Taylor & Francis (2007) 4-56

[21] David R. Lide, CRC Handbook of Chemistry and Physics, 88th Edition, Taylor & Francis (2007) 4-61

CHAPTER 6

PREPARATION OF GRAPHITE DISPERSED COPPER COMPOSITE WITH ADDITION OF GRAPHITE INTO MOLTEN COPPER

6.1 Introduction

Because graphite-dispersed copper composite is a good heat and electric good conductor and self-lubricity, it is suitable for sliding contact materials like a pantograph, brush for a DC motor and so on. Many methods for preparation this composite have been reported until now [1-14]. However, it has been usually prepared with the sintering. The phase diagram of copper-carbon system has revealed that the solubility of graphite into molten copper increased with an increased in the temperature. the recent study revealed that the solubility of carbon into molten copper increased with an increase in the temperature. the recent study revealed that the solubility of carbon into molten copper steeply increased the temperature of more than approximately 2100 K [15]

In Chapter 4 and Chapter 5, it was tried to prepare the graphite-dispersed copper composite on the copper plate locally. In Chapter 2, it was tried to prepare the composite using precipitation from the molten carbon saturated copper-nickel alloy. Then, in this chapter, it was tried to prepare the composite using additive amount of graphite particles that was more than the amount of graphite predicted from the carbon saturated copper alloy.

6.2 Experimental

6.2.1 Specimen preparation

1) Materials

Copper (the purity: 99.9 mass%) and graphite powder (99.9 mass%) were used for preparation of copper-graphite composite. Nickel (99.99 mass%) and iron powder (99.9 mass%) were used as alloying elements. The graphite powder can be divided into two types. The first type of graphite particles were ground particles with an agate mortar and pestle to reduce the size of the graphite particle. Figs. 6.1 (a) and (b) showed us the microstructure of the graphite before and after grinding. The ground particles were passed through the sieve with opening size of 20 μm. The ground graphite particles were approximately 5 μm in average size. The small graphite particles in Fig. 6.1 (b) were flat and angular in shape respectively.

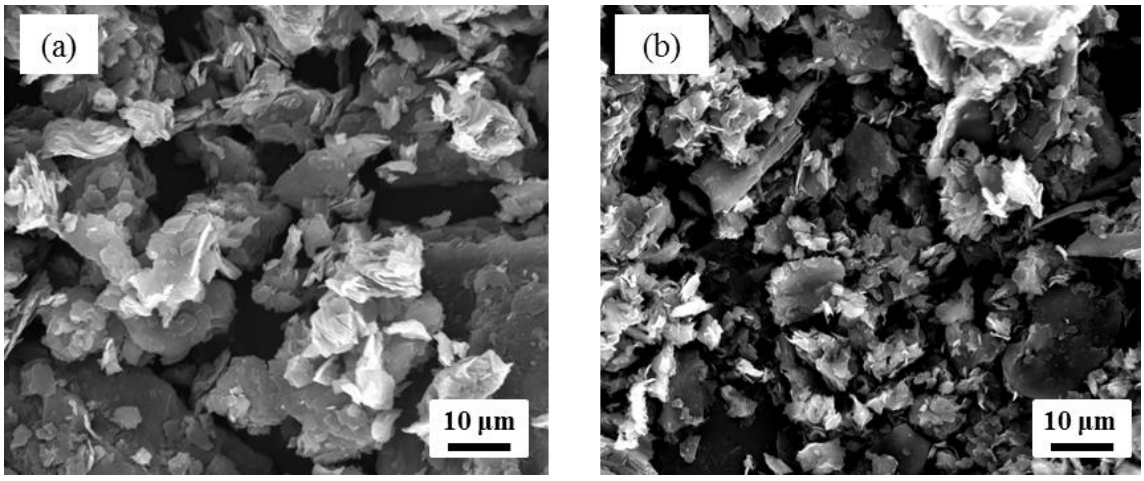

Fig. 6.1 SEM images of graphite particles used in this work. (a) was the particles before grinding and (b) was the particles after grinding.

The second type of particles were the ball-milled graphite particles. The grinding was performed on the condition that the graphite particles were ball-milled with copper ball for 20 hours inside centrifuge. The average diameter of the copper ball was 1 mm. Copper balls used in the milling process were for preparation of certain specimen. Fig. 6.2 showed the surface of the copper ball after milling process. The milled copper ball was dark black in color due to coating with graphite. The composition of modified graphite particles were analyzed using the EDX. Table 6.1 showed the chemical composition of the ground graphite particles and copper balls. The intensity of copper was low in these graphite powder as could be seen in Fig. 6.3, but the powders included copper.

Table 6.1 Chemical composition of ground graphite particles and copper ball.

	Copper content, C_{Cu} / mass %	Carbon content, C_C / mass %
Graphite particles	1.34	98.66
Copper ball	77.95	22.05

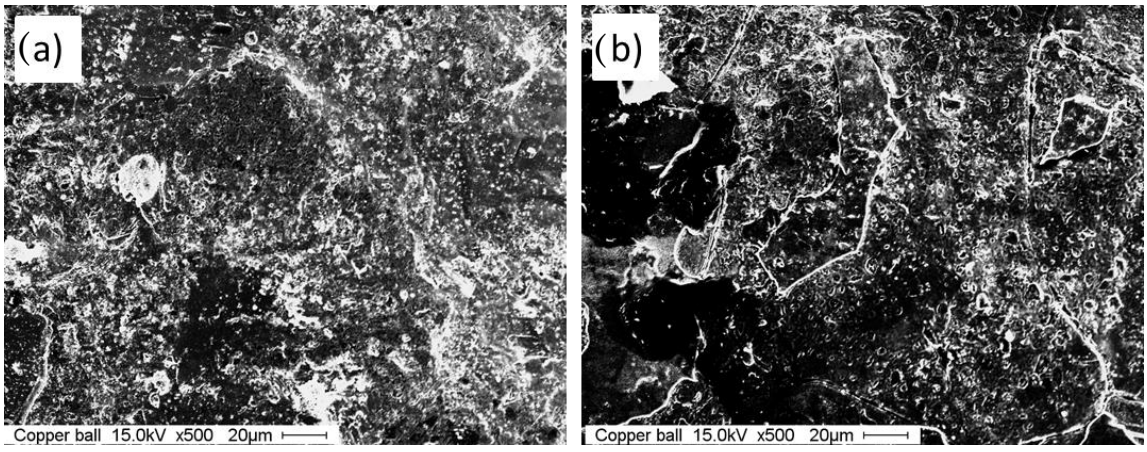

Fig. 6.2 Copper ball surfaces before ball-milling, (a) and after ball-milling, (b).

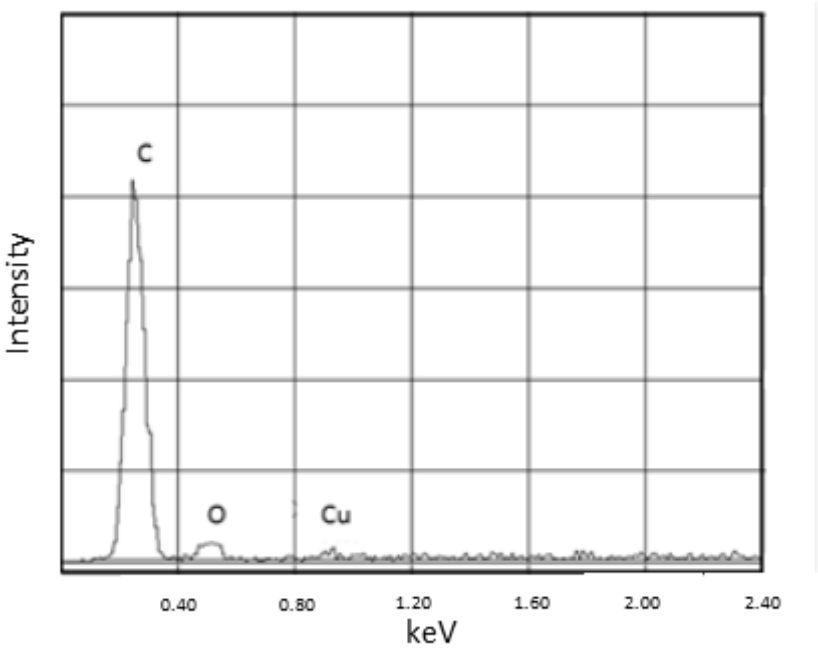

Fig. 6.3 Intensities of elements in grounded graphite powder analyzed with EDX.

In current work, a specially designated copper rod with hole inside of the rod where graphite powder or graphite powder with copper balls was placed was used as shown in Fig. 6.4. The volume of the hole was 294.4 mm^3. To remove unnecessary substances such as grease, laboratory dust and so on, the copper holder was washed in an ultrasonic cleaner filled with acetone. The copper holder weight was approximately 12.9 ± 0.1 g and the weight of graphite filled inside copper hole was approximately 0.25 ± 0.01 g.

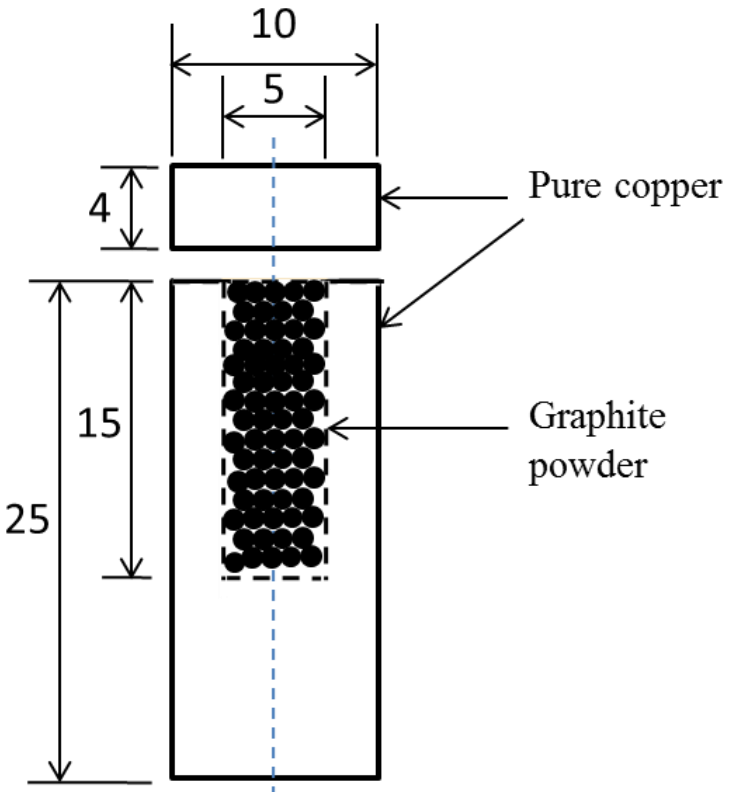

Fig. 6.4 Schematic of designated copper holder.

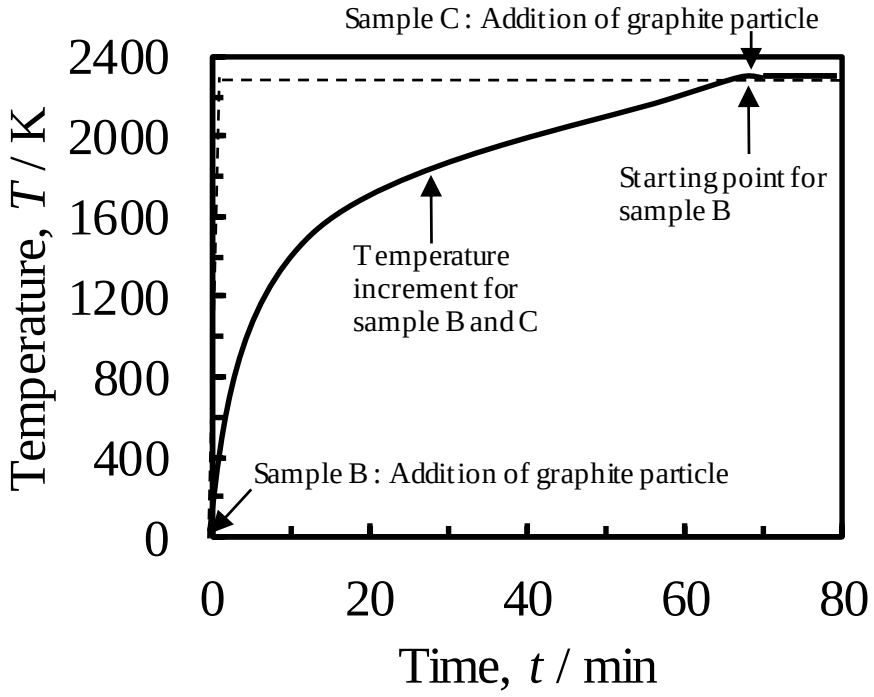

Fig. 6.5 Time dependencies of temperature for sample B and sample C

2) Apparatus

High frequency induction furnace was used to heat the sample, as shown in Fig. 6.6. The two color thermometer (CHINO series IR-FL2AH04) which equipped with a laser pointing system was used for measurement of the graphite crucible temperature. The temperature at the laser pointed place could be measured with this thermometer. When the temperature of the surface of the molten metal in crucible was measured, it was differed with the measuring spot due to the emissivity of copper and graphite. Then, the temperature of the graphite crucible was measured, because the graphite could be estimated to be black body.

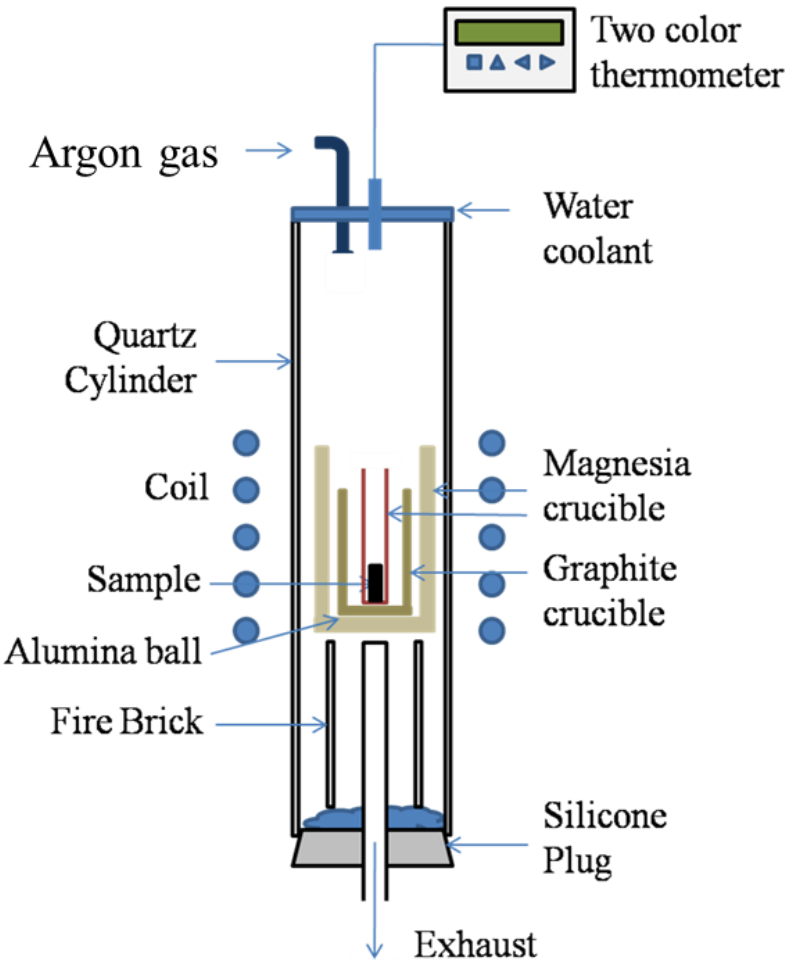

Fig. 6.6 High frequency induction furnace

6.2.2 Experiment and analysis

1) Experiment

Argon gas with a flow rate of $2.0 \times 10^{-5} m^3 s^{-1}$(293 K, 101.3 kPa (NTP)) was introduced into the furnace to displace the air and prevent oxidation during experiment. The specimens were melted on the conditions as listed in Table 6.2. For sample C, after the graphite crucible temperature reached 2073 K, copper rod filled with graphite powder was put using copper wire from above of quartz tube.

After the sample was held at 2073 K for 2 hour, the sample was cooled in the furnace to room temperature. After that, the specimen was taken from the magnesia crucible. The copper composite could not to be taken out from magnesia crucible easily. The lower part of the specimen adhered to the with magnesia crucible. Then, the magnesia crucible was crushed to take out the specimen. The specimen was carefully cleaned with emery paper to eliminate magnesia attached with the copper composite. Then the sample was cleaned using ultrasonic cleaner.

2) Experimental condition for preparation of composite

Graphite dispersed copper composite had been prepared on 6 different conditions in attempt to increase carbon content in the composite. The preparation conditions were listed in Table 6.2. The samples were named A, B, C, D, E and F prepared on each condition.

Samples A and B were heated at 1673 K and 2073 K respectively. The ground graphite powder was used in sample A and B. For sample C, it had the same experiment condition with B except temperature at the addition of graphite powder. The addition for sample C was done by inserting with graphite powder enveloped with copper film into

the molten copper when the temperature of the furnace reached 2073 K. Fig. 6.4 showed the changes in the temperature for samples B and C with time and the addition time of the graphite

Table 6.2 condition of preparation of graphite dispersed copper composite.

Sample	Parameters		
	Temperature, *T* / K	Alloying element	Graphite type
A	1673	No	Ground
B	2073	No	Ground
C	2073	No	Ground (Addition at 2073 K)
D	2073	No	Milled with copper
E	2073	Nickel 5 mass%	Ground
F	2073	Iron 5 mass%	Ground

Mixture of copper balls and ball-milled graphite powder instead of grinded graphite powder was used for preparation of the sample D. Copper balls which were used to mill graphite and ball-milled graphite were put together in the copper holder. Samples E and F were prepared with addition of nickel or iron in attempt to increase carbon solubility. The sample E contained 5 mass% of nickel in itself, while sample F contained 5 mass% of iron in itself. All specimens were heated for 2 hours at temperature of 2073 K.

3) EDX and observation of surface and cross-section

The sample was cut along the center axes of the samples for observation of the cross section. The sample was put in liquid resin and was held for a day to harden the resin. The sample was polished by the emery paper, abrasive of alumina and colloidal silica in this order, and was observed by a laser microscope (Keyence VK8500) and a scanning electron microscope (SEM, JEOL JSM-6300) equipped with an EDS. For SEM observation, the samples were coated with platinum of around 20 nm in thickness. It was important to coat the sample with platinum, otherwise the sample will be charged up.

4) Vickers hardness

Micro hardness tester (Shimadzu HMV Micro Hardness Tester) was used to investigate the Vickers hardness of the alloy. Vickers hardness of the alloy was measured on the condition of the test force of 980 mN and holding time of 10 s. The hardness was measured for the lower, middle and upper part of the specimen. The hardness was measured for 7 different positions of each part. The highest and lowest measured hardness were eliminated, and the average of the remaining 5 points was used as actual hardness. The scattering of the measured hardness was ± 50 MPa. The hardness of the copper composite after annealed was also investigated. All the specimens were annealed at 923 K for 1 hour..

6.3. Result and discussion

6.3.1 Microstructure and EDX

1) Chemical composition

Table 6.3 showed the carbon content and alloy content in each sample analyzed

using the EDX. The carbon content was the value for the surface of the cross-section of the samples. The quantity of graphite adhered to the copper plate was evaluated with this carbon content. The carbon contents at seven different places were measured with an area analysis of the EDX. The measured area size was approximately 0.02 mm^2. The carbon content was evaluated with the mean of seven measured values.

Table 6.3 Carbon content and alloy content in each sample analyzed using EDX

Sample	**Carbon content, C_c / mass%**			**Nickel or iron content, C_{Ni} or C_{Fe} / mass%**		
	Upper	**Middle**	**Lower**	**Upper**	**Middle**	**Lower**
A	**0.35**	**0.03**	**0.00**	**-**	**-**	**-**
B	**2.64**	**1.14**	**1.24**	**-**	**-**	**-**
C	**2.56**	**1.80**	**1.74**	**-**	**-**	**-**
D	**2.70**	**1.91**	**2.00**	**-**	**-**	**-**
E	**4.16**	**3.26**	**2.39**	**5.30**	**5.05**	**4.72**
F	**4.02**	**3.34**	**2.61**	**2.61**	**2.49**	**3.68**

2) Effect of melting temperature

Figs. 6.7 (a), (b) and (c) showed morphologies of graphite particles at the cross sections of samples A, B and C respectively. In sample A which was melted at 1673 K, graphite particle was hardly observed in comparison with samples B which were melted at 2073 K. The temperature dependency of carbon content roughly agreed with previous that the solubility of carbon increased with the temperature of approximately 2073 K [15].

3) Influence of addition way of graphite

From Fig. 6.7 (b) and (c), the graphite precipitated near upper surface for sample B and C. The EDX results analyzed in Table 6.2 showed that the carbon content in sample B and sample C were 2.64 mass% and 2.56 mass% respectively. This showed that the solubility of carbon is not influenced by addition way of graphite. However, it was found that graphite particles distributed at center area of the cross-section as shown in Fig. 6.8. In contrast to the other samples, it was only sample C that graphite precipitations could been found at center area.

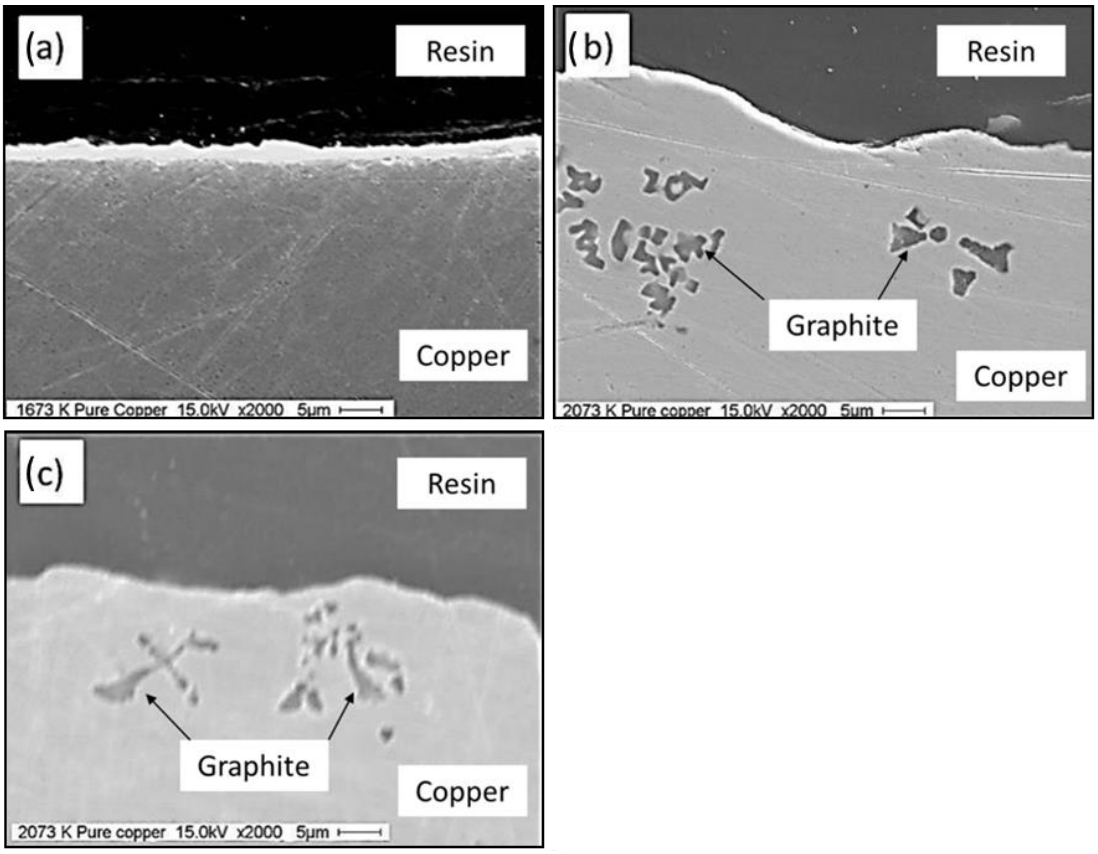

Fig 6.7 Cross sections of sample A (a), sample B (b) and sample C (c)

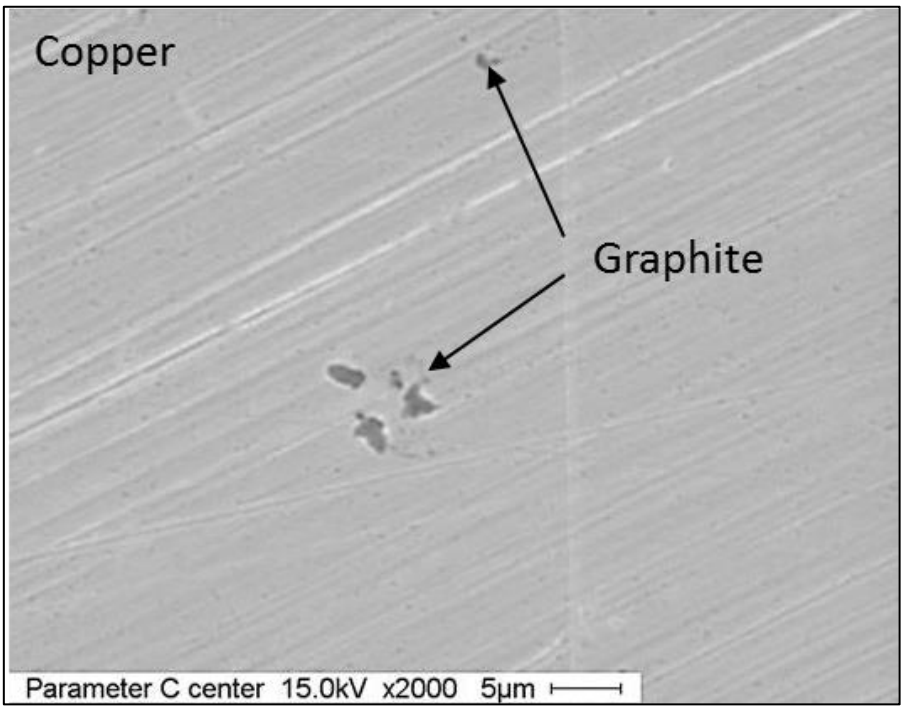

Fig. 6.8 Graphite particles distributed at middle area of sample C.

4) Influence of ball-milled graphite particle

Figs. 6.9 (a) and (b) showed the cross-section of sample D and sample B respectively. Both samples were prepared with the same procedure except for the preparation condition of graphite. Graphite particles were ball-milled with copper ball in sample D, while it was just ground to smaller particle size in sample B. The number of graphite precipitated near the surface in Fig. 6.9 (a) was higher than in Fig. 6.9 (b). In Fig. 6.9 (c) and Fig. 6.9 (d), the graphite precipitation in sample D was agglomerated and had various shapes. The microstructure of the graphite precipitation in sample D was different from the one in sample B. An EDX analysis on these spots showed a high contain of graphite precipitation. In spot 1 and 2 the carbon content were 36.9 mass% and 56.8 mass % while in spot 3 it was none. In sample B, the carbon content of the graphite precipitation was approximately 2.47 mass %.

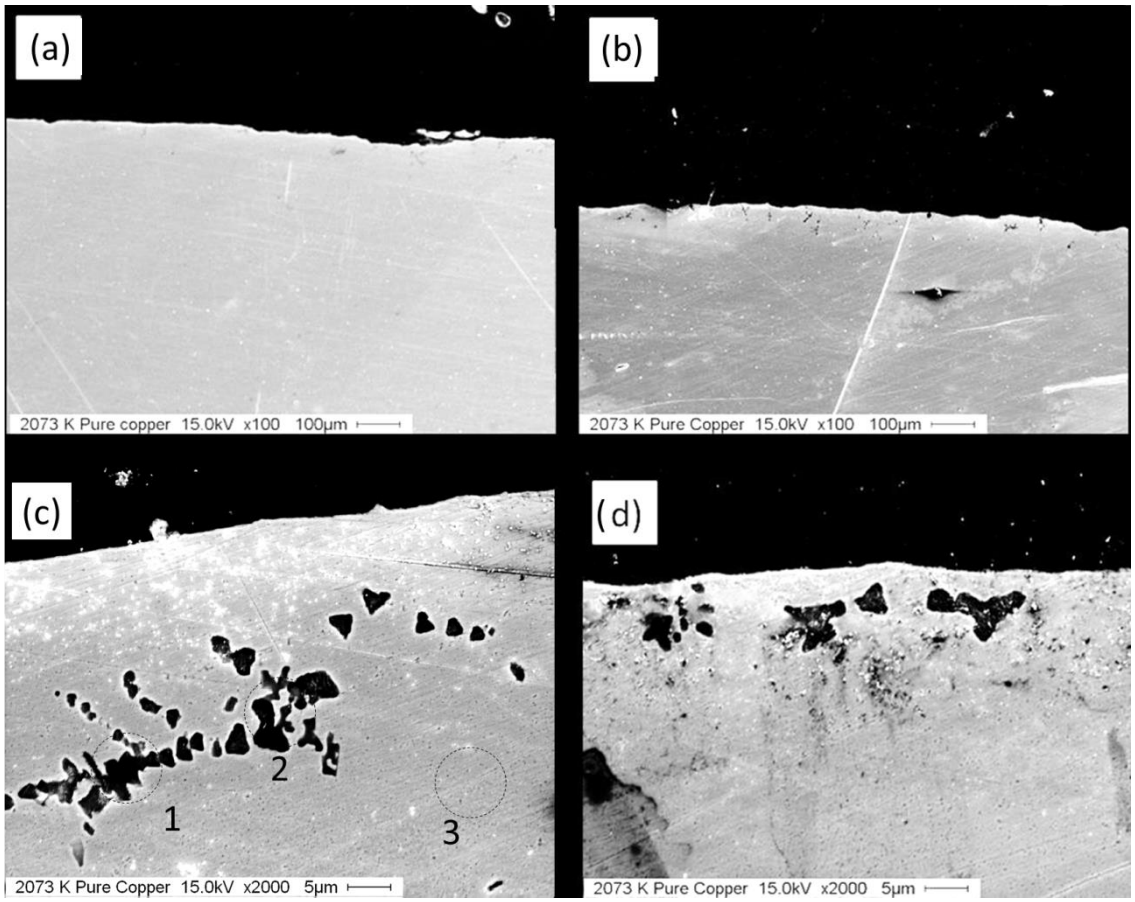

Fig. 6.9 (a) showed cross sections of sample B, and (b) showed cross section of sample D. (c) and (d) showed enlarged image of sample D.

5) Effect of nickel

In sample E, nickel was added so that the content of nickel was 5 mass%. Figs. 6.10 (a), (b) and (c) showed the cross section of the sample E. In sample E, graphite precipitated could be classified in 2 shapes. In Fig. 6.10 (a), darker black spots had higher carbon content with average of 64.4 mass%, while the carbon content in the lighter black spot was only 2.92 mass% in average. The nickel content in darker spot was lower than lighter spot. The lighter spot was similar with the one in sample B. The graphite precipitates could be in agglomerated and various in shapes. It was found in

sample E that the darker black spots diameter sizes were from 5 μm to 10 μm. These were similar to the diameter size of the graphite particles used in the experiment. However, the shapes of the graphite particles were roundish. In contrast, the shapes of graphite particles used in this work before melting were flat and angular as shown in Fig. 6.1. It was possible that these black spots could be graphite precipitation. Fig. 6.10 (c) showed the distribution of graphite precipitates inside the copper composite. Almost all the precipitations existed at the upper part of the composite.

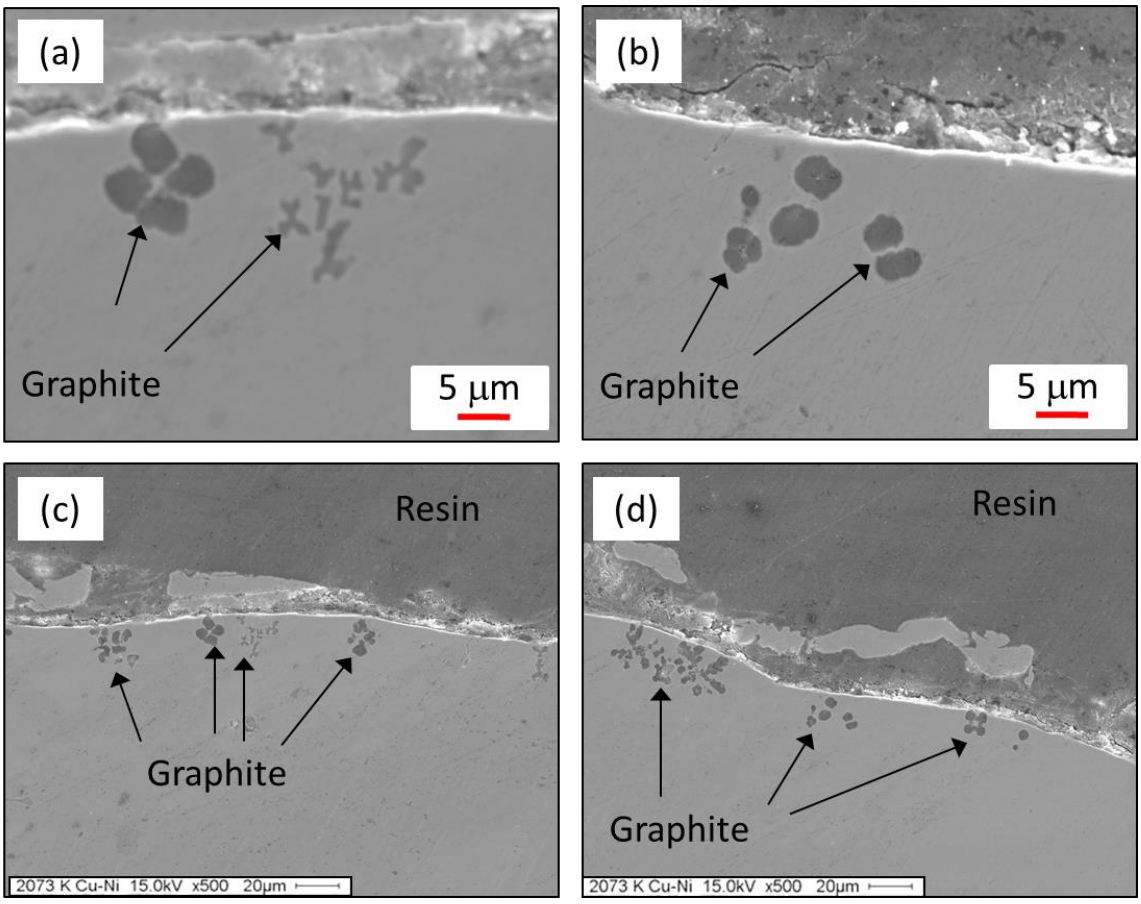

Fig. 6.10 Cross sections of sample F. Figs. (c) and (d) were enlarged pictures of graphite particles in Figs. (a) and (b).

6) Effect of iron

Fig. 6.11 (a) showed the cross section of copper-iron 5 mass% at temperature 2073 K. The morphology of graphite precipitated in this specimen was different from that in copper-nickel 5 mass%. Areas surrounding the graphite precipitations were darker than other area. EDX analysis showed that iron content in this phase was high. Fig. 6.11 (b) showed macroscopic view of the cross section of sample F. Graphite precipitation in sample F only occurred inside high iron content phases. In some cases, graphite particles adhered to the surface of alloy.

Fig. 6.12 showed the mapping of iron element in the middle area of copper. The distribution of the iron was not uniform. The average iron content in area without high iron phase was 2.49 mass% for the upper. Meanwhile the average iron content in the center area of the composite was 2.61 mass% and 3.68 mass% at lower area. The iron content was lower than added iron content which was 5 mass%.

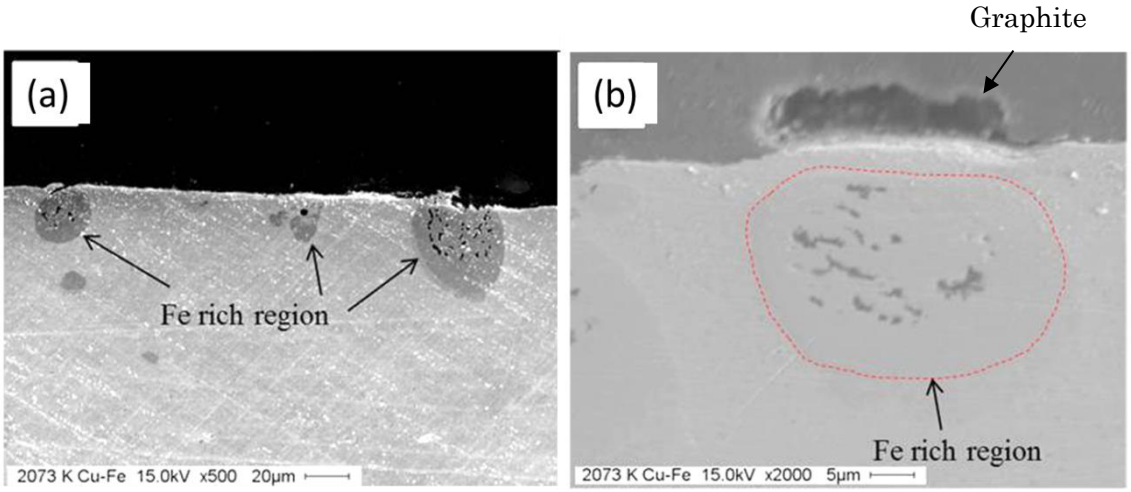

Fig. 6.11 Cross sections of sample F. Figure (b) was magnified image of iron rich region.

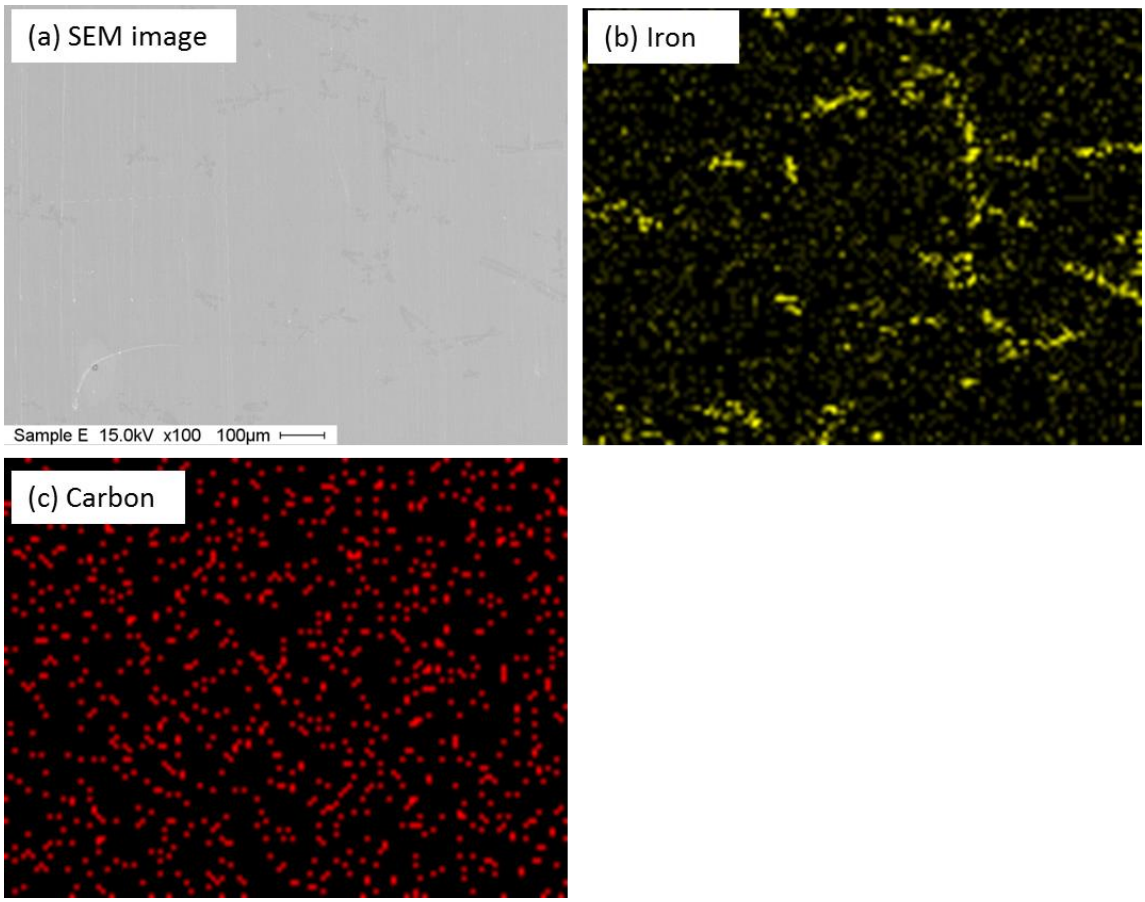

Fig.6.12 Segregation of iron content in copper composite. (a) was the SEM image, (b) the mapping distribution of iron and (c) the distribution of carbon

Fig. 6.13 showed the center area of copper composite prepared in sample F. There was no graphite precipitate in this area. This showed that during melting, graphite particles scattered to the surface. Then it was difficult for graphite particles to enter the molten alloy due to the buoyance. Therefore, it was difficult to observe graphite precipitates in area far from the surface.

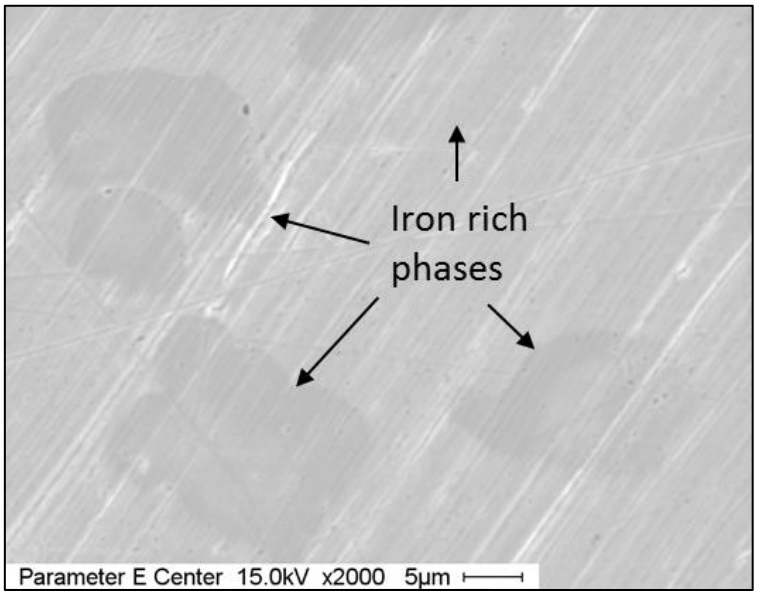

Fig. 6.13 Center area of sample F.

6.3.2 Mechanism of melting process at 2073 K

1) Motion of graphite particles during melting

Generally, a graphite is a lightweight material with density of 2.2 g/cm^{-3} [18] comparing with copper which is 8.96 g/cm^{-3} [19]. During melting process, graphite particle moved to copper surface. This was true because all copper composite prepared by each sample showed that graphite particles were found near surface except sample C. In addition, remaining graphite particles appeared on top of the solidified copper composite after the experiment. Fig. 6.14 showed the schematic how the copper holder deformed due to melting.

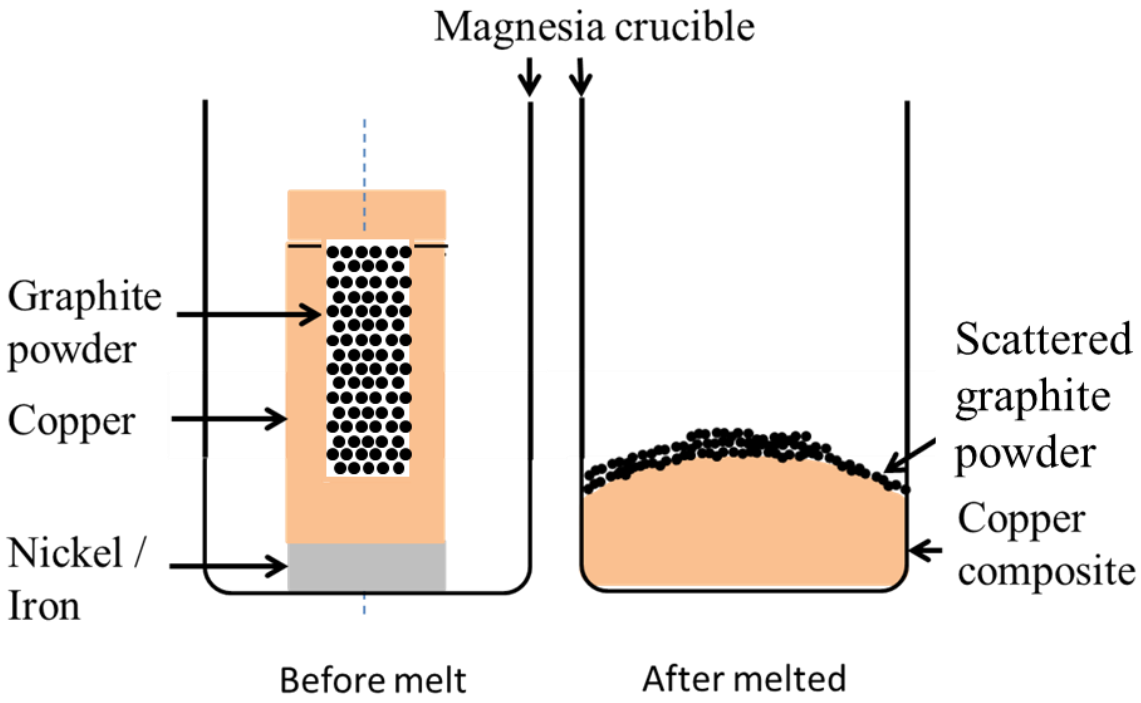

Fig. 6.14 Schematic of copper composite condition before melted and after melted.

During melting process, the motion of the graphite particle in molten copper could be related to Stokes' law as:

$$F_d = 6\pi\eta r v \tag{6-1}$$

Where F_d was drag force, η was viscosity, r was radius of the particle and v was the terminal velocity. Because of the graphite density is lower than copper, it would rise during melting. The buoyancy force and gravitational force could express as:

$$F_b = \rho_{Cu}(4\pi r^3/3)g \tag{6-2}$$

$$F_g = \rho_g(4\pi r^3/3)g \tag{6-3}$$

Where ρ_{Cu} and ρ_g were the density of the molten copper and graphite particles respectively, and g was gravitational acceleration. Because the graphite rose in molten alloy, the forces could be explained as:

$$F_b = F_g + F_d \tag{6-4}$$

From the Eq. (6-4), the velocity of the particles was obtained by using Eq. (6-5).

$$v = \frac{(\rho_{Cu} - \rho_g)(4\pi r^3/3)g}{6\pi\eta r} \tag{6-5}$$

Viscosity of the molten copper decreased with an increase of temperature [20]. The rising of graphite particles were estimated to start from the copper melting. The velocity of the graphite particles inside molten copper was 0.034 mm/s, assuming that the particles diameter was 5 μm

Fig. 6.15 showed the explanation of the motion of graphite particles during melting. Firstly when copper melted, graphite scattered to surface. In sample B, the time for all graphite particles to rise to the surface was estimated to be 441 s. If all graphite particles were floated after 441 s, the temperature of the molten copper was just approximately 1400 K during that time. This temperature was so lower than temperature 2073 K where the solubility increased. After reaching the temperature of 2073 K and held it for 2 hours, the graphite particles dissolved into molten copper. After certain time, the carbon content at the area near the surface reached a saturated phase. As a result, graphite precipitated at the near surface from the melt. This explained why there were no graphite particles at the middle and lower part.

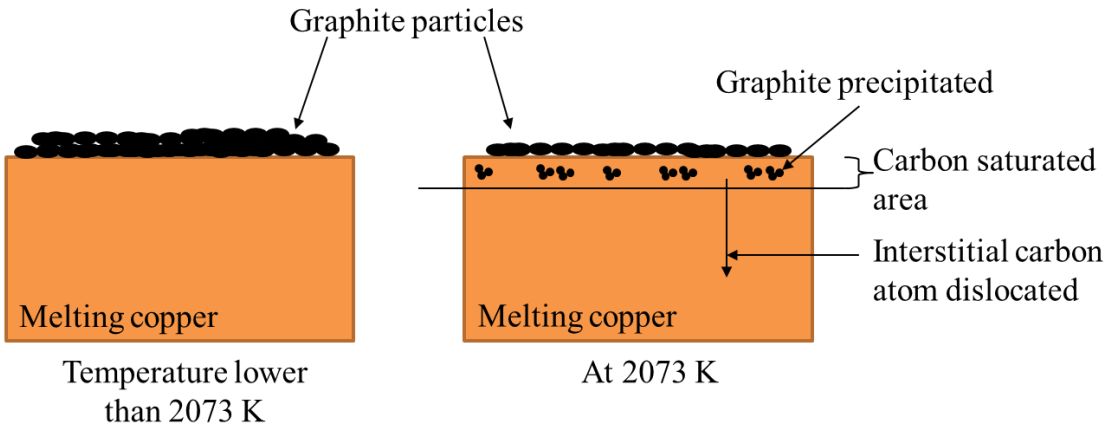

Fig. 6.15 Explanation of motion of graphite particles during melting

2) Mechanism in sample E

In previous Chapter 2, the distribution of graphite precipitates was not uniform but distributed throughout the copper-nickel alloy. However, in sample E, the graphite precipitates could only be observed near surface. Graphite particles were used in this work. In contrast, graphite crucible was used in Chapter 2. In Chapter 2, molten copper surface touched with graphite crucible at every surface. In contrast, in sample E, graphite particles rose to the upper surface, and as a resulted only touched to molten copper at only the upper surface. At temperature of 2073 K, when the Cu-Ni alloy at near surface saturated with carbon, the dissolved carbon just diffused from the surface to the inside of the molten copper. It was difficult for graphite to precipitate at the inside of it. The segregation of nickel inside copper was hardly observed because at Cu-Ni alloy was an all proportional solid solution.

3) Mechanism in sample F

In sample F, graphite only precipitated inside high iron content phases. Generally,

carbon solubility in iron is so higher than that in copper. Fig. 6.16 showed that graphite precipitated inside phase with high iron content. It was also found that graphite particles agglomerated on the surface of the phase with high iron content. This was resulted from that the graphite particles could wet with iron rich phase. In sample E, the liquid phase was not homogeneous and can be classified as two phases. One was liquid phase with high copper content, and the other was liquid phase with high iron content. Usually, liquid phases with high iron content were darker grey in SEM image as shown in Fig. 6.16.

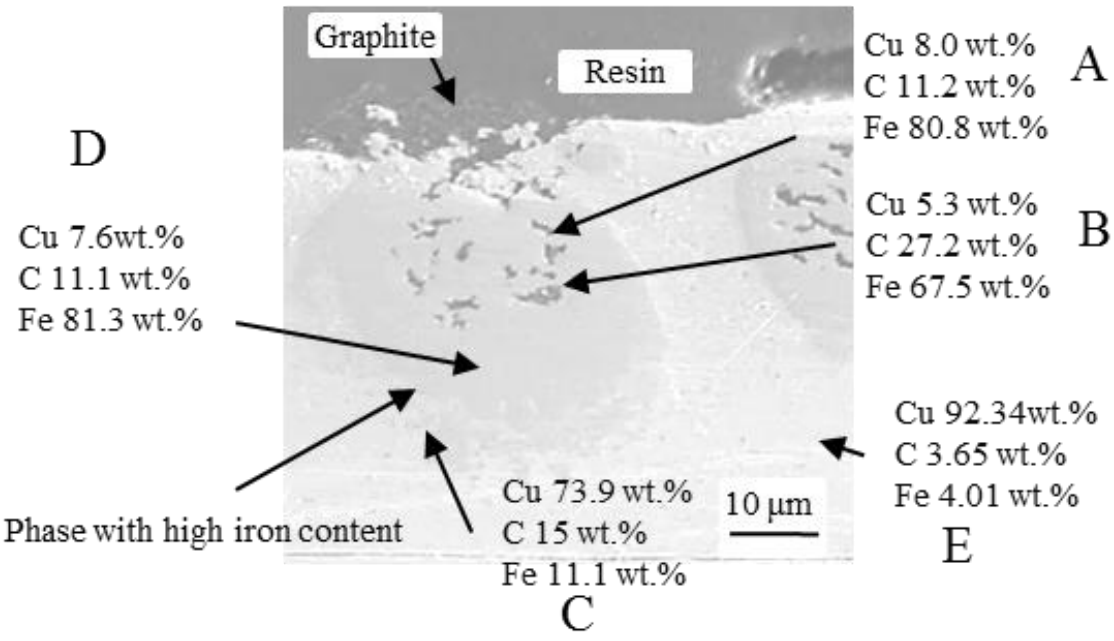

Fig. 6.16 Elemental contents around area with high iron content.

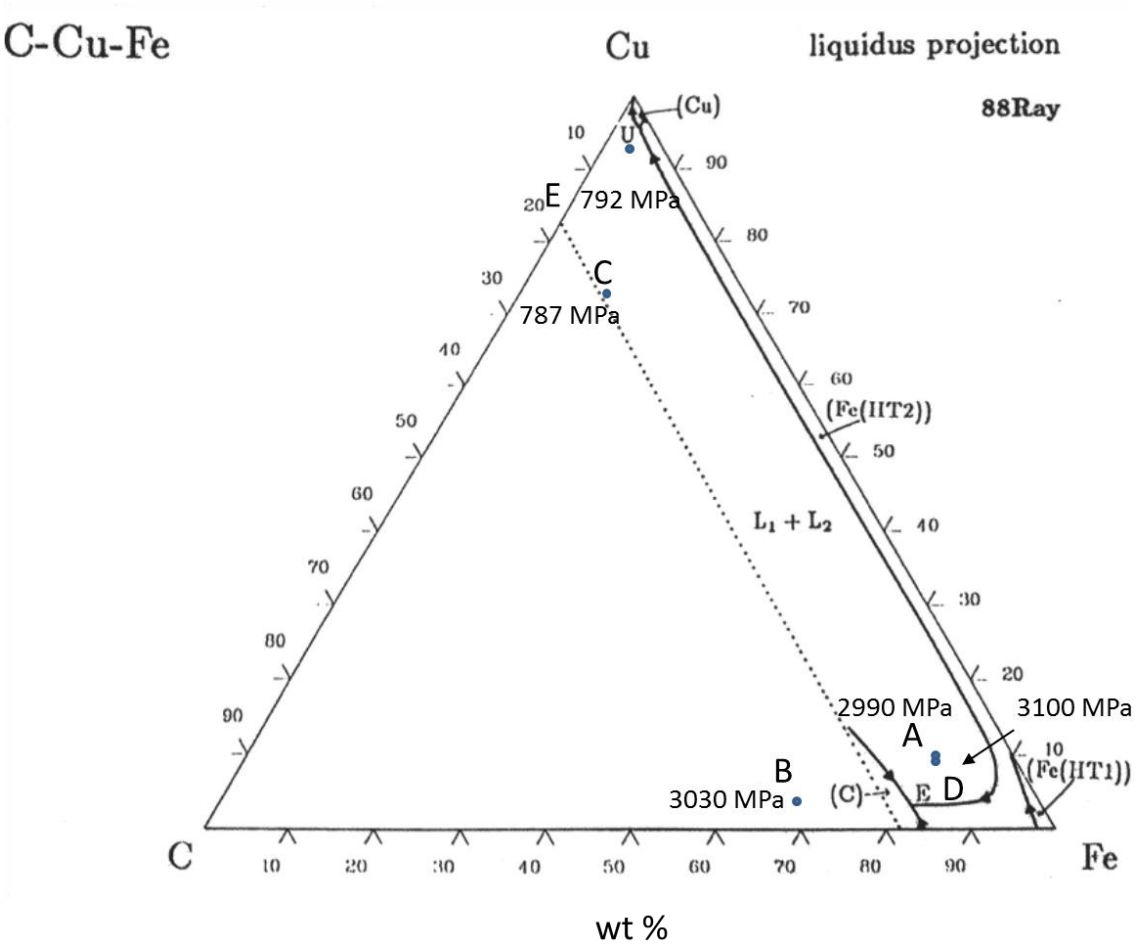

Fig. 6.17 Ternary phase diagram of C-Cu-Fe [17] with plotted spots from Fig. 6.15. Label of A, B, C, D and E were the same as those shown in Fig. 6.15.

Elements content in Fig. 6.16 which represented as spots A, B, C, D and E were plotted in the ternary phase diagram of C-Cu-Fe at liquidus as shown in Fig. 6.17. As described later, the number was the hardness of the phases was in the figure. For spot A and spot B, which were graphite precipitates, they were near to carbon phase in the ternary phase diagram. According to the ternary phase diagram, two liquid phases can be achieved if the carbon content is less than 17.2 mass%. This could be related to two phases in spot C and spot D. Spot C was phase with high in copper content and near to high iron phase, while spot D was phase with high iron content. Lastly, spot E represent

phase with lower iron content and was the main phase in sample F. Because the graphite had good solubility and wettability to iron, graphite particles adhered on top surface of the liquid phase with high iron content.

6.3.3 Vickers hardness

1. Before and after annealed

The Vickers hardness was measured for all samples. Fig. 6.18 showed us the Vickers hardness for each parameter before and after annealed at 923 K for 1 hour. Here, the hardness was mean value for the upper, the middle and the lower part of the sample. Generally, the hardness of copper composite in all samples reduced after annealed. The Vickers hardness of the composite after annealing was smaller than before annealing because of the relaxation of solid-solution strengthening of carbon. Hardness of copper composite prepared in sample A, B, and D which contained copper and graphite were slightly higher than the hardness of pure copper. However copper composite prepared in sample C was slightly higher than sample A, B and D. This might be resulted from the precipitation of the graphite not only near the surface area but also in other area. This showed that these samples were hardened by the precipitation hardening of graphite.

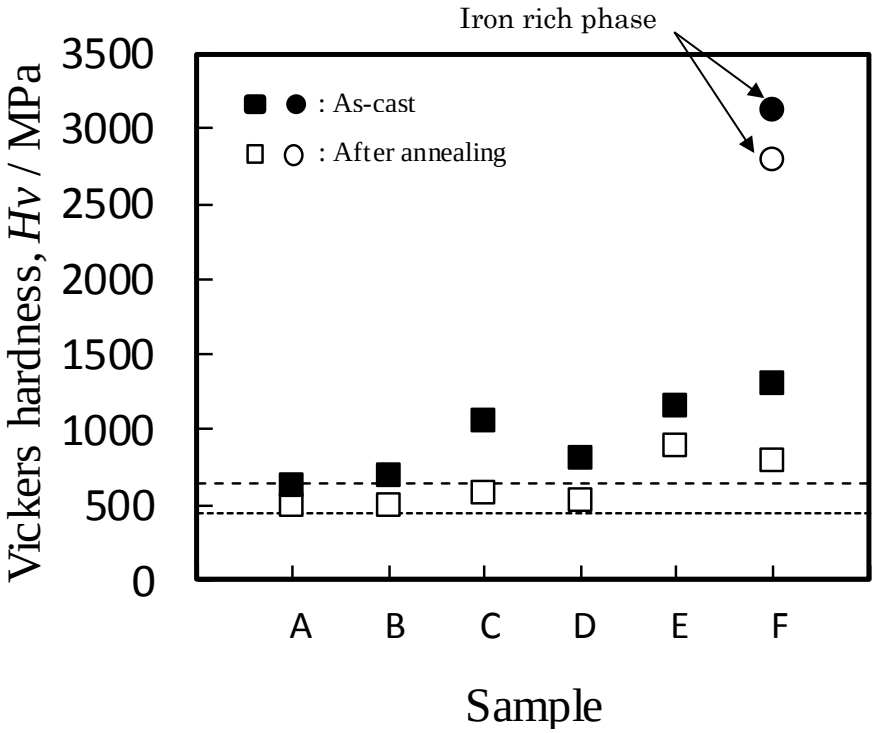

Fig. 6.18 Vickers hardness of copper composite before annealed

.

2. Vickers hardness of sample B, sample C and sample D

The Vickers hardness in sample B, C and D were compared with previous works prepared using a spot welder and a laser irradiation. Fig. 6.19 showed that the Vickers hardness of copper composite of sample B, C and D were nearly to equal the hardness of copper spot welded with electrical current flow and also prepared with laser irradiation for 12 s. This also suggested that during preparation using laser and spot welding with electrical current, the surface was melted.

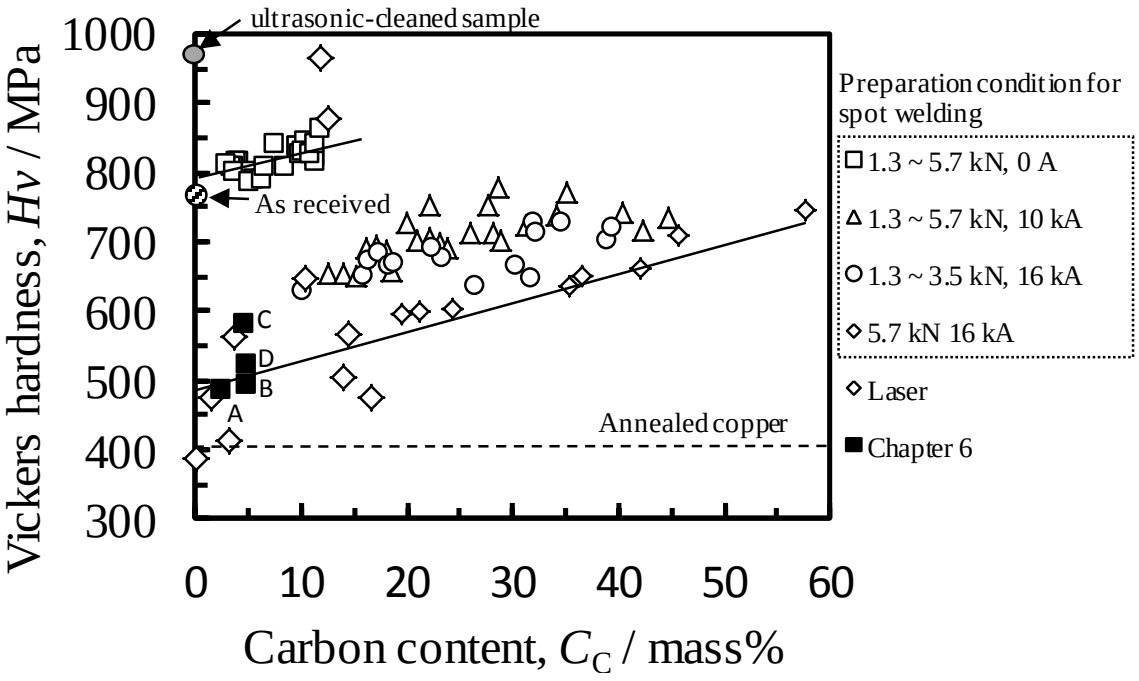

Fig. 6.19 Relation between hardness in sample B and C with previous chapter.

3. Vickers hardness of sample E

Sample E was hardened by precipitation hardening of the graphite particles and solution hardening of nickel. However the hardness in sample E was higher than previous results in Chapter 2 as shown in Fig. 6.18 and Fig. 6.20. Insufficient of annealing might affect the Vickers hardness. The sample in Chapter 2 was smaller than sample E. As a results, sample E was not annealed in comparison with the sample in Chapter 2. In addition the annealing temperature in chapter 2 (973 K) was higher than that for sample E (923 K).

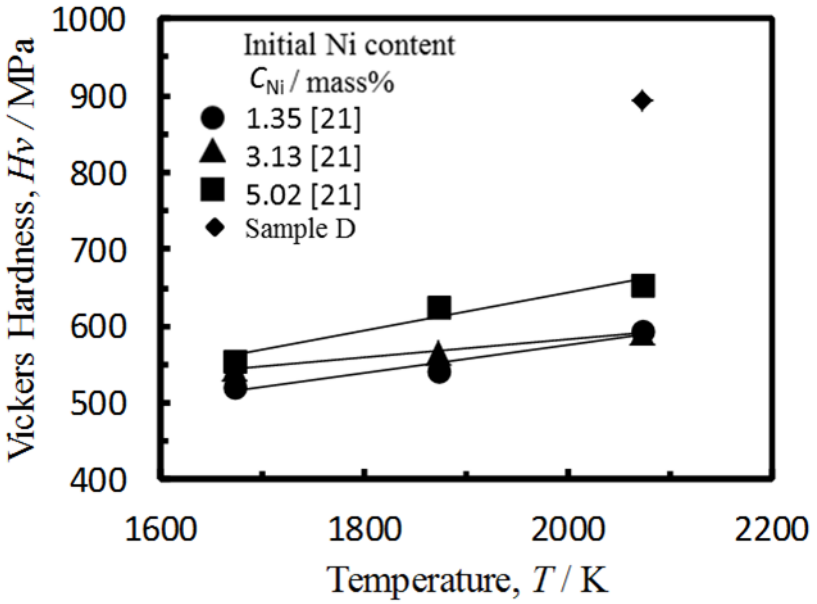

Fig. 6.20 Relation between hardness of sample E and temperature.

4. Vickers hardness in sample F

In sample F, the hardening of the composite was influenced by the solid-solution hardening of iron phases. The hardness at area with high iron content filled with and without graphite precipitations were also measured. In the previous ternary phase diagram Fig. 6.17, it showed the Vickers hardness of each phase in Fig. 6.16. Generally, phases near to carbon phase have higher Vickers hardness than the other phases. Fig. 6.21 showed where the measured area was. In this area, the hardness was extremely higher than area with high copper content. The average hardness measured was 2786 MPa, which was approximately 2000 MPa higher than the average hardness. The region with high iron content not only limited at near surface but middle and lower area. Another thing that influenced the hardness was the precipitation hardening of graphite and solid-solution hardening of iron. Overall, the hardness of sample F was influenced by the high iron content phase throughout the composite and the solid-solution hardening by solid-soluted carbon and iron.

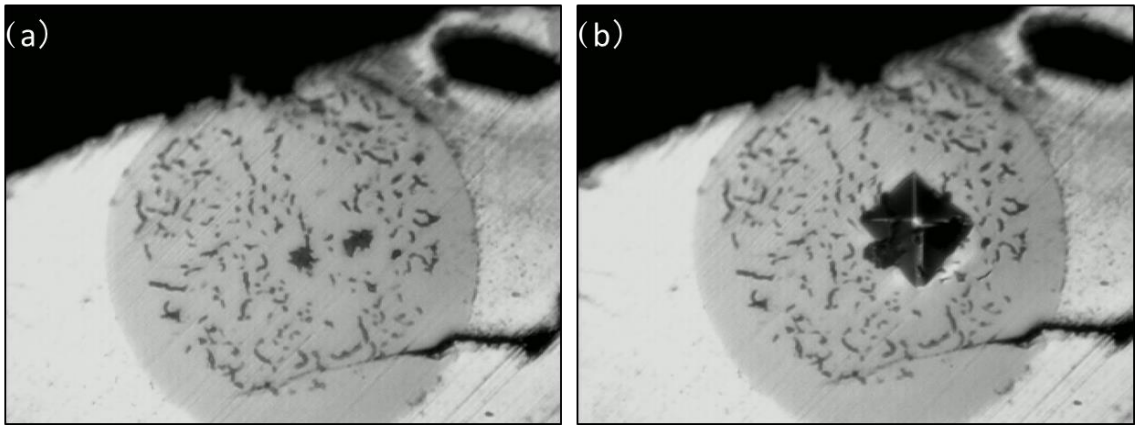

Fig. 6.21 Microscopic image of region with high iron content. (a) was the region before hardness measurement and (b) was after the measurement.

6.4 Conclusions.

Bulks of graphite dispersed copper composite were prepared on the six different conditions to investigate the influence of the condition on the morphologies of graphite and the Vickers hardness. The results obtained were summarized as follows:

1) Graphite particles in the prepared composite were mainly formed by the precipitation from the melt under solidification, because the particles in the composite were different in shape and size from the initial graphite particles. Therefore, temperature of 2073 K and addition of the graphite particles at this temperature were desirable to prepare the composite because of prevention of the scattering of the particles under heating. Because the addition of nickel or iron in the copper increased solubility, the addition of them was advantageous to production of the composite. However, the composite prepared with the addition of iron consisted of graphite, copper rich phase and iron rich phase.

2) The Vickers hardness of as-casted composite were higher than that of annealed

composite due to the solid-solution hardening. The Vickers hardness of graphite dispersed nickel- or iron-copper composite was higher than that of graphite dispersed copper composite because of the solid-solution hardening of each alloying element.

It was tried that the graphite dispersed copper alloy composite prepared with addition of graphite particles. The carbon content in the prepared composite was up to approximately 5 mass%. This composite did not satisfied lower level of the carbon content of usual composite which demanded carbon content from approximately 20 mass% to 85 mass%.

This study could not clear whichever quantity of graphite in the composite was higher than that of carbon solubility or not. A further study was necessary to understand quantitatively the relation between additive amount of graphite particles and amount of precipitated graphite particles and so on.

REFERENCES

[1] W. D. W. Ángel, L. T. Jurado, J. F. C. Alcalá, E. C. Martínez, Víctor F. V. Cedeño: "Effect of copper on the mechanical properties of alloys formed by powder metallurgy", Materials & Design, vol. 58 (2014) pp. 12–18

[2] S. Saji, T. Kadokura, H. Anada, K. Notoya, N. Takano: "Solid Solubility of Carbon in Copper During Mechanical Alloying", Mater. Trans. JIM, vol. 39 (7) (1998) pp. 778-781

[3] J. Wang: "Research on Preparation of Copper-Graphite Composite Powder by Mechanical Alloying", Composite Powder, vol. 34 (2016) pp. 291-294

[4] S. Abe, S. Saji, S. Hori: "Mechanical alloying of Al-20 mass%Ti mixed powders", Japan Inst. Metals, vol. 54 (1990) pp. 895-902

[5] K. Uenishi, K. Kobayashi, S. Nasu, H. Hatano, K Ishihara, P. Shingu: "Mechanical alloying in the Fe-Cu system", Z. Metallk., vol. 83 (1992) pp. 132

[6] S. Saji, H. Araki, K. Hashimoto, E. Murata: "Amorphization of Al-12at.%Ti-X (X=Cr,Fe,Ni,Cu) mixed powders by mechanical alloying", Mater. Trans. JIM, vol. 37 (1996) pp. 1061-1066

[7] U. Mizutani, T. Takeuchi, T. Fukunaga: "Formation of quasicrystals and approximant crystals by mechanical alloying in Mg-Al-Zn alloy system", Trans. JIM, vol. 34 (1993) pp. 102-108

[8] W. Zhang, DS. Zhou, D. Zhang, X. Li: "Microstructural evolution of Cu-10at%C nanocomposite powder during high energy mechanical milling", Mat. Res., vol. 18 (2015) pp. 152-157

[9] J. Zhang, T. Wang, C. Liu, Y. He: "Effect of brazing temperature on microstructure and mechanical properties of graphite/copper joints", Mater. Sci. Eng., vol. 594 (2014)

pp. 26-31

[10] K. Rajkumar, S. Aravindan: “Microwave sintering of copper–graphite composites”, J. Mater. Process. Tech., vol. 209 (15-16) (2009) pp. 5601-5605

[11] J. P. Chu, C. H. Chung, P. Y. Lee, J. M. Rigsbee, J. Y. Wang: “Microstructure and properties of Cu-C pseudoalloy films prepared by sputter deposition”, Metall. Mater. Trans. A, vol. 29 (1998) pp. 647-658

[12] P. R. Subramanian, D. E. Laughlin: “Phase diagrams of binary alloys. Monograph series on alloy phase diagrams”, Materials Park, OH: ASM International, vol. 10 (1994) pp. 562

[13] M. Zhao, Y. Xing, Z. Jia, Q. Liu, X. Wu: “Effects of heating rate on the hardness and microstructure of Al-Cu and Al-Cu-Zr-Ti-V alloys”, J. Alloys Compd.,vol. 686 (2016) pp. 312–317

[14] Q. Yu, Q. Liang, T. Tsuru, R. Traylor, D. Rugg: “Origin of dramatic oxygen solute strengthening effect in titanium”, Science, vol. 347 (2015) pp. 635-639

[15] S. Yokoyama, Y. Takashima, M. Nor, Y. Murata, H. Kanematsu, J. Sasano, M. Izaki: “Solubility of carbon and Vickers hardness of copper saturated with carbon”, AMPT, Sept. (2012) pp. 1-8

[16] T. B. Massalski, J. L. Murray, L. H. Bennett, H. Baker: “Bynary Alloy phase diagrams”, American Society for Metals, Ohio U.S.A, vol. 1 (1986) pp. 561-566

[17] A. Pierre Villars, Alan Prince, Hiroaki Okamoto: “Handbook of Ternary Alloy Phase Diagrams”, ASM International (1995)

[18] David R. Lide, CRC Handbook of Chemistry and Physics, 88th Edition, Taylor & Francis (2007) 4-56.

[19] David R. Lide, CRC Handbook of Chemistry and Physics, 88th Edition, Taylor &

Francis (2007) 4-61.

[20] M. Kehr, W. Hoyer, I Egry: “A New High-Temperature Oscillating Cup Viscometer”, Int. J. Thermophys, vol. 28 (2007) pp. 1017-1025

[21] Abdul Muizz bin Mohd Noor and Seiji Yokoyama: “Solubility of Carbon in Molten Copper-Nickel Alloy and Vickers Hardness of Copper-Nickel-Saturated Carbon”, Materials Transactions, vol. 58 no.1 (2017) pp.11-15

CHAPTER 7

RESEARCH SUMMARY

Several experiments have been carried out to in order to prepare graphite dispersed copper composite. In Chapter 2, Cu-Ni alloy which included nickel content up to approximately 5 mass% was melted in the graphite crucible to prepare graphite dispersed Cu-Ni alloy. Solubility of carbon in the molten Cu-Ni alloy and Vickers hardness were measured in this study. The solubility of carbon in the molten Cu-Ni alloy increased with the temperature rise and with the nickel content. The relation between solubility of carbon in molten Cu-Ni alloy and temperature, *T* (1673 K ~ 2143 K) could be given by Eqs. (2-1) ~ (2-3). It was cleared that the interaction parameter, ω_C^{Ni}, for Cu-Ni-Csat (saturated carbon) was -17.1. Graphite particles were precipitated from the molten Cu-Ni-Csat. Vickers hardness of Cu-Ni-Csat system increased with carbon content and nickel content. The heat treated Cu-Ni-Csat alloy was hardened by precipitation hardening of the graphite particles and solution hardening of nickel.

In Chapter 3, solubility of nitrogen gas into a molten copper was measured at the temperature range of 1993 K to 2443 K using a levitation-melting apparatus. The dissolution of nitrogen gas into molten copper obeyed the Sieverts' law, which meant that absorption of nitrogen gas into molten copper was expressed as:

$$\frac{1}{2}N_2(\text{gas}) = \underline{N} \tag{7-1}$$

Solubility of nitrogen gas into a molten copper of which oxygen content was 60

massppm to 120 massppm was expressed as:

$$\ln[\text{mass\%N}] = -\frac{7406}{T} - 5.863 \text{ (T: 1993 K} \sim \text{2443 K)} \quad (7\text{-}2)$$

The standard reaction Gibbs energy was expressed as:

$$\Delta_r G^0 = 61573 + 48.75T \text{ [J/(mol·k)]} \quad (7\text{-}3)$$

In Chapter 4, the copper plates which contained graphite particles between them were spot-welded to prepare the graphite dispersed copper composite on a copper plate. Several conclusions had been made. The composite which was prepared only by the compression of graphite particles without an electric current flow was produced by plunging the relatively small graphite particles. The carbon content in the composite increased with the repetition number of the compression and the compressive load. When an electric current was energized through the sample at the compression, the copper around the graphite particle melted locally. The graphite particles partially or wholly dissolved into the copper melt. Undissolved graphite particles adhered to the copper by the melting. The graphite particles were precipitated from the molten copper under cooling. The carbon content in the composite became higher than that prepared without an electric current flow. The Vickers hardness of the copper matrix in the composite and the volume fraction of graphite were expressed by the rule of mixtures given by eq. (4-3) and eq. (4-4).

In Chapter 5, it was tried in this study that graphite dispersed copper composite was prepared locally on the surface of the copper plate with the CO_2 laser. Then, after

graphite particles were plunged into a copper plate by rolling, the laser was irradiated on the plate. A laser could heat a substance and catch a particle. When the laser was irradiated on the graphite particles for a short time, the graphite particles which were pushed deeply into the plate adhered on the surface of the plate, whereas the graphite particles which were pushed shallowly were eliminated by the laser trapping. When the laser was irradiated for a longer time, the copper surrounding of the remained graphite particles was melted. Most graphite particles were eliminated from the surface by the laser trapping. The graphite particles at out of the laser spot were easy to remain on the copper plate because the laser trapping did not act there in comparison with the spot. The area out of the laser spot was heated by the heat conduction from the laser spot and melted. The particles was fixed by the wetting. The graphite dispersed copper composite could be prepared if the laser was irradiated near the place where we want to form the composite However, the graphite particles were half-afloat from the copper plate. Lastly, Vickers hardness decreased with an increase in the laser irradiation time due to the annealing. The hardness at the outside of the laser spot where the graphite particles more remained was larger by approximately 100 MPa than that at the center.

In Chapter 6, I had studied about preparation of graphite dispersed copper composite with addition of graphite particles into molten copper. Copper composite had been prepared on six different conditions. The microstructure, elemental analysis and hardness of the composite were investigated. Graphite particles in the prepared composite were mainly formed by the precipitation from the melt under solidification, because the particles in the composite were different in shape and size from the initial graphite particles. Therefore, temperature of 2073 K and addition of the graphite particles at this temperature were desirable to prepare the composite because of

prevention of the scattering of the particles under heating. Because the addition of nickel or iron in the copper increased solubility, the addition of them was advantageous to production of the composite. However, the composite prepared with the addition of iron consisted of graphite, copper rich phase and iron rich phase. The Vickers hardness of as-casted composite were higher than that of annealed composite due to the solid-solution hardening. The Vickers hardness of graphite dispersed nickel- or iron-copper composite was higher than that of graphite dispersed copper composite because of the solid-solution hardening of each alloying element. This study could not clear whichever quantity of graphite in the composite was higher than that of carbon solubility or not. A further study was necessary to understand quantitatively the relation between additive amount of graphite particles and amount of precipitated graphite particles and so on.

In this study, the processes for preparation of the graphite dispersed copper alloy composite has been developed and discussed physico-chemically. Conventionally, carbon content in the composite was 20 mass% to 85 mass%. The maximum carbon content in the graphite dispersed copper composite prepared with the spot welding method was approximately 50 mass%. Therefore, the spot welding method produced a graphite dispersed copper composite which satisfied this carbon content range. Because the maximum carbon content in the composite prepared with the laser was approximately 20 mass%, this method can produced a graphite dispersed copper composite somehow. These two methods prepare the composite only on the surface of a copper plate.

This study provides the following guidance for the preparation of the composite.

(1) Presently, we must add more nickel into copper and raise the temperature of the

molten copper alloy higher to prepare the composite with the dissolution – solidification method with addition of nickel. However, the excessive addition of nickel may lost copper characteristics. In addition, higher temperature will bring much loss of metal by evaporation of it. Therefore, we must search for a new alloy element which increases the solubility of graphite in molten copper alloy for the preparation of the composite with the dissolution – solidification method.

(2) The spot welding is a suitable method to prepare the graphite the graphite dispersed copper composite only on a copper surface. It will be the key in this method to prepare the composite at a larger area. In the process with using the laser, it is important to prevent the elimination of graphite particles by the laser trapping. By putting thin boards on powder, it is necessary to attach a particle by the heat conduction from it. The surface will be smooth by rolling for example because the particles will half-floating on a copper plate.

(3) The method of addition of graphite particles has possibility of preparation of bulk of a graphite dispersed copper alloy composite. It is the key to this method to prevent scattering of the particles under heating and at the time of the addition. A vacuum melting will be useful for the preparation of the composite.

ACKNOWLEDGEMENT

This thesis is the outcome of my research from October 2014 until September 2017 at Toyohashi University of Technology, Aichi, Japan. The completion of this thesis not solely depended on the devotion of my time to research, but also on a lot of assistances and supports from a lot of peoples to whom I would like to express my unlimited thankful acknowledgement.

First of all, I would like to give my infinite gratefulness and appreciation to my respected supervisor, Assoc. Prof. Dr. Seiji Yokoyama for his patience, ideas, discussions, supports, advices, comments, heart-kind and many other things in many ways. I also want to thank my Thin Film Laboratory advisor, Prof. Dr. Masanobu Izaki for recommended me to do research in Dr. Yokoyama group, giving varieties of comments and suggestions. I also like to thank Prof. Dr. Masahiro Fukumoto and Assoc. Prof. Dr. Masakazu Kobayashi for giving varieties of comments and suggestions that helped me a lot to improve my work. I also want to thank to Dr. Junji Sasano, for his comments and ideas especially during the discussion in laboratory's seminars and when using laboratories facilities. Then, I would like to thank Prof. Dr. Yoshikazu Todaka for giving me permission to conduct several experiments in his laboratory.

Next to all Thin Film Laboratory members, I would like to thank them for their support, comment and advices during my 3 and half years at this laboratory. This is especially to Mr. Yusuke Inoue, Mr. Shahrul Shazwan and Mr. Yoshikazu Ishikawa, which whom I mostly worked with. I also like to thank members of Material Function Control Laboratory for their cooperation during conducting several experiments at their laboratory

My study in Toyohashi University of Technology was supported by NGK Foundation, in which I received scholarship for 1 and a half years. I like to thank to all staff in the foundation especially to Mrs. Yaeko Tasaki, who always takes care and advice the scholarships students. I also like to thanks to all my friends in this foundations. Beside the busy of the study life, we had all joyful stories we shared together during monthly meeting at Nagoya.

To all my fellow Malaysian in Toyohashi, I would like to thank to you all. It was a long journey since I came in Toyohashi in 2010. Without all of you, I could not get to what I am doing now. Thank you for those encouragements, advices, ideas, activities, football and many more.

Last but not least, I would like to give my uncountable thanks for my beloved wife, Siti Hajar binti Muhammad Anuar for her unlimited support, caring and love all the time. I also want to thank to my parents, Prof. Dr. Mohd Noor bin Ahmad and Norizan binti Mamat, my sibling, Nor Zainira, Nor Baizura, Aishah, Anas and Nur Syakirah for their unlimited support, and of course to my relatives and friends in Malaysia and Japan.

RESEARCH ACHIEVEMENTS

List of Journals:

[1] Abdul Muizz bin Mohd Noor and Seiji Yokoyama: “Solubility of Carbon in Molten Copper-Nickel Alloy and Vickers Hardness of Copper-Nickel-Saturated Carbon”, Materials Transactions, vol. 58 no.1 (2017) pp.11-15

[2] Abdul Muizz Mohd Noor, Nik Hisyamudin Muhd Nor and Seiji Yokoyama: “Solubility of Nitrogen Gas into Molten Copper at Temperature Range of 1,993 K to 2,443 K”, High Temperature Materials Processes, (2017) Published Online DOI: https://doi.org/10.1515/htmp-2016-0174

[3] Abdul Muizz Mohd Noor, Yoshikazu Ishikawa and Seiji Yokoyama: “Preparation of Graphite Dispersed Copper Composite on Copper Plate with Spot Welding”, Materials Transactions, vol. 58 No. 8 (2017) pp. 1138-1144

List of Proceedings of International Conferences:

[1] Abdul Muizz Mohd Noor, Yoshikazu Ishikawa and Seiji Yokoyama: “Preparation of Graphite dispersed Copper Composite with Intruding Graphite Particles in Copper Plate”, AIP Conference Proceedings, vol. 1807 (1) (2017) DOI: http://dx.doi.org/10.1063/1.4974798